FINAL REPORT

Synergistic Treatment of Mixed 1,4-Dioxane and Polyfluorinated Chemical Contaminations by Combining Electrolytic Degradation with Electrobiostimulation

SERDP Project ER-2718

OCTOBER 2021

Jens Blotevogel
Thomas Sale
Colorado State University

Shaily Mahendra
University of California, Los Angeles

SERDP
DOD ▪ EPA ▪ DOE

REPORT DOCUMENTATION PAGE

Form Approved
OMB No. 0704-0188

1. REPORT DATE *(DD-MM-YYYY)*	**2. REPORT TYPE**	**3. DATES COVERED** *(From - To)*
18/10/2021	SERDP Final Report	9/29/2017 - 9/29/2022

4. TITLE AND SUBTITLE

Synergistic Treatment of Mixed 1,4-Dioxane and Polyfluorinated Chemical Contaminations by Combining Electrolytic Degradation with Electrobiostimulation

5a. CONTRACT NUMBER
17-C-0054

5b. GRANT NUMBER

5c. PROGRAM ELEMENT NUMBER

6. AUTHOR(S)
Jens Blotevogel
Thomas Sale
Colorado State University

Shaily Mahendra
University of California, Los Angeles

5d. PROJECT NUMBER
ER-2718

5e. TASK NUMBER

5f. WORK UNIT NUMBER

7. PERFORMING ORGANIZATION NAME(S) AND ADDRESS(ES)
Colorado State University
1320 Campus Delivery
Fort Collins, CO 80523

8. PERFORMING ORGANIZATION REPORT NUMBER
ER-2718

9. SPONSORING/MONITORING AGENCY NAME(S) AND ADDRESS(ES)
Strategic Environmental Research and Development Program (SERDP)
4800 Mark Center Drive, Suite 16F16
Alexandria, VA 22350-3605

10. SPONSOR/MONITOR'S ACRONYM(S)
SERDP

11. SPONSOR/MONITOR'S REPORT NUMBER(S)
ER-2718

12. DISTRIBUTION/AVAILABILITY STATEMENT
DISTRIBUTION STATEMENT A. Approved for public release: distribution unlimited.

13. SUPPLEMENTARY NOTES

14. ABSTRACT
1,4-Dioxane and per- and polyfluoroalkyl substances (PFASs) co-occur in mixed plumes at several Department of Defense (DoD) sites and are resistant to many natural and engineered degradation processes. Costly ex situ treatment technologies are often required to break them down. More costefficient destructive treatment approaches are urgently needed that can (1) generate synergistic ffects and (2) optionally be applied in situ. Our previous work has shown that electrochemical water treatment, one of the few processes that can break the C-F bond in PFASs, can be installed in situ. Building on this work, the objective of this project was to advance the efficacy of combining electrochemical with biological oxidation for the in situ remediation of groundwater contaminated by mixed COCs.

15. SUBJECT TERMS
Emerging contaminants, 1,4-dioxane, chlorinated solvents, PFAS, PFOS, PFOA, perfluorinated, polyfluorinated, precursor, AFFF, electrochemical oxidation, advanced oxidation processes, defluorination, groundwater remediation, destructive treatment, biodegradation, Pseudonocardia dioxanivorans CB1190, fungal degradation, mycoremediation, extracellular, enzymes ligninolytic, wood-rotting, peroxidase, laccase, aerobic, biotransformation, in situ, sustainability, treatment train

16. SECURITY CLASSIFICATION OF:			**17. LIMITATION OF ABSTRACT**	**18. NUMBER OF PAGES**	**19a. NAME OF RESPONSIBLE PERSON**
a. REPORT	**b. ABSTRACT**	**c. THIS PAGE**			Jens Blotevogel
UNCLASS	UNCLASS	UNCLASS	UNCLASS	102	**19b. TELEPHONE NUMBER** *(Include area code)* 970-491-8880

TABLE OF CONTENTS

LIST OF FIGURES

LIST OF TABLES

LIST OF ACRONYMS

1,4-D	1,4-Dioxane
4:2 FTSA-PrAn	4:2 Fluorotelomer sulfonamido propyl amine
6:2 FTSA-PrAn	6:2 Fluorotelomer sulfonamido propyl amine
AEO	Alkyl ethoxylate
AFFF	Aqueous film-forming foam
AmPr-FPeSA	*N*-dimethyl ammonio propyl perfluoropentane sulfonamide
AmPr-FPrSA	*N*-dimethyl ammonio propyl perfluoropropane sulfonamide
AMS	Ammonium mineral salts
AOP	Advanced oxidation process
ATP	Adenosine triphosphate
BDD	Boron-doped diamond
CCA	Canonical correspondence analysis
CCH	Center for Contaminant Hydrology
CSU	Colorado State University
CT	Carbon tetrachloride
COC	Contaminant of concern
CVOC	Chlorinated volatile organic compound
DBP	Disinfection by-product
DC	Direct current
DCE	Dichloroethene
DCM	Dichloromethane
DET	Direct electron transfer
DNA	Deoxyribonucleic acid
DO	Dissolved oxygen
DoD	Department of Defense
DXMO	Dioxane monooxygenase
EO	Electrochemical oxidation
ESI	Electrospray ionization
ESTCP	Environmental Security Technology Certification Program

GAC	Granular activated carbon
FOSA	Perfluorooctane sulfonamide
FTS	Fluorotelomer sulfonate
GC	Gas chromatograph(y)
GW	Groundwater
HBT	Hydroxybenzotriazole
HPLC	High-performance liquid chromatography
IC	Ion chromatography
ID	Inner diameter
IPR	In-Progress Review
LC	Liquid chromatograph(y)
LOD	Limit of detection
MMO	Mixed metal oxide
MS	Mass spectrometer/spectrometry
OD	Outer diameter
OEP	Oxygen evolution potential
O&M	Operation & maintenance
ORP	Oxidation-reduction potential
PCA	Principal component analysis
PCM	Polarizable Continuum Model
PES	Polyethersulfone
PFAA	Perfluoroalkyl acid
PFAS	Per- and polyfluoroalkyl substance
PFC	Polyfluorinated chemical
PFCA	Perfluoroalkyl carboxylic acid
PFHpS	Perfluoroheptane sulfonic acid
PFHxS	Perfluorohexane sulfonic acid
PFPeS	Perfluoropentane sulfonic acid
PFBS	Perfluorobutane sulfonic acid
PFOA	Perfluorooctanoic acid
PFOS	Perfluorooctane sulfonic acid

PFSA	Perfluoroalkane sulfonic acid
PIGE	Particle-induced gamma-ray emission
POP	Persistent organic pollutant
PRB	Permeable reactive barrier
PVC	Polyvinyl chloride
qPCR	Quantitative polymerase chain reaction
QqQ	Triple quadrupole
QToF	Quadrupole time-of-flight
RLU	Relative light units
RNA	Ribonucleic acid
ROS	Reactive oxygen species
rRNA	Ribosomal ribonucleic acid
SERDP	Strategic Environmental Research and Development Program
SHE	Standard hydrogen electrode
SIM	Selective ion monitoring
SPE	Solid-phase extraction
TCA	Trichloroethane
TCE	Trichloroethene
Ti-MMO	Titanium - mixed metal oxide
TOC	Total organic carbon
TOP	Total oxidizable precursor
UCLA	University of California, Los Angeles
UHPLC	Ultra-high-performance liquid chromatography
UNCD	Ultrananocrystalline diamond
UV	Ultraviolet

KEYWORDS

Emerging contaminants, 1,4-dioxane, chlorinated solvents, PFAS, PFOS, PFOA, perfluorinated, polyfluorinated, precursor, AFFF, electrochemical oxidation, advanced oxidation processes, defluorination, groundwater remediation, destructive treatment, biodegradation, *Pseudonocardia dioxanivorans* CB1190, fungal degradation, mycoremediation, extracellular, enzymes ligninolytic, wood-rotting, peroxidase, laccase, aerobic, biotransformation, *in situ*, sustainability, treatment train

ACKNOWLEDGEMENTS

The authors thank the following contributors at Colorado State University: Dr. Nasim Pica, Dr. Andrea Hanson, Dr. Greg Dooley, Brian Cranmer, Dr. Hamidreza Sharifan, Dr. Anthony Rappé, Cathelyne Powers, Jenna Salvat, and Dr. Amy Sullivan.

The authors thank the following contributors at the University of California, Los Angeles: Dr. Yu Miao, Dr. Shashank Singh Kalra, Dr. Nicholas W. Johnson, and Pia Ramos.

Furthermore, the authors thank Dr. Christopher Higgins and his team at the Colorado School of Mines for generously providing an extensive PFAS suspect screening list; Dr. Graham Peaslee and Yukun Jin at the University of Notre Dame for PIGE analyses; Dr. Thomas Holsen and Elizabeth Brown at Clarkson University for total organofluorine analyses; Rob Sterner and Jay Huang at Magneli Materials, LLC for custom-fabricating and donating the Magnéli-phase titanium mesh anodes; Dr. Paul Hatzinger for donating the AFFF sample.

Finally, the authors thank Angelo Fenti as well as Dr. Pasquale Iovino, Dr. Stefano Salvestrini, and Dr. Dino Musmarra at the University of Campania “Luigi Vanvitelli” for their collaboration on electrochemical flow-through treatment of PFAS.

Partial support for this research was provided by the Colorado State University Scott Undergraduate Research Experience (SURE) and the P.O.R. CAMPANIA FSE 2014/2020 Fund.

ABSTRACT

Introduction and Objectives

1,4-Dioxane and per- and polyfluoroalkyl substances (PFASs) co-occur in mixed plumes at several Department of Defense (DoD) sites and are resistant to many natural and engineered degradation processes. Costly *ex situ* treatment technologies are often required to break them down. More cost-efficient destructive treatment approaches are urgently needed that can (1) generate synergistic effects and (2) optionally be applied *in situ*. Our previous work has shown that electrochemical water treatment, one of the few processes that can break the C-F bond in PFASs, can be installed *in situ*. Building on this work, the objective of this project was to advance the efficacy of combining electrochemical with biological oxidation for the *in situ* remediation of groundwater contaminated by mixed COCs.

Technical Approach

Our bioelectrochemical treatment train approach is based on creating synergistic effects between two processes: (1) rapid electrochemical oxidation on dimensionally stable electrodes and (2) enhancement of aerobic biodegradation processes via electrochemically generated oxygen with concurrent removal of inhibiting co-contaminants. Here, we tested various mesh electrode materials in both commercial and custom-fabricated flow-through electrochemical reactors and investigated the coupling with 1,4-dioxane biodegradation by *Pseudonocardia dioxanivorans* CB1190 and aqueous film-forming foam (AFFF) pretreatment by the laccase-producing fungus *Trametes versicolor*.

Results

Bioelectrochemical treatment rapidly reduced concentrations of 1,4-dioxane by several orders of magnitude even in the presence of biologically inhibitory chlorinated solvents, demonstrating the technology's viability for both source zone and plume treatment. Coupling electrochemical with biological oxidation reduced energy consumption, material usage, and treatment costs by about one order of magnitude while mitigating oxidation by-product formation. Several mesh anode materials were shown to be effective for flow-through PFAS mineralization, Magnéli-phase titanium suboxides being the most efficient. Over 99% of PFAS removal was achieved, demonstrating fluoride generation without aqueous organofluorine intermediate formation. Fungal AFFF pretreatment did not conclusively lead to PFAS transformation, possibly due to time limitations, but aerobic degradation of non-fluorinated AFFF components decreased the energy consumption of subsequent electrochemical treatment by 20%. The energy consumption of *in situ* electrochemical PFAS treatment under mass transfer-limitations is high, however, and further efforts on process configuration, material development, and implementation should be explored.

Benefits

At many sites, remediation of groundwater impacted with 1,4-dioxane, chlorinated solvents, and PFASs requires costly *ex situ* treatment. In this project, we provided DoD site managers with a new technology to treat mixed persistent contaminants *in situ*. Bioelectrochemical treatment is sufficiently developed and understood to move ahead with field application, and is currently being tested at the pilot-scale. More work is needed to establish *in situ* (bio)electrochemical PFAS treatment, but this research provides a solid foundation and critical early insights.

EXECUTIVE SUMMARY

Introduction

A recent review showed that the groundwater at 59% of Department of Defense (DoD) sites was impacted by more than one chemical, including chlorinated volatile organic compounds (CVOCs), 1,4-dioxane, and per- and polyfluoroalkyl substances (PFASs). 1,4-Dioxane and PFASs are persistent organic pollutants that are widespread in the environment. Due to its application as stabilizing agent in chlorinated solvents, 1,4-dioxane frequently co-occurs with CVOCs such as 1,1,1-trichloroethane (1,1,1-TCA) and trichloroethene (TCE). PFASs are a highly complex group of anthropogenic chemicals comprising thousands of individual species and critical components of aqueous film-forming foams (AFFFs). While labile non-fluorinated moieties of PFASs are prone to partial abiotic and biotic transformation processes, the chemical and thermal stability of the perfluoroalkyl tails translates into an extraordinary recalcitrance in the environment.

1,4-Dioxane and PFASs are resistant to many natural degradation processes and traditional water treatment technologies. Costly *ex situ* treatment technologies involving strong oxidants and/or ultraviolet light are often required to break it down. Consequently, more cost-efficient treatment approaches are acutely needed that can (1) generate synergistic effects between treatment processes and (2) optionally be applied *in situ*.

In our previous work, we have gathered valuable insights in the implementation of electrochemical water treatment both *in situ* and *ex situ*. The final design of an *in situ* electrolytic barrier ("e^- Barrier", Figure ES 1) installed at Pueblo Chemical Depot for the treatment of energetic compounds included a sequence of multiple active electrodes mounted on vinyl sheet pile sections.

Our first-generation laboratory-scale studies on bioelectrochemical degradation of 1,4-dioxane in bench-scale flow-through reactors had shown that concurrent stimulation of *Pseudonocardia dioxanivorans* CB1190 leads to an over-additive treatment effect by (1) providing O_2 to aerobic microorganisms via anodic oxidation of water and (2) concurrent degradation of inhibiting trichloroethene (TCE). However, critical questions remained to be addressed on the path to field-scale installation regarding performance optimization, oxidation by-product formation, and sustainability. Furthermore, while mixed metal oxide electrodes have been shown to oxidize PFASs, other electrode materials such as boron-doped diamond (BDD) and Magnéli-phase titanium suboxides were reported to be potentially more efficient. Consequently, two critical steps were required before *in situ* electrochemical water treatment can be (cost-)effectively implemented at PFAS-impacted field sites: (1) the testing of dimensionally stable mesh electrode materials, and (2) the determination of optimum design and operational parameters to optimize synergistic treatment effects.

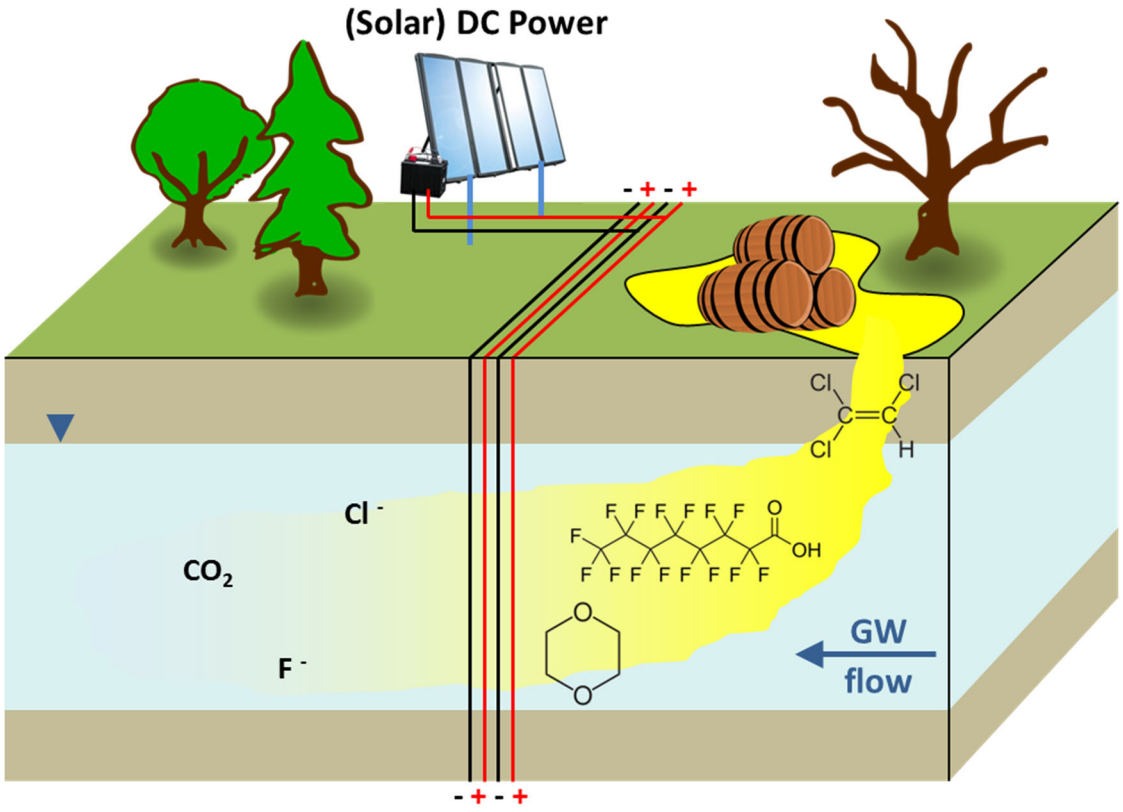

Figure ES 1: Conceptual design of an *in situ* electrolytic barrier ("e⁻Barrier").

Objectives

The overarching objective of this project was to advance the efficacy of bioelectrochemical treatment for the remediation of groundwater contaminated by mixed contaminants of concern (COCs), focusing on PFASs as well as 1,4-dioxane in the presence of CVOCs. The guiding idea was to establish contaminant degradation by flow-through mesh electrodes, enabling *in situ* implementation as permeable reactive barrier, providing DoD site managers with guidance on treatment options and design for specific remedial goals with the following specific objectives:

- to test dimensionally stable electrodes that enable rapid oxidation of COCs in flow-through reactors;
- to enhance aerobic biodegradation processes via electrochemically generated molecular oxygen;
- to remove co-occurring COCs that inhibit biodegradation;
- to remove readily biodegradable co-contaminants and thereby increase the electrochemical treatment efficiency for more refractory COCs;
- to develop a greater understanding of potential treatment synergies that could lead to cost savings and improved remedial strategies.

Technical Approach

Bioelectrochemical treatment of mixed 1,4-dioxane and CVOC contaminations was tested in bench-scale flow-through column reactors with doped tin oxide-coated titanium (Ti/SnO_2-X) mesh anodes. The columns were packed with sand, either sterilized or inoculated with the aerobic metabolic 1,4-dioxane degrader *Pseudonocardia dioxanivorans* CB1190. The experiments were performed in the presence and absence of 1,1-dichloroethene (1,1-DCE). Two different potentials were compared.

In situ treatment of PFASs was first tested in custom-fabricated flow-through electrochemical reactors with three different types of anode mesh materials: Magnéli-phase titanium suboxides Ti_nO_{2n-1}, boron-doped diamond (BDD), and IrO_2-Ta_2O_5 mixed metal oxides. The impacts of varying current density, flow velocity, electrolyte conductivity, initial PFAS concentration, PFAS chain length/branching, and PFAS functional head group on electrochemical oxidation kinetics were compared. A fluorine mass balance was established based on both aqueous-phase and gas-phase analyses.

To explore bioelectrochemical treatment of PFASs, biological and electrochemical oxidation processes were tested independently due to substantially different kinetics. For biological pretreatment of AFFF-spiked water, fungal degradation was investigated in aerobic batch containers. Electrochemical oxidation was performed in a commercial flow cell with a BDD anode. Three treatment experiments were conducted: (1) PFOS only in synthetic electrolyte solution, (2) AFFF in the same pure electrolyte solution, and (3) AFFF solution pretreated with *Trametes versicolor*, a laccase-producing fungus.

Results and Discussion

Bioelectrochemical treatment degraded 1,4-dioxane significantly faster than electrochemical treatment alone. 1,4-Dioxane influent concentrations were rapidly reduced from around 100,000 µg/L by more than four orders of magnitude to below our detection limit of 3 µg/L (Figure ES 2). The application of an electric potential was associated with a higher abundance of *P. dioxanivorans* CB1190 in both sessile and planktonic states. The presence of 5 mg/L 1,1-DCE, one of the strongest known inhibitors of 1,4-dioxane biodegradation, reduced 1,4-dioxane degradation rates but did not stall the process. Compared to electrochemical treatment only, the coupling with biological metabolism reduced energy consumption, material usage, and consequently overall treatment costs by about one order of magnitude while generating lower amounts of oxidation by-products such as chlorate and perchlorate. Our results establish that bioelectrochemical treatment is a synergistic, sustainable technology for water contaminated with 1,4-dioxane and chlorinated co-contaminants to meet strict regulatory thresholds.

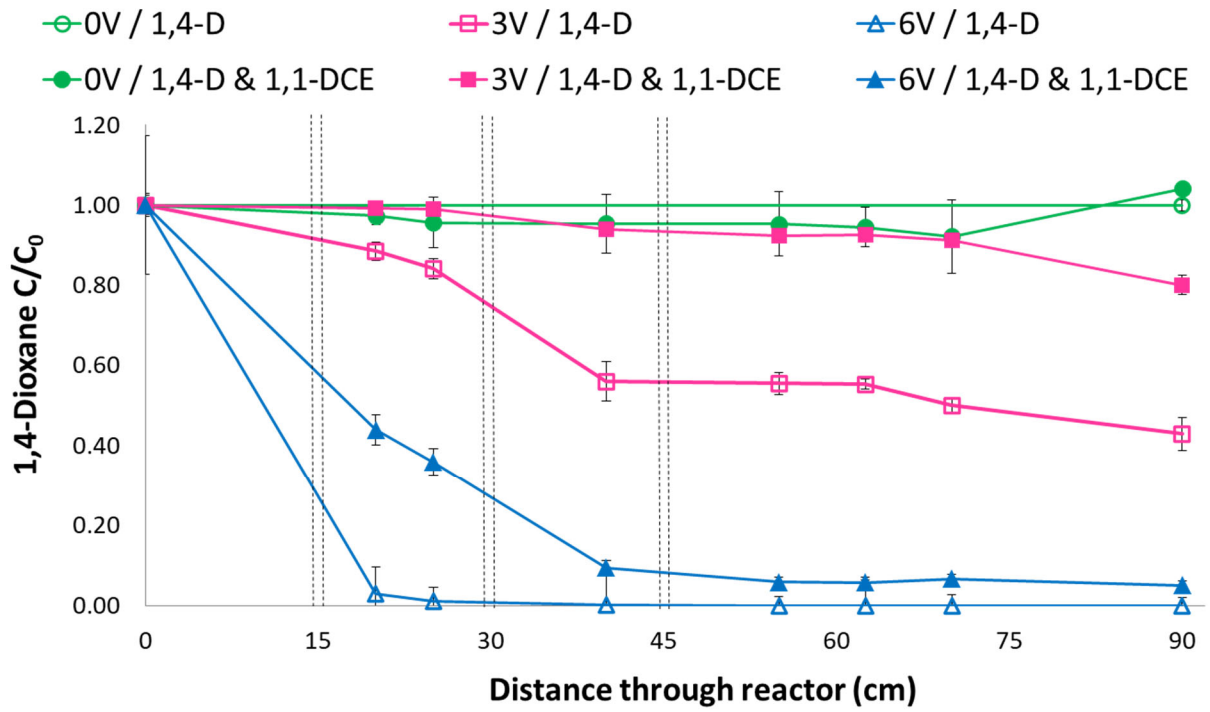

Figure ES 2: 1,4-Dioxane removal for bioelectrochemical treatment. Open markers represent absence, solid markers show the presence of the co-contaminant 1,1-DCE in the feed water. The vertical dashed lines indicate the location of (leading) anode and (trailing) cathode pairs.

The Magnéli-phase titanium suboxides anode achieved higher perfluorooctane sulfonate (PFOS) oxidation rates and lower energy consumption than BDD and IrO_2-Ta_2O_5, and was thus chosen for further testing. Electrochemical oxidation rates increased with increasing current density, decreasing water conductivity, increasing seepage velocity, and decreasing PFOS concentration. Over 99% of PFOS removal was achieved under continuous flow conditions (Figure ES 3). The fluorine mass balance showed that most PFOS-bonded F was released as fluoride, while no organic intermediates were detected in the aqueous phase. Each ~2% of fluorine was recovered as HF and organofluorine intermediates in the gas phase. A comparison of 10 PFAS revealed a hydrophobicity-driven increase in oxidation rate with increasing perfluoroalkyl chain length as well as faster oxidation kinetics for perfluoroalkyl carboxylic acids (PFCAs) compared to perfluoroalkane sulfonic acids (PFSAs), likely due to contributions from electrochemically activated sulfate. The energy consumption of PFAS treatment under simulated slow-flow groundwater conditions was substantially higher than in *ex situ* electrochemical systems optimized for enhanced mass transfer. Consequently, future work should focus on in situ treatment design optimization with an emphasis on power requirements. Collectively, our investigations demonstrate that among the few water treatment technologies capable of breaking the carbon-fluorine bond, electrochemical treatment is a promising approach for *in situ* destruction of PFAS in the subsurface.

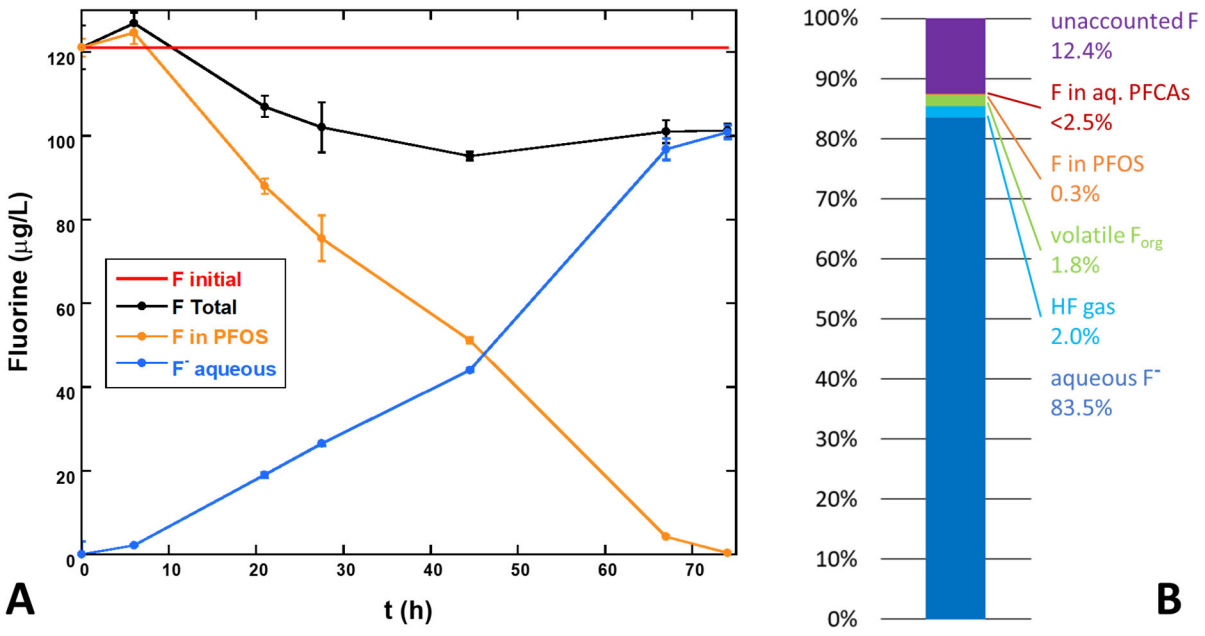

Figure ES 3: A) Aqueous fluorine mass balance for the electrochemical oxidation of ~200 µg/L PFOS at a Magnéli-phase Ti_nO_{2n-1} mesh anode, showing the time-dependent concentrations of F bonded in the parent PFOS (orange), generated fluoride in aqueous solution (blue) and the sum of these two species as total F (black). The red line indicates F concentration in the system at the start of the experiment. B) Total fluorine mass balance at the end of the 74-hour experiment.

In the commercial flow cell with a BDD anode, we showed that electrochemical oxidation of PFOS only in synthetic electrolyte solution proceeds faster than in complex AFFF solution due to competition by other AFFF components. Fungal treatment of a dilute complex AFFF sample for 19 days showed losses of PFSAs as well as some PFCAs and polyfluorinated species compared to a killed control (Figure ES 4), but no fluoride generation as evidence for C-F bond cleavage could be observed. In contrast, fungal degradation of non-fluorinated AFFF components was readily observed (Figure ES 4). This latter process alone led to a 20% lower energy consumption during electrochemical treatment of the dilute AFFF sample compared to direct electrochemical oxidation without fungal pretreatment. Consequently, remediation cost savings are possible by granting natural degradation processes time and space, and focusing these expensive treatment methods on the most persistent PFAAs only.

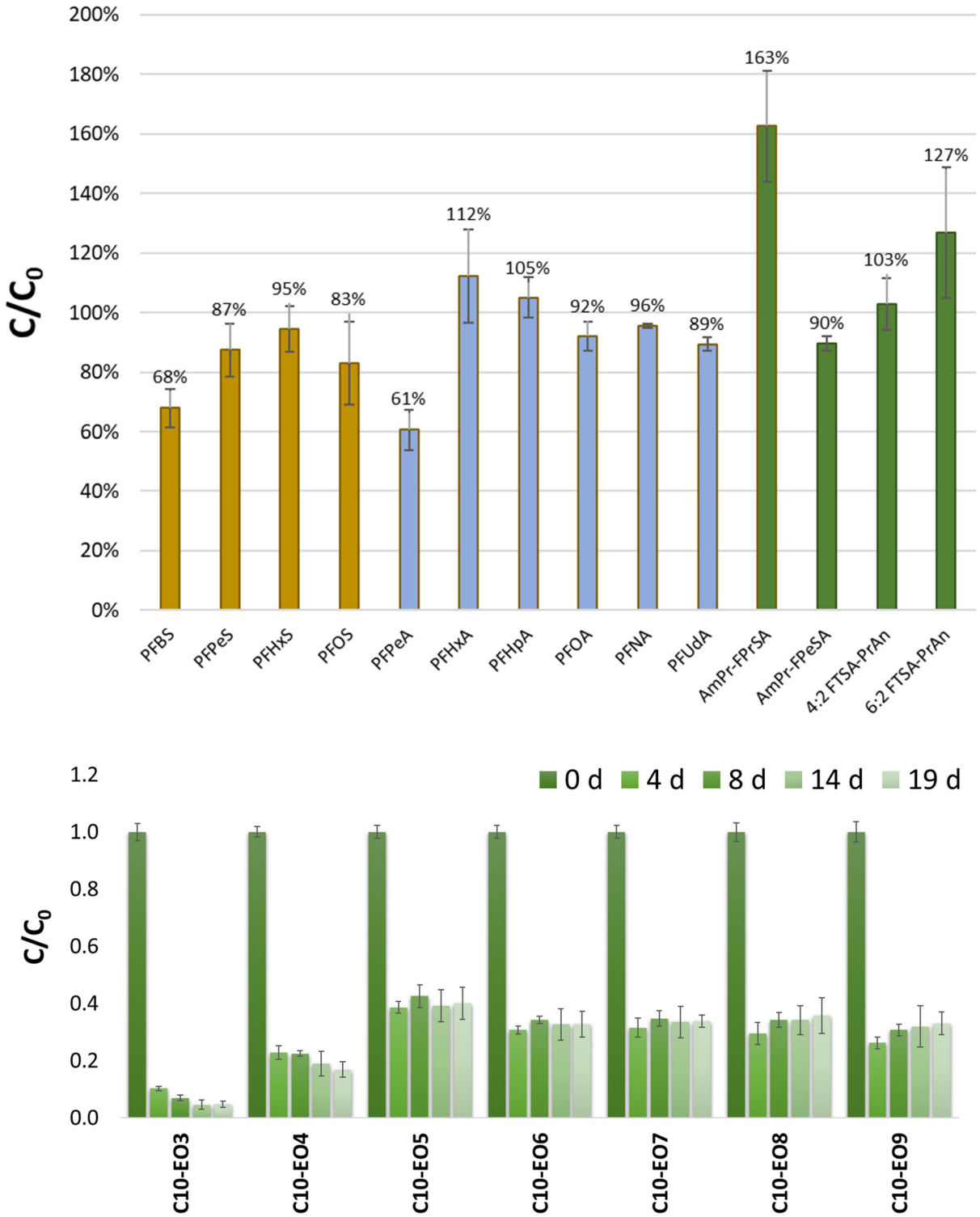

Figure ES 4: Top: Normalized PFAS concentrations after 19 days of fungal pretreatment normalized to the initial concentrations. Bottom: C_{10}-alkyl ethoxylate surfactant concentrations over time during fungal pretreatment normalized to the initial concentrations.

Implications for Future Research and Benefits

Our research shows that bioelectrochemical treatment can effectively, efficiently, and sustainably reduce 1,4-dioxane concentrations by several orders of magnitude, even in the presence of inhibitory chlorinated solvents. Consequently, this technology should be effective in source zones as well as in dilute plumes, possibly meeting the strict low- or sub-ppb 1,4-dioxane regulatory limits where purely (co-)metabolic bioremediation approaches are challenged. Dimensionally stable mesh electrodes can be operative for extended periods (i.e., months, years) if proper scale management via polarity reversals is performed. Due to the success of our research performed within this project, bioelectrochemical treatment of mixed 1,4-dioxane and CVOC contaminations has been scaled up and is currently pilot-tested in drum-scale reactors at an undisclosed non-DoD site in the U.S. We believe that future efforts should be focused on further scale-up and explore whether bioelectrochemical treatment is effective with other types of bacteria including co-metabolizing strains and mixed cultures. Installations other than permeable reactive barriers such as integration into a subgrade biogeochemical reactor seem possible. With these findings, DoD site managers have one more technology option in their toolbox for sites at which 1,4-dioxane and chlorinated solvents impacts require active remediation.

Regarding PFASs, our findings show that various mesh electrode materials are capable of breaking down even the most persistent perfluoroalkyl acids (PFAAs), paving the way for *in situ* electrochemical groundwater treatment. While we were unable to find conclusive evidence of fungal PFAS defluorination during the relatively short experimental time frame, our experiments did demonstrate that biodegradation of non-fluorinated AFFF components have the potential to significantly lower treatment costs. However, electrochemical PFAS oxidation is notoriously mass transfer-limited, and typically slow groundwater seepage velocities in combination with high current densities needed for PFAS destruction results in low faradaic efficiency, causing excessive gas formation and low direct electron transfer rates to the target PFAS molecules.

As water treatment and remediation technologies have matured in recent years, combining processes in efficient treatment trains promises further economic and environmental benefits. In this project, we have advanced the efficacy of bioelectrochemical treatment for the remediation of groundwater contaminated by mixed contaminants of concern. While this technology appears to be ready for field application at 1,4-dioxane- and CVOC-impacted sites, more research and work remains to be performed for *in situ* electrochemical treatment of more persistent PFASs. At the moment, any destructive PFAS treatment is expensive, but process and material optimizations leading to considerable cost savings are still waiting to be discovered.

1 OBJECTIVE

This project was conducted based on the SERDP Statement of Need ERSON-17-01, addressing the need for improved strategies for remediating mixed contaminants in groundwater. A recent review had shown that the groundwater at 59% of Department of Defense (DoD) sites was contaminated by more than one compound, including chlorinated volatile organic compounds (CVOCs), 1,4-dioxane, and per- and polyfluoroalkyl substances (PFASs).

The overarching objective of this project was to advance the efficacy of bioelectrochemical treatment for the remediation of groundwater contaminated by mixed contaminants of concern (COCs), focusing on PFASs as well as 1,4-dioxane in the presence of CVOCs. The guiding idea was to establish contaminant degradation by flow-through mesh electrodes, enabling *in situ* implementation as permeable reactive barrier ("e^-Barrier", Figure 1), providing DoD site managers with guidance on treatment options and design for specific remedial goals with the following specific objectives:

- to test dimensionally stable electrodes that enable rapid oxidation of COCs in flow-through reactors;
- to enhance aerobic biodegradation processes via electrochemically generated molecular oxygen;
- to remove co-occurring COCs that inhibit biodegradation;
- to remove readily biodegradable co-contaminants and thereby increase the electrochemical treatment efficiency for more refractory COCs;
- to develop a greater understanding of potential treatment synergies that could lead to cost savings and improved remedial strategies.

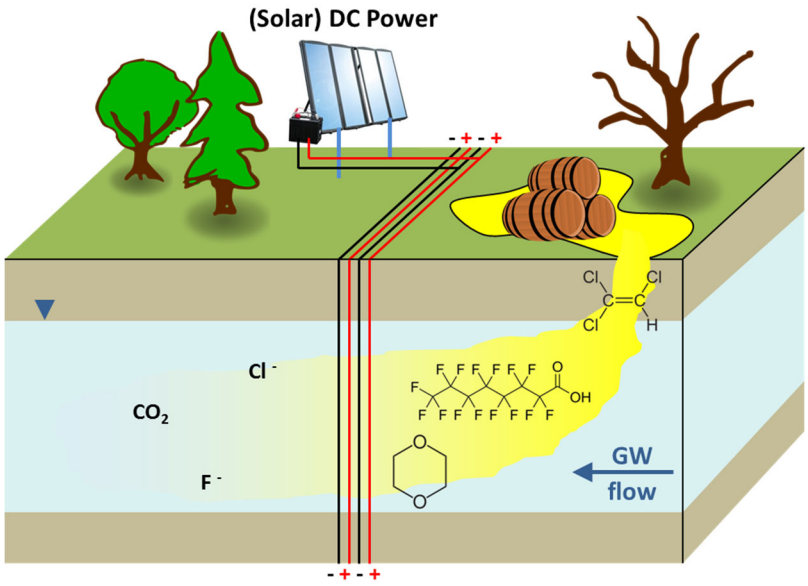

Figure 1: Conceptual design of an *in situ* electrolytic barrier.

2 BACKGROUND

1,4-Dioxane and PFASs are persistent organic pollutants (POPs) that are widespread due to their frequent use and resistance to many natural degradation processes. 1,4-Dioxane is a water-miscible chemical with low potential for adsorption to soil and therefore capable of rapid migration in groundwater.[1] Its physicochemical properties make 1,4-dioxane resistant to many of the traditional water treatment technologies like air stripping and sorption to activated carbon, and costly *ex situ* technologies involving ultraviolet light in combination with strong oxidants are often required to break it down.[2] U.S. state-specific drinking water criteria for 1,4-dioxane currently range from 0.25 to 50 µg/L, while groundwater criteria range from 0.3 to 200 µg/L.[3] PFASs are a highly complex group of anthropogenic chemicals comprising thousands of individual species,[4] and critical components of aqueous film-forming foams (AFFFs). PFASs may vary in functional group substitution, ionization state, chain length, degree of branching and other characteristics, but their perfluoroalkyl moiety provides a common chemical and thermal stability along with both hydrophobic and oleophobic properties.[5] In addition, polar and ionizable headgroups cause surface-active behavior.[6] While labile non-fluorinated moieties of PFASs are prone to partial abiotic and biotic transformation processes, the chemical and thermal stability of the perfluoroalkyl groups translates into an extraordinary recalcitrance in the environment.[7] The U.S. Environmental Protection Agency (EPA) recently established health advisory levels for PFOS and PFOA in drinking water of 70 ng/L, both separately and combined.[8]

Due to its application as stabilizing agent in chlorinated solvents, 1,4-dioxane frequently co-occurs with CVOCs such as 1,1,1-trichloroethane (1,1,1-TCA) and trichloroethene (TCE). While aerobic biodegradation of 1,4-dioxane has been shown to occur, the presence of CVOCs typically inhibits the responsible microorganisms.[9,10] Furthermore, the use of AFFFs in firefighting training has led to PFAS contamination of groundwater at DoD sites that are already contaminated with COCs such as 1,4-dioxane and TCE. Weathers et al. (2016)[11] showed that PFASs may inhibit reductive dechlorination of TCE by repressing *Dehalococcoides*. Thus, synergistic treatment approaches are critically needed to enable and enhance both chemical and biological degradation of mixed COCs.

Due to different physicochemical properties, biodegradability and inhibiting co-solvent interactions, complex treatment trains or harsh advanced oxidation processes are necessary to treat mixed contaminants. Owing to these processes' size or involvement of ultraviolet (UV) light, treatment typically has to occur *ex situ*, and thus presents an insurmountable cost challenge for the remediation of mixed groundwater plumes. Consequently, more cost-efficient treatment approaches are acutely needed that can (1) generate synergistic effects between treatment processes and (2) optionally be applied *in situ*.

In our previous work, we have gathered valuable insights in the implementation of electrochemical water treatment both *in situ*[12,13] and *ex situ*[14]. The final design of the e$^-$Barrier installed at Pueblo Chemical Depot for the treatment of energetic compounds (Figure 2, Figure 3, Sale et al. (2010)[13]) included a sequence of multiple active electrodes mounted on vinyl sheet pile sections. The total

width of the e$^-$Barrier was 35 feet and intercepted a 240 ft^2 section of the plume. The e$^-$Barrier was successfully operated for 770 days by a solar power supply.

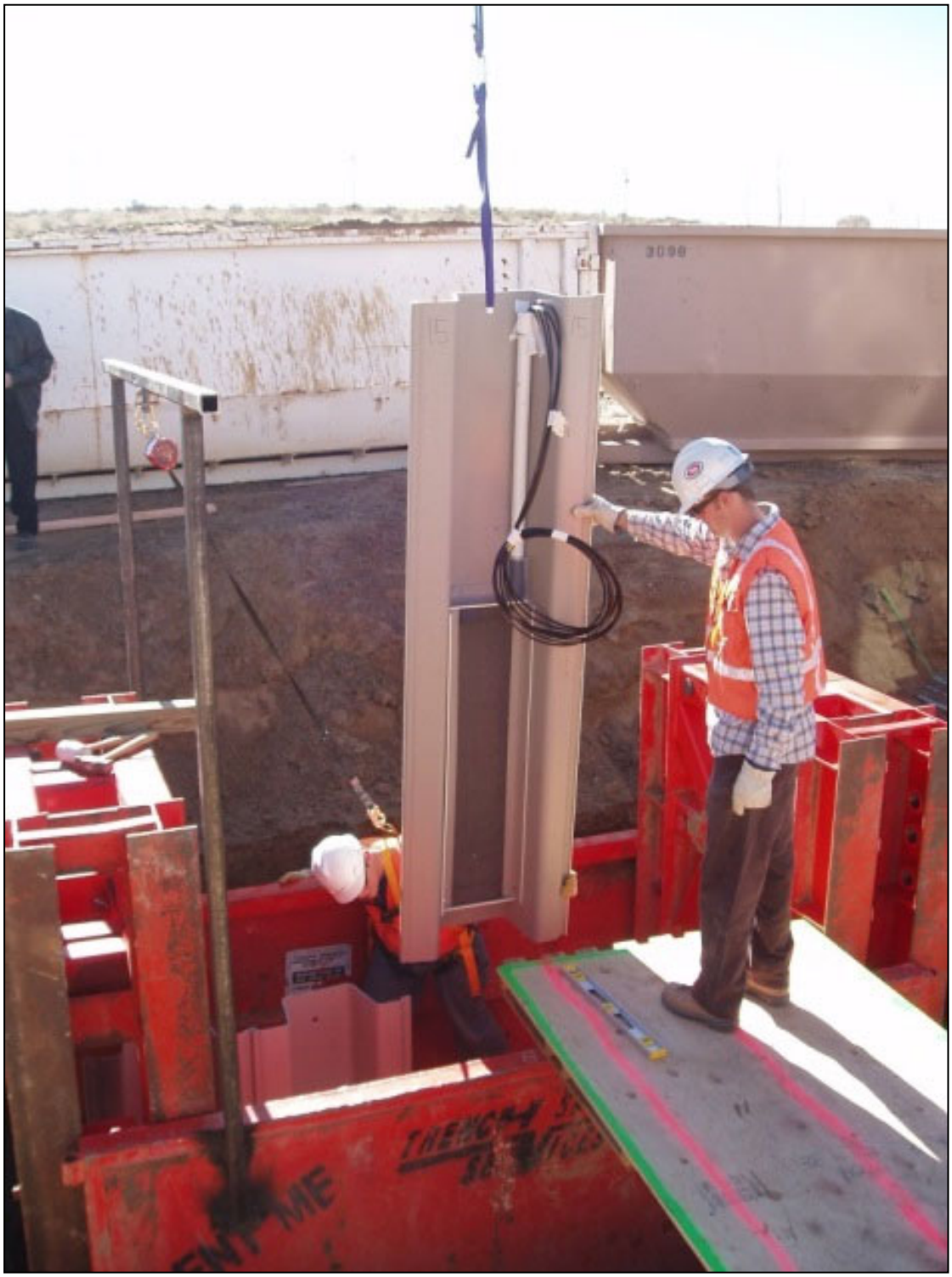

Figure 2: Installation of *in situ* e$^-$Barrier at Pueblo Chemical Depot.

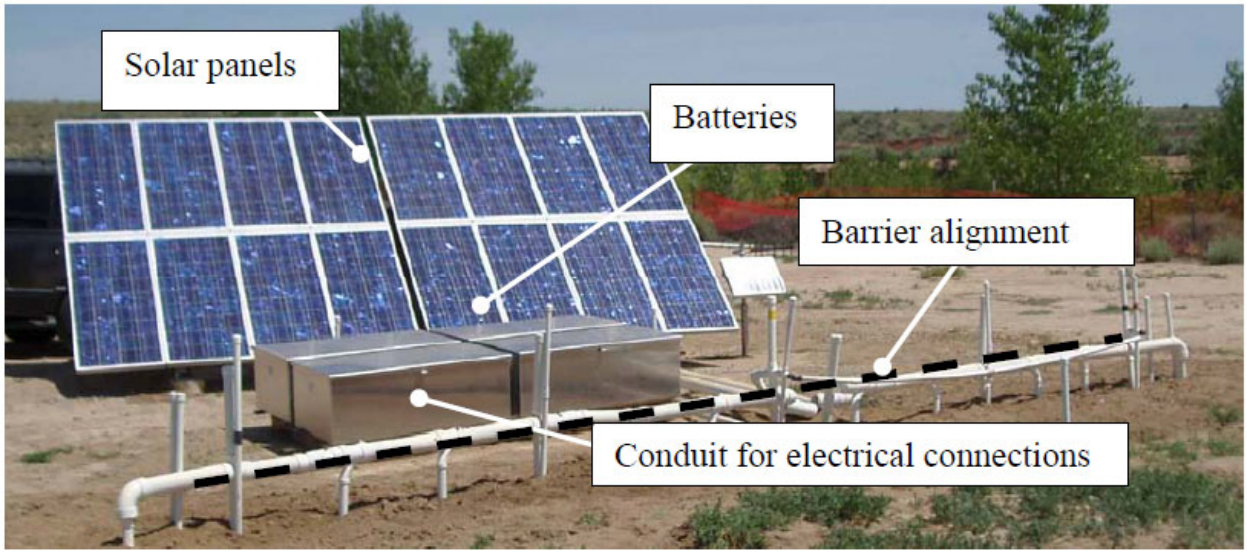

Figure 3: *In situ* e$^-$Barrier at Pueblo Chemical Depot including solar power supply.

Figure 4: Ti-MMO mesh electrode processed for flow-through column installation.

Our first-generation laboratory-scale studies on bioelectrochemical degradation of 1,4-dioxane using titanium - iridium/tantalum mixed metal oxide (Ti-MMO) electrodes (Figure 4) in bench-scale flow-through reactors had shown that concurrent stimulation of *Pseudonocardia dioxanivorans* CB1190 leads to an overadditive treatment effect by (1) providing O_2 to aerobic microorganisms via anodic oxidation of water and (2) concurrent degradation of inhibiting trichloroethene (TCE).[15] However, critical questions remained to be addressed on the path to field-scale installation regarding performance optimization, oxidation by-product formation, and sustainability. Furthermore, while mixed metal oxide electrodes have been shown to oxidize PFASs[16], other electrode materials such as boron-doped diamond (BDD) and Magnéli-phase titanium suboxides Ti_nO_{2n-1} were reported to be potentially more efficient.[17,18] Consequently, two critical steps were required before *in situ* electrochemical water treatment can be (cost-)effectively implemented at PFAS-impacted field sites: (1) the testing of dimensionally stable mesh electrode materials, and (2) the determination of optimum design and operational parameters to optimize synergistic treatment effects.

2.1 Literature References

1) Adamson, D. T.; Mahendra, S.; Walker, K. L.; Rauch, S. R.; Sengupta, S.; Newell, C. J. A. Multisite Survey to Identify the Scale of the 1,4-dioxane Problem at Contaminated Groundwater Sites. *Environ. Sci. Technol. Lett.* 2014, *1*, 254-258, DOI: 10.1021/ez500092u.

2) U.S. EPA. Treatment Technologies for 1,4-Dioxane: Fundamentals and Field Applications. Office of Solid Waste and Emergency Response (5203P). EPA-542-R-06-009. December 2006.

3) Broughton, A.; Sepulveda, A.; Foster, K.; Kruk, T.; Nickelsen, M. G.; Gillan, M.; Mohr, T. K. G. 1,4-Dioxane: Emerging technologies for an emerging contaminant. *Remediation* 2019, *29*, 49-63.

4) Barzen-Hanson, K. A., S. C. Roberts, S. Choyke, K. Oetjen, A. McAlees, N. Riddell, R. McCrindle, P. L. Ferguson, C. P. Higgins, and J. A. Field. 2017a. 'Discovery of 40 Classes of Per- and Polyfluoroalkyl Substances in Historical Aqueous Film-Forming Foams (AFFFs) and AFFF-Impacted Groundwater', *Environ Sci Technol*, 51: 2047-57.

5) Buck, Robert C, James Franklin, Urs Berger, Jason M Conder, Ian T Cousins, Pim De Voogt, Allan Astrup Jensen, Kurunthachalam Kannan, Scott A Mabury, and Stefan PJ van Leeuwen. 2011. 'Perfluoroalkyl and polyfluoroalkyl substances in the environment: terminology, classification, and origins', *Integrated Environmental Assessment and Management*, 7: 513-41.

6) Schaefer, Charles E, Veronika Culina, Dung Nguyen, and Jennifer Field. 2019. 'Uptake of Poly-and Perfluoroalkyl Substances at the Air–Water Interface', *Environmental Science & Technology*, 53: 12442-48.

7) Sharifan, H.; Bagheri, M.; Wang, D.; Burken, J.G.; Higgins, C.P.; Liang, Y.; Liu, J.; Schaefer, C.E.; Blotevogel, J. (2021): Fate and transport of per- and polyfluoroalkyl substances (PFASs) in the vadose zone. *Science of the Total Environment*, 771, 145427.

8) U.S. Environmental Protection Agency Office of Water (4304T) Health and Ecological Criteria Division Washington, Drinking Water Health Advisory for Perfluorooctanoic Acid (PFOA), DC 20460, 2016. https://www.epa.gov/sites/default/files/2016-05/documents/pfoa_health_advisory_final-plain.pdf.

9) Hand, S.; Wang, B.; Chu, K.-H. Biodegradation of 1,4-dioxane: Effects of enzyme inducers and trichloroethylene. *Sci. Total Environ.* 2015, 520, 154–159.

10) Mahendra, S.; Grostern, A.; Alvarez-Cohen, L. The Impact of Chlorinated Solvent Co-contaminants on the Biodegradation Kinetics of 1,4-Dioxane. *Chemosphere* 2013, 91, 88-92.

11) Weathers, T.S.; Harding-Marjanovic, K.C.; Higgins, C.P.; Alvarez-Cohen, L.; Sharp, J.O. Perfluoroalkyl acids inhibit reductive dechlorination of trichloroethene by repressing *Dehalococcoides*. *Environ. Sci. Technol.* 2016, 50, 240-248.

12) Sale, T.; Gilbert, D. Electronically Induced Redox Barriers for Treatment of Groundwater: Cost & Performance Report. Final Report ESTCP ER-0112, Oct 2006.

13) Sale, T.; Olson, M.; Gilbert, D.; Petersen, M. Field Demonstration/Validation of Electrolytic Barriers for Energetic Compounds at Pueblo Chemical Depot. Final Report ESTCP ER-0519, Jan 2010.

14) Blotevogel, J.; Pijls, C.; Scheffer, B.; de Waele, J.P.; Lee, A.; van Poecke, R.; van Belzen, N.; Staal, W. Pilot-Scale Electrochemical Treatment of a 1,4-Dioxane Source Zone. *Groundwater Monitoring & Remediation*. 2019, *39*, 36-42.

15) Jasmann, J.R.; Gedalanga, P.B.; Borch, T.; Mahendra, S.; Blotevogel, J. Synergistic Treatment of Mixed 1,4-Dioxane and Chlorinated Solvent Contaminations by Coupling Electrochemical Oxidation with Aerobic Biodegradation. *Environ. Sci. Technol.* 2017, 51, 12619–12629.

16) Schaefer, C.E.; Andaya, C.; Urtiaga, A.; McKenzie, E.R.; Higgins, C.P. Electrochemical treatment of perfluorooctanoic acid (PFOA) and perfluorooctane sulfonic acid (PFOS) in groundwater impacted by aqueous film forming foams (AFFFs). *J. Hazard. Mater.* 2015, 295, 170-175.

17) Wang, Y.; Pierce, R.; Shi, H.; Li, C.; Huang, Q. Electrochemical degradation of perfluoroalkyl acids by titanium suboxide anodes. *Environ. Sci. Water Res. Technol.* 2020, 6, 144–152.

18) Le, T.X.H.; Haflich, H.; Shah, A.D.; Chaplin, B.P. Energy-Efficient Electrochemical Oxidation of Perfluoroalkyl Substances Using a Ti_4O_7 Reactive Electrochemical Membrane Anode. *Environ. Sci. Technol. Lett.* 2019, 6, 504–510.

3 BIOELECTROCHEMICAL TREATMENT OF MIXED 1,4-DIOXANE AND CVOC CONTAMINATIONS

3.1 Introduction

1,4-Dioxane (1,4-D) is a synthetic industrial chemical that has been frequently detected in groundwater and industrial wastewater. Due to its widespread use as solvent stabilizer, it often co-occurs with chlorinated volatile organic compounds (CVOCs) such as 1,1-dichloroethene (1,1-DCE), trichloroethane (TCA), and trichloroethene (TCE).[1] The U.S. Environmental Protection Agency has classified 1,4-dioxane as "likely to be carcinogenic to humans" by all routes of exposure.[2] In the U.S., state-specific drinking water criteria for 1,4-dioxane currently range from 0.25 to 50 µg/L, while groundwater criteria range from 0.3 to 200 µg/L.[3] It is estimated that more than 20% of U.S. water bodies have been contaminated with 1,4-dioxane at concentrations exceeding 0.35 µg/L, and in some instances concentrations in groundwater and industrial wastewater may be as high as tens or hundreds of mg/L.[1,4-7]

In the environment, 1,4-dioxane has shown remarkable recalcitrance to natural biological and chemical attenuation processes, and has proven challenging to be removed by traditional water treatment approaches. Generally, strong oxidants are needed to activate the diether ring.[5-9] Several studies have demonstrated that advanced oxidation processes (AOPs) such as H_2O_2, plasma, UV, peroxymonosulfate, and ozone treatment are effective in generating reactive oxygen species (ROS) to degrade 1,4-dioxane.[10-27] Electrochemical oxidation has emerged as a promising technology to remove persistent organic pollutants[28-32] because it is cost-competitive with other AOPs[33] and can be implemented for *in situ* groundwater treatment by using mesh electrodes.[34-35] Indirect oxidation through generated ROS such as $^{\cdot}OH$ and direct electron transfer were shown as the main degradation mechanism of this technology.[36] However, despite the effectiveness of electrochemical oxidation processes, high capital costs and considerable energy consumption have thus far deferred field-scale applications.

Biological degradation of 1,4-dioxane has been studied as an alternative remedial strategy to treat contaminated water bodies. Laboratory-scale studies have demonstrated metabolic and co-metabolic pathways for 1,4-dioxane under aerobic conditions for instance by *Pseudonocardia dioxanivorans* CB1190 (referred to as "CB1190" hereafter), *Mycobacterium sp.* PH-06, *Pseudonocardia sp.* ENV478, *Methylosinus trichosporium* OB3b, *Mycobacterium austroafricanum* JOB5, and *Rhodococcus ruber* ENV425.[37-46] However, in both metabolic and co-metabolic degradation of 1,4-dioxane, it has been proven challenging to reduce 1,4-dioxane concentrations to sub-ppb regulatory limits for *in situ* application of bioremediation either due to dependency on 1,4-dioxane as the only carbon source or lack of sufficient primary substrates.[47-48] Furthermore, it is well-documented that the presence of CVOCs significantly inhibits 1,4-dioxane degrading microorganisms due to delayed ATP production as well as down-regulation of both 1,4-dioxane monooxygenase (*dxmB*) and aldehyde dehydrogenase (*aldH*) genes.[46,49] Consequently, the lack of oxygen and the presence of chlorinated co-contaminants limit the effectiveness of biodegradation as the sole water treatment strategy.

Recently, we coupled electrochemical with biological oxidation by CB1190, a microaerophilic bacterium that can grow on 1,4-dioxane as its sole electron donor and carbon source, to degrade 1,4-dioxane in contaminated water.[31] However, this limited proof-of-principle study employed only one pair of electrodes, did not allow for spatial sampling and thus determination of degradation kinetics along the column, and assessed a relatively weak inhibitor compound (TCE). Thus, more detailed investigations are critically needed on the technology's path toward scale-up for field application.

In this study, we designed a 2nd generation bioelectrochemical flow-through reactor with the objectives (1) to optimize process performance, (2) to obtain a thorough understanding of bioelectrochemical oxidation by CB1190 based on parameters critical for future scale-up and application in real-world contamination management, and (3) to consider the sustainability of this technology based on material usage and energy footprint. As model CVOC, we chose 1,1-DCE to challenge the process with worst-case conditions as 1,1-DCE has shown the highest inhibition effect on 1,4-dioxane biodegradation by CB1190.[46,49] Finally, we characterized the reactor effluent for disinfection by-products (DBPs) and toxicity to obtain a holistic evaluation of bioelectrochemical oxidation systems as effective treatment for 1,4-dioxane-contaminated water.

3.2 Materials and Methods

3.2.1 Chemicals

1,4-Dioxane (99.5%, Fisher Scientific), 1,1-DCE (99.5%, Alfa Aesar), vinyl chloride (99%, Restek), chloromethane, chloroform and carbon tetrachloride (99.99%, Restek) were used for calibration standards and/or in influent contaminant mixtures. Dichloromethane and toluene (99.96%, OmniSolv Millipore EMD) were used as extraction solvents. 1,4-Dioxane-d_8 (99% and 99 atom %D, Sigma-Aldrich) was used for isotopic dilution quantitation.

3.2.2 Sterilization and disinfection protocol

All reactor components such as tubing, valves, reactor body (polyvinyl chloride, PVC) were disinfected by soaking in 70% ethanol overnight. The feed water tank and all glassware were autoclaved at 121 °C for ≥60 minutes. Acid-washed sand was heat-sterilized at 450 °C overnight and then autoclaved at 121 °C for ≥60 minutes.

3.2.3 Flow-through column reactors

89 cm-long reactors were built using 10-cm diameter clear PVC pipe (Figure 5). Three dimensionally stable, disc-shaped pairs of mesh electrodes (1.0 mm thick with 1.0 × 2.8 mm openings) were installed at 15 cm distance to leave sufficient space for biodegradation processes, designed based on our previous observations that the highest cell abundance in bioelectrochemical columns was ~10 cm downstream of the trailing cathode.[31] The mesh anodes were doped tin oxide-coated titanium (Ti/SnO_2-X; Optima™ IRSA, Evoqua Water Technologies). Doped tin oxide coatings have substantially lower cost compared to boron-doped diamond, faster oxidation kinetics compared to many other metal oxide-based coatings such as RuO_2 and Ta_2O_5, and a long service life.[28,50-51] The mesh cathodes were Ti/IrO_2-Ta_2O_5 (ELGARD™, Corrpro).[30-31] Six liquid sampling

ports and five solid sampling ports were distributed throughout the reactors. The reactors were equipped with seven gas vents along the reactor to collect generated gasses in a 20-L Tedlar® bag. The columns were packed with sterilized or inoculated 8-12 mesh quartz silica sand for abiotic and biotic experiments, respectively.

3.2.4 Bioelectrochemical experiments

(Bio)electrochemical oxidation was studied at two applied cell potentials of 3 and 6 volts, resulting in anode potentials of 2.2 V versus standard hydrogen electrode (SHE) and 5.0 V vs. SHE, respectively, as measured with a Dri-Ref 5 reference electrode (World Precision Instruments, Inc.). We note that a high anode potential likely prevents direct attachment of microorganisms, and bioelectrochemical processes occur spatially separated with electrolytically generated O_2 as electron transfer mediator. A biological control experiment was run with inoculated sand and no potential applied to the electrodes.

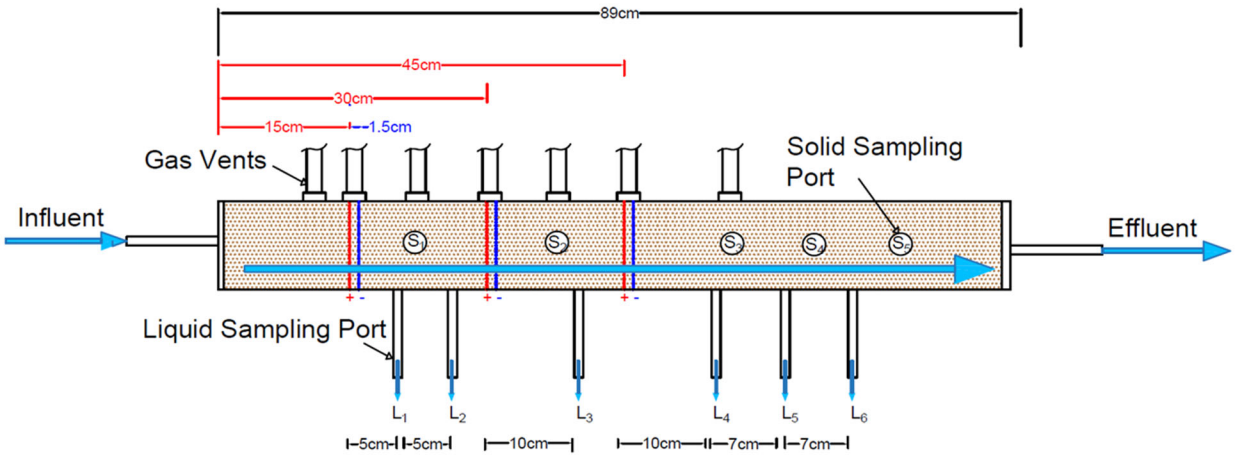

Figure 5: Schematic of the flow-through bioelectrochemical reactors. The red and blue vertical lines represent the locations of the mesh anodes and cathodes, respectively. Additional sampling ports for liquid samples were present at both inlet and outlet of the column reactors.

In all biotic experiments, sterilized sand was inoculated with CB1190 in 3 L ammonium mineral salt (AMS) medium[44] with 100 to 500 mg/L 1,4-dioxane for >6 days after the 1,4-dioxane biodegradation rate had reached 200 $mg \cdot L^{-1} \cdot d^{-1}$. In the case of combined biological and electrochemical oxidation, the power supply was turned on once the column had been packed with inoculated sand.

The influent solution was made in 20-L batches and contained AMS medium (Table 1) spiked with 100 mg/L of 1,4-dioxane and 5 mg/L of 1,1-DCE for co-contaminant experiments. The chosen 1,4-dioxane concentration is higher than found at many contaminated sites, though not uncommon.[1,4-7,52] Also, when used as solvent stabilizer, 1,4-dioxane concentrations are typically lower than those of co-occurring chlorinated solvents. However, at many sites, 1,4-dioxane and

chlorinated solvents were released independently.[52] We chose these rather high concentrations to demonstrate the effectiveness of our process over a large range of concentrations, so that at an advanced stage of treatment the removal performance could still be evaluated for waters with low 1,4-dioxane and chlorinated solvent concentrations. Prior to adding the contaminants, the solution was purged with nitrogen gas for several hours to lower the dissolved oxygen (DO) concentration to below 2 mg/L. The carboys were then connected to a 20-L Tedlar® bag filled with nitrogen gas to maintain constant headspace pressure with decreasing water levels.

Table 1: Composition of stock A and trace element solutions.

Stock A	5.0	g/L	Fe-Na EDTA
	2.0	g/L	$NaMoO_4 \cdot 2H_2O$
Trace Elements Stock	0.5	g/L	$FeSO_4 \cdot 7H_2O$
	0.4	g/L	$ZnSO_4 \cdot 7H_2O$
	0.02	g/L	$MnSO_4 \cdot H_2O$
	0.015	g/L	H_3BO_3
	0.01	g/L	$NiCl_2 \cdot 6H_2O$
	0.25	g/L	EDTA
	0.05	g/L	$CoCl_2 \cdot 6H_2O$
	0.005	g/L	$CuCl_2 \cdot 2H_2O$

All experiments were run at 43 cm/d seepage velocity simulating groundwater flow conditions, and ambient temperature in the dark. To eliminate physical losses of 1,4-dioxane and 1,1-DCE in the experiments, the power supply was turned on after influent and effluent concentrations were equal (eliminating sorption/volatilization effects and serving as abiotic no-voltage control). Performance data were collected after the system had reached steady-state effluent 1,4-dioxane concentrations.

An activated C18 solid-phase extraction (SPE) cartridge (Maxi Clean 500 mg) was used to collect volatile organics, and 1 mL of HPLC-grade toluene was used to extract the volatiles for gas chromatography analysis. C18 cartridges were preconditioned by eluting with 5 mL of toluene, followed by 5 mL of air, and let dry overnight.

A minimum of three complete sampling rounds were performed. 1,4-Dioxane, 1,1-DCE, and DBPs were measured throughout the column. Oxidation-reduction potential (ORP), pH and dissolved oxygen (DO) were measured throughout the column using an OAKLON PC450, pH strips (PANPEHA), and DO meter (Hach HQ 40d) and probe (Hach LOD101), respectively. Measurements of pH were taken in triplicate, while DO and ORP measurements were only performed on the last sample under steady-state conditions before ending the experiment due to larger sample volume requirements. Aqueous samples were filtered using 0.2-µm nylon syringe filters (VWR International) and extracted into dichloromethane for analysis of 1,4-dioxane, 1,1-DCE, and organic DBPs. Voltage and current were measured daily using a Fluke digital multimeter (Global Test Supply, USA). At the end of each experiment, solid and liquid samples were taken

and sent overnight on dry ice to the University of California, Los Angeles (UCLA) for nucleic acids extraction, quantitative polymerase chain reaction (qPCR) analysis, and toxicity tests.

To assess the energy requirements of (bio)electrochemical treatment, the electric energy per order of magnitude of 1,4-dioxane removed (E_{EO}) was calculated:[32]

$$E_{EO}\left(\frac{kWh}{m^3}\right) = \frac{P\,t}{V\,log\left(\frac{C_0}{C_t}\right)} \quad (2)$$

where P is power (kW), t is treatment time (h), V is the water volume (m^3), and C_0 and C_t are initial and final 1,4-dioxane concentrations, respectively. The anode surface area per order of 1,4-dioxane removed (ASA_O) was determined based on Pica et al. (2019):[53]

$$ASA_O\left(\frac{m^2h}{m^3}\right) = \frac{A\,t}{V\,log\left(\frac{C_0}{C_t}\right)} \quad (3)$$

where A is anode area (m^2).

3.2.5 Chemical analyses

An Agilent 6890N gas chromatograph (GC) coupled with Agilent 5973N mass spectrometer (MS) was used to measure 1,4-dioxane and CVOCs. For 1,4-dioxane, injections of 1 µL were made using a 4:1 split flow ratio and an inlet temperature of 250°C. The column was Restek Rxi-624Sil MS mid-polarity (30 m * 0.25 mm ID * 1.4 µm df). The Helium carrier gas was set to constant flow at 2.0 mL/min. The initial oven temperature was set at 40 °C for 2 min, then ramped at 8 °C/min to 100 °C, followed by an additional ramp of 40 °C to 160 °C and held for 1 min. Isotopic dilution calibration was used to quantify 1,4 dioxane in all experiments, using 1,4 dioxane-d_8 as the internal standard to correct for any losses during sample preparation and/or instrument response. The MS was programmed to scan for *m/z* 58 and 88 (1,4-dioxane) as well as *m/z* of 64 and 96 (deuterated 1,4-dioxane) at 6 to 8 min after injection. Further details on analytical methods can be found in ref. 31. The limit of detection (LOD) for 1,4-dioxane was 3 µg/L.

For chlorinated methane and ethenes, the initial oven temperature was set at 40 °C for 2 min, then ramped at 8 °C/min to 100 °C, followed by an additional ramp of 40 °C to 160 °C and held for 1 min. The MS was programmed to scan for *m/z* 50 and 52 (chloromethane) in segment 1, and 62 and 64 (vinyl chloride) in segment 2 from 1.0 to 3.0 min after injection. Segment 3 was set to scan for *m/z* 61 and 96 (1,1-DCE). In segment 4, *m/z* of 49 and 84 were scanned to analyze for dichloromethane (DCM). *m/z* of 83 and 85 were scanned for chloroform in segment 5, and segment 6 was set to scan for *m/z* of 117 and 119 (carbon tetrachloride, CT). Each ion was assigned a dwell time of 100 µs. Quantification with GC/MS(SIM) for all chlorinated compounds was performed using external calibration standards. The LODs for chloromethane, vinyl chloride, 1,1-DCE, DCM, chloroform, and CT were 92, 72, 209, 76, 328, and 13 µg/L, respectively.

Ion chromatography on a Dionex DX-1500 was used to quantify chloride, chlorate and perchlorate. The columns were a Dionex™ IonPac™ AS16 (250 m x 4.0 mm ID) with an IonPac™ AG16 Guard Column (4 x 50 mm).

3.2.6 Bacterial strain and culture conditions

Pseudonocardia dioxanivorans strain CB1190 was cultured by a 10% (v/v) dilution from an actively grown pure culture. CB1190 was grown aerobically in AMS media and sequentially cultured by 10% (v/v) dilution into larger volumes so that ultimately 6 L of pure culture stock was prepared for sand inoculation. 1,4-dioxane served as the sole carbon source during the culturing process at concentrations between 100 and 500 mg/L. The culture was incubated at 30 °C with constant agitation at 150 rpm. To assess CB1190 growth, ATP and 1,4-dioxane concentration were monitored daily. To track ATP, luminescence analysis (BioTekSynergy HT) was completed within 2 h of sampling using Promega BacTiter-Glo Microbial Cell Viability Assay following Promega Technical Bulletin #TB337 and Protocol for Measuring ATP from Bacteria Bulletin.

3.2.7 Total nucleic acids extraction and quantitative polymerase chain reaction (qPCR)

qPCR was used to quantify both total bacterial 16S rRNA gene and a 1,4-dioxane biodegradation biomarker, dioxane monooxygenase (DXMO) gene (*dxmB*). Total nucleic acids were extracted using a modified phenol/chloroform/isoamyl alcohol method as described in ref. 37. Universal 16S rRNA gene was amplified to quantify total biomass, and the CB1190-like 16S rRNA gene was used to quantify the abundance of the 1,4-dioxane metabolizer *Pseudonocardia dioxanivorans* CB1190 or closely related bacteria. All reactions were run on a StepOnePlus thermocycler (Life Technologies, Carlsbad, CA) using a total volume of 20 µL containing 10 µL 2 × Luminaris Color HiGreen-HiROX qPCR Master Mix (Thermo Scientific, Waltham, MA), 0.3 mM primers (Table S2), and 2 µL of DNA (1-10 ng/µL) template. The cycling parameters to amplify the gene fragment started with holding at 50 °C for 2 min and 95 °C for 10 min, followed by 40 cycles of 95 °C for 15 s and annealing at respective temperatures for 45 s. All reactions were accompanied by a melt-curve analysis to confirm the specificity of quantitative polymerase chain reaction products. Melt-curve analyses 81.5-83.6 °C were considered specific to target genes. Details of the method can be found in Table 2 and in ref. 31.

3.2.8 Cytotoxicity assay

Cytotoxicity of the experimental column effluent was determined by conducting an adenosine triphosphate (ATP) assay using BacTiter-Glo Microbial Cell Viability Assay kit (Promega). The assays work on the basis of enzymatic reactions emitting luminescence when the assay reagent is reacted with ATP molecules, which are directly proportional to the amount of ATP present in the cell sample used, and can provide insight into the toxic effect of the effluent samples in question.[46] Column effluent sample toxicity was assessed by combining 1-part CB1190 culture suspension to 9-parts column effluent in snap cap tubes for a total volume of 1 mL and left to incubate for 4 hours. Each column effluent sample was tested in duplicate. Following incubation, 50 µL of sample were mixed with 50 µL of BacTiter-Glo Reagent in white flat-bottom 96-well plates and incubated for 5 min in the dark at ambient temperature. These samples were then measured in a spectrophotometer using a 600 nm to measure luminescence specifically.

Table 2: Primer sequences and annealing temperatures.

Gene	For-Primer (5'→ 3')	Rev-Primer (5'→ 3')	Annealing temperature (°C)
Universal 16S rRNA	ATGGCTGTCGTCAGCT	ACGGGCGGTGTGTAC	45
CB1190-like 16S rRNA	ACGGTCTCGCAGCCCTCTGT	AGCGGGTTATGCCGGGGACT	60
***dxmB*/dioxane monooxygenase (DXMO)**	CCAAACGGGCGTCAGTCAT	AGAACGTGCGCTCCCAAAG	60
***aldH*/aldehyde dehydrogenase (ALDH)**	ACCAAGGACCTCACCTCGTA	AACGGATGCGCGTTGTTC	60

3.2.9 Statistical analysis

Principal component analysis (PCA) was computed with "vegan" packages in RStudio to further explore the multivariate variation among reactors in terms of effluent variables.

3.3 Results and Discussion

3.3.1 Operational parameters

DO, ORP, and pH were measured to understand the impacts of electrolysis on water quality and bacterial growth. After N_2-purging, DO concentrations in the influent tank were generally <2.0 mg/L. As a result of anodic water oxidation, DO levels increased within the reactive area of the reactors (i.e., inter-electrode space between the 1st and 3rd pair of electrodes) in all electrochemical experiments (Figure 6). As expected, the increases in DO were more pronounced at the higher anode potential, with the highest concentration recorded at 18 mg/L in the non-augmented reactor at 5.0 V in the absence of co-contaminant. A similar trend was observed for ORP (Figure 7), where elevated potentials close to the electrodes indicated a reactive zone favorable for 1,4-dioxane oxidation. Bulk pH (Figure 8) remained circumneutral within the optimum growth range of 5.0 < pH < 8.5 for CB1190[46,54] under all experimental conditions.

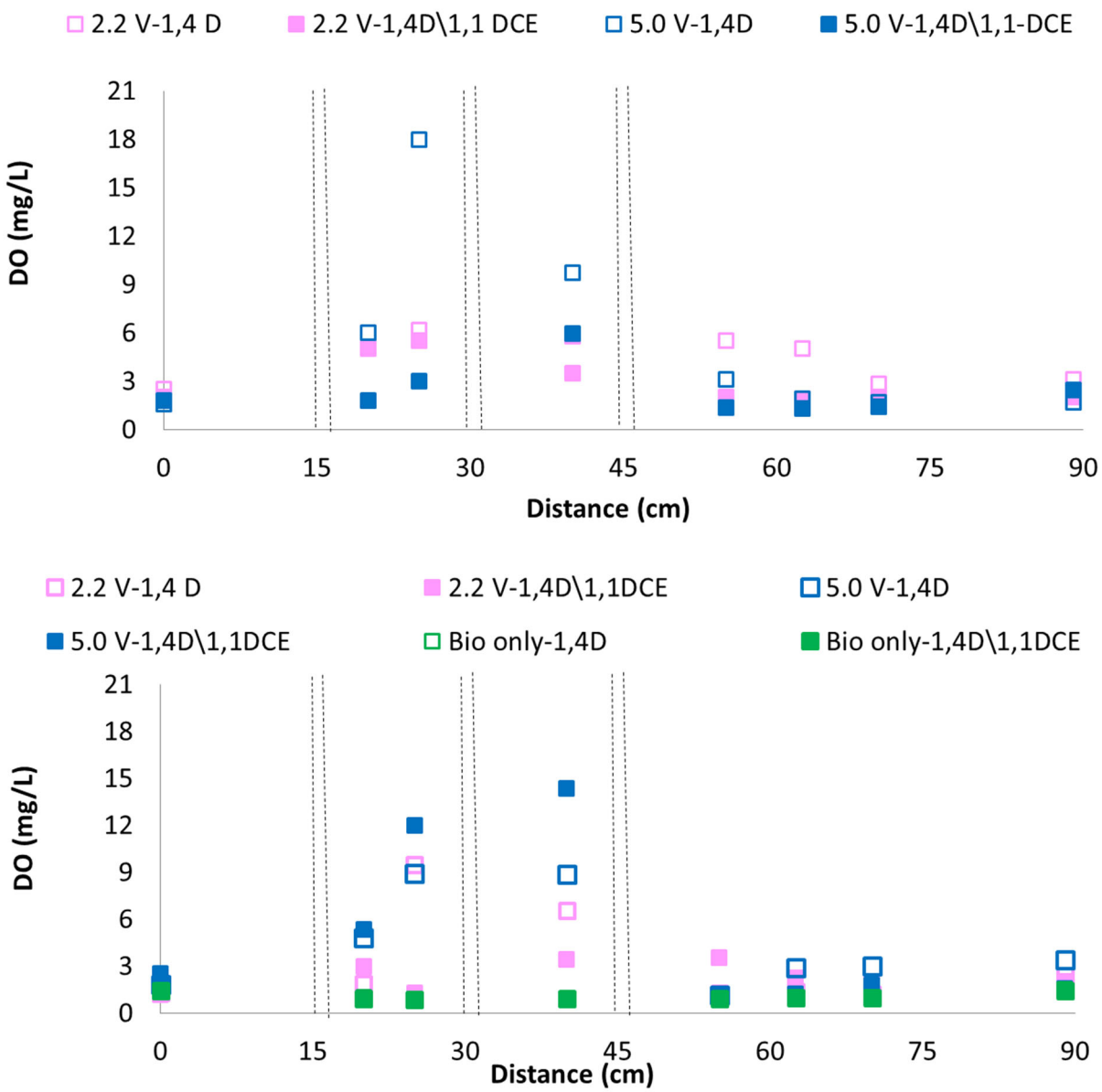

Figure 6: Profiles of dissolved oxygen (DO) throughout the reactors under abiotic (top) and bioaugmented conditions (bottom). The vertical dashed lines indicate the location of the electrodes. Pink markers represent 2.2 V, blue represent 5.0 V, and green markers show the biological control experiment at 0 V anode potential. Open markers represent the absence of 1,1-DCE while solid markers represent the presence of 1,1-DCE.

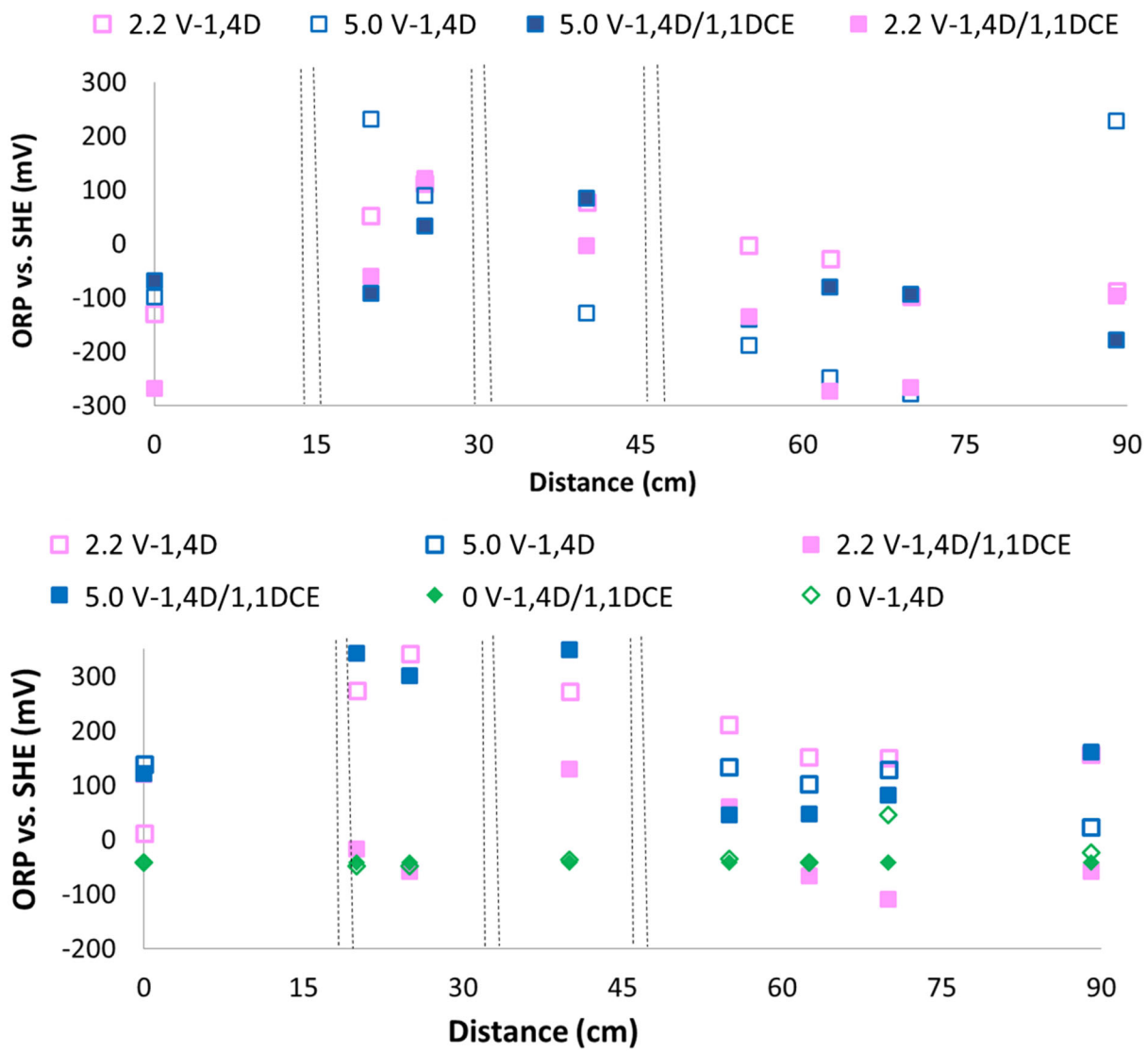

Figure 7: Profiles of bulk ORP throughout the reactors under abiotic (top) and bioaugmented conditions (bottom). The vertical dashed lines indicate the location of electrodes. Pink markers represent 2.2 V, blue represent 5.0 V, and green markers show the biological control experiment at 0 V. Open markers represent the absence of 1,1-DCE while solid markers represent the presence of 1,1-DCE.

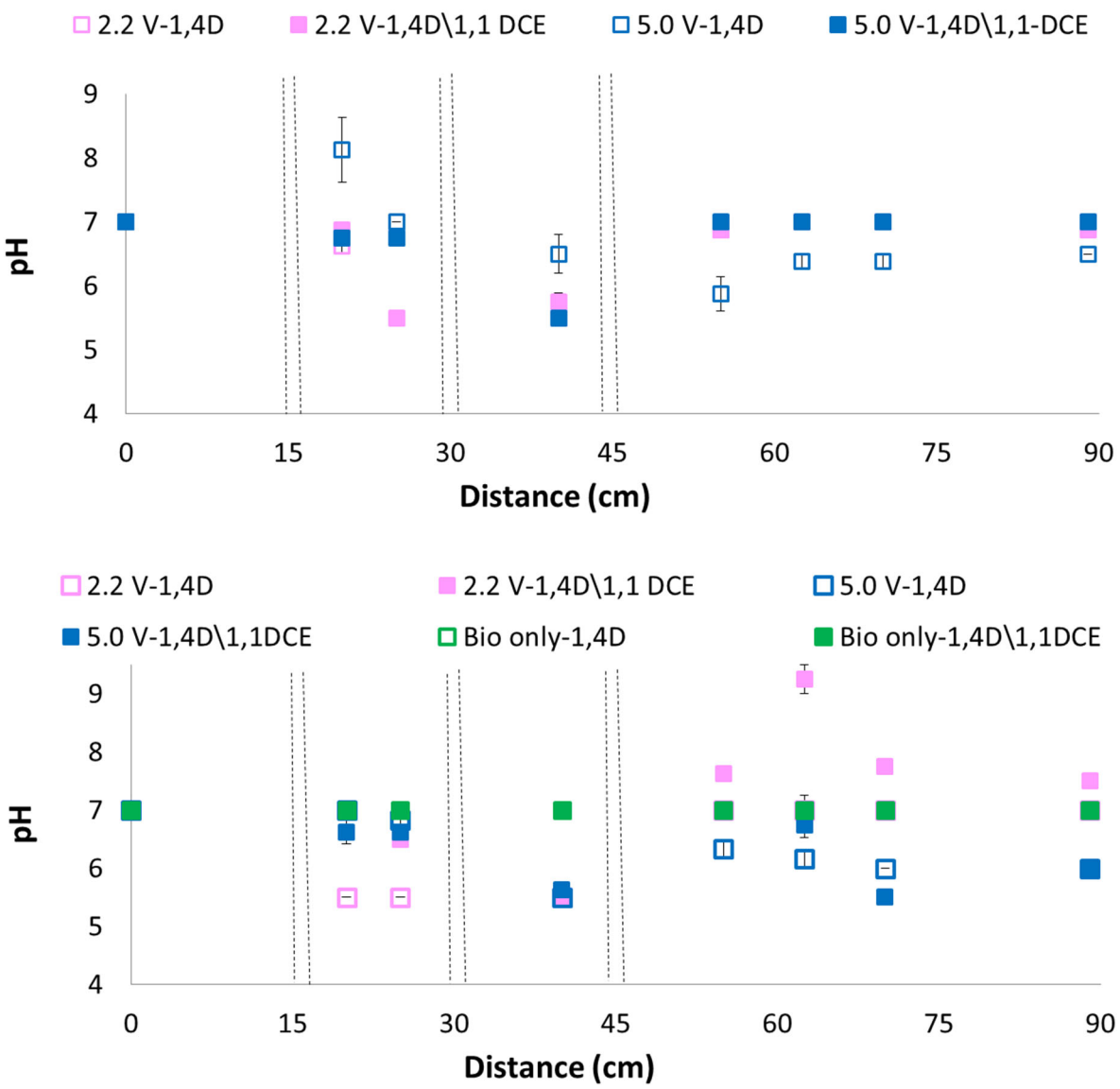

Figure 8: Profiles of pH throughout the reactors under abiotic (top) and bioaugmented conditions (bottom). The vertical dashed lines indicate the location of electrodes. Pink markers represent 2.2 V, blue represent 5.0 V, and green markers show the biological control experiment at 0 V. Open markers represent the absence of 1,1-DCE while solid markers represent the presence of 1,1-DCE.

3.3.2 1,4-Dioxane removal

The removal of 1,4-dioxane during electrochemical and bioelectrochemical treatment throughout the column reactors is shown in Figure 9. During the non-augmented run at 2.2 V anode potential, only 4% of 1,4-dioxane removal was observed, similar to the low removal reported at the same cell potential for Ti/IrO_2-Ta_2O_5 anodes.[31] At 3 V applied cell potential, the measured anode

potential of 2.2 V was only slightly above the oxygen evolution potential for doped tin oxide electrodes of ~1.9 V.[55-56]

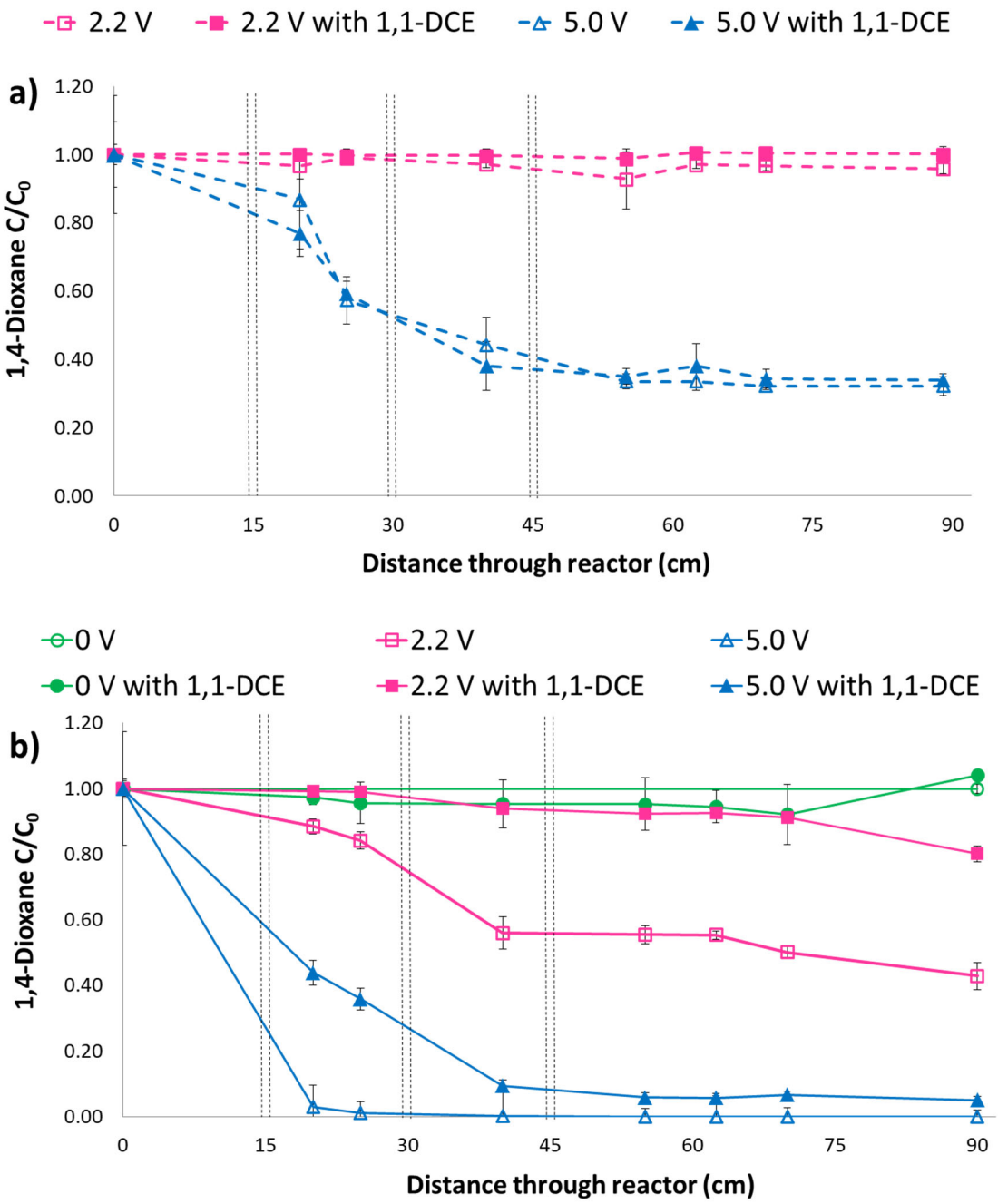

Figure 9: 1,4-Dioxane removal for electrochemical (a) and bioelectrochemical (b) treatment in the presence and absence of 1,1-DCE. The dashed lines represent abiotic conditions, whereas the solid lines illustrate the presence of CB1190. Open markers represent absence, solid markers show the presence of the co-contaminant 1,1-DCE in the feed water. The vertical dashed lines indicate the location of (leading) anode and (trailing) cathode pairs.

At the higher anode potential of 5.0 V, 1,4-dioxane concentrations decreased more rapidly. At the end of the electrochemically reactive zone (i.e., past the third electrode pair at 55 cm), 66% of 1,4-dioxane had been removed, reducing the 1,4-dioxane concentration from 98.1 mg/L to 32.9 mg/L. At the end of the column (89 cm), total 1,4-dioxane removal reached 68%, negligibly greater than right past the third electrode pair, indicating that electrochemical oxidation was only operative in the direct vicinity of the electrodes. The increase in 1,4-dioxane removal rate with increasing anode potential and current under the same flow (i.e., mass transfer) regime indicates current-limited conditions.[55] Since 1,4-dioxane is readily oxidized by hydroxyl radicals,[30] whose generation increases with increasing current,[57] the low removal rates can be attributed to low generation of ROS at the lower anode potential.[4]

No detection of 1,4-dioxane in the gas-phase samples and minor 1,4-dioxane removal in the 2.2 V experiments support the conclusion that 1,4-dioxane was oxidized and transformed by ROS, and that other removal mechanisms such as sorption, photolysis and volatilization did not contribute to the overall removal, in agreement with a low reported sorption affinity and Henry constant.[46]

To assess and harness the synergy between biological and electrochemical oxidation, the column reactors were inoculated with CB1190. In the biological control experiment at 0 V applied, no removal of 1,4-dioxane was observed, again ruling out sorption, photolysis and volatilization as loss mechanisms, as well as anaerobic degradation. The DO concentration below 2 mg/L proved insufficient for the microaerophilic CB1190 to biodegrade 1,4-dioxane during the 2-day residence time in the reactors. At 2.2 V, 45% of 1,4-dioxane was removed within the electrochemically active zone, concurrent with the observed increases in DO and ORP. Removal increased to 57% by the end of column (89 cm). This removal beyond the electrochemically active area of the column indicated continuing 1,4-dioxane biodegradation by CB1190, inferring the effectiveness of a polishing zone in the reactor design. The anode surface area-normalized 1,4-dioxane degradation rate r_{ASA} (103 $mg \cdot h^{-1} \cdot m^{-2}$) was 12 times higher during bioelectrochemical treatment at 2.2 V compared to electrochemical treatment only (9 $mg \cdot h^{-1} \cdot m^{-2}$), illustrating the synergistic effects of this technology.

At 5.0 V, the bioelectrochemical 1,4-dioxane degradation rate r_{ASA} further increased to 774 $mg \cdot h^{-1} \cdot m^{-2}$, five times higher than during electrochemical treatment at 5.0 V (168 $mg \cdot h^{-1} \cdot m^{-2}$), and equally five times higher than the highest bioelectrochemical rate achieved in our 1st generation reactor.[31] Furthermore, the bioelectrochemical degradation rate was eight times higher at 5.0 V compared to 2.2 V applied. The highly variable DO concentrations in the (abiotic) electrochemical experiments at 2.2 V and 5.0 V (Figure 6) do not clearly support higher DO availability as the cause of this observation. It is also possible that the increased electrochemical transformation of 1,4-dioxane at 5.0 V led to the generation of more readily biodegradable oxidation intermediates that provided higher energy yields for the bacteria, especially at low 1,4-dioxane concentrations. Electrochemical oxidation of 1,4-dioxane generates intermediate ring opening products such as diethylene glycol, ethylene glycol diformate, and various organic acids including glycolate before

being fully mineralized.[4,30] Glycolate is a central intermediate of 1,4-dioxane degradation by CB1190 and readily supports its growth.[38,54]

Overall, bioelectrochemical oxidation at 5.0 V applied achieved a reduction in 1,4-dioxane concentration from 100,000 µg/L in the influent to an average effluent concentration of 53 µg/L. We emphasize that two of the three effluent replicate 1,4-dioxane measurements were below our method detection limit of 3 µg/L. Small variations in effluent concentrations may arise from temporary preferential flow paths in the porous media, for instance generated by evolving gas bubbles.

3.3.3 1,1-DCE inhibition and removal

As CVOCs often co-occur with 1,4-dioxane and inhibit its degradation,[4,31,46,49] it was critical to assess the fate and impact of 1,1-DCE in the column experiments. Figure 10 depicts 1,1-DCE normalized concentrations throughout the column reactors under the five experimental conditions tested. In the biological control column at 0 V applied, 1,1-DCE concentrations decreased slightly by 20%, which can be attributed to sorption or volatilization losses, although no 1,1-DCE was detected on the SPE cartridges connected to the gas vents. At 2.2 V, 80% of 1,1-DCE was removed after the first electrode pair, and 97% after all three electrode pairs (55 cm) under both non-augmented and CB1190-augmented conditions, indicating that 1,1-DCE removal was due to electrochemical removal. Since the presence of 5 mg/L 1,1-DCE did not affect the electrochemical oxidation of 1,4-dioxane under current-limiting conditions in a meaningful way (Figure 9), non-competing mechanisms such as volatilization by electrolytically generated gasses and/or cathodic reductive dechlorination likely contributed to 1,1-DCE removal from the aqueous phase. However, no potential 1,1-DCE reduction product was detected in any of the samples. At 5.0 V during both electrochemical and bioelectrochemical treatment, more than 98% 1,1-DCE was removed after the first electrode, and >99% throughout the entire reactor passage. This increase was likely driven by higher gas generation at the anode.

Despite the high electrochemical removal of 1,1-DCE, inhibitory effects of this co-contaminant were still apparent (Figure 9). At 2.2 V, the bioelectrochemical 1,4-dioxane degradation rate r_{ASA} dropped from 103 $mg \cdot h^{-1} \cdot m^{-2}$ to 48 $mg \cdot h^{-1} \cdot m^{-2}$. At 5.0 V, r_{ASA} dropped from 774 $mg \cdot h^{-1} \cdot m^{-2}$ to 201 $mg \cdot h^{-1} \cdot m^{-2}$. While inhibitory effects by other commonly co-occurring CVOCs are expected to be less pronounced,[46] these observations highlight the need for (near-)complete removal of 1,1-DCE for biodegradation-based water treatment approaches.

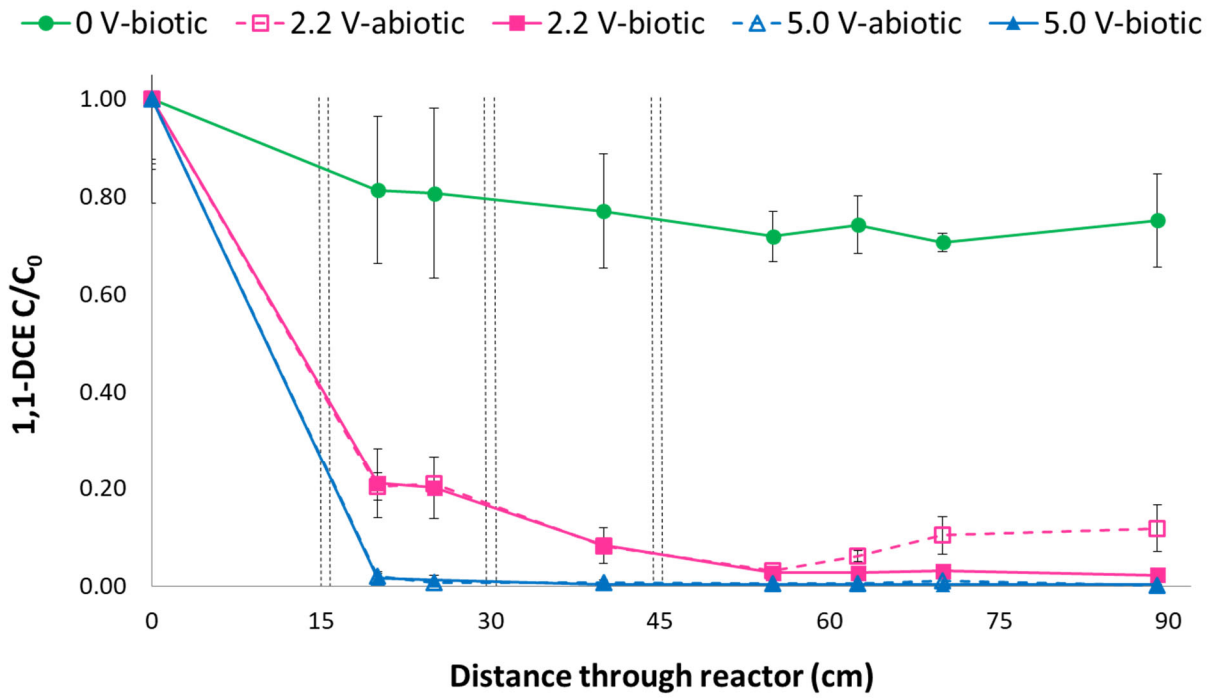

Figure 10: 1,1-DCE removal for electrochemical (abiotic) and bioelectrochemical treatment (biotic) at anode potentials of 2.2 V (magenta) and 5.0 V (blue). Green markers show the biological control (0V) experiment. Dashed lines represent abiotic electrochemical oxidation and solid lines represent bioelectrochemical oxidation. The vertical dashed lines indicate the location of (leading) anode and (trailing) cathode pairs.

3.3.4 Bacterial abundance

To locate and quantify bacterial distribution throughout the bioelectrochemical column reactors, qPCR analyses were performed on both aqueous and solid samples. Previous research had suggested that bacterial abundance and activity may become adversely impacted if anode potentials reach a range in which electrochemical processes cause cellular disruption associated with the production of ROS.[31,58] Complete profiles for the six bioaugmented experiments can be found in Figure 11. As 1,4-dioxane had been almost completely removed after the first electrode pair in the 5.0 V experiment without 1,1-DCE present (Figure 9), we focus our discussion on the bacterial abundance in the interelectrode space between the first two electrode pairs (15-30 cm), where the electron donor conditions were most comparable (Figure 12).

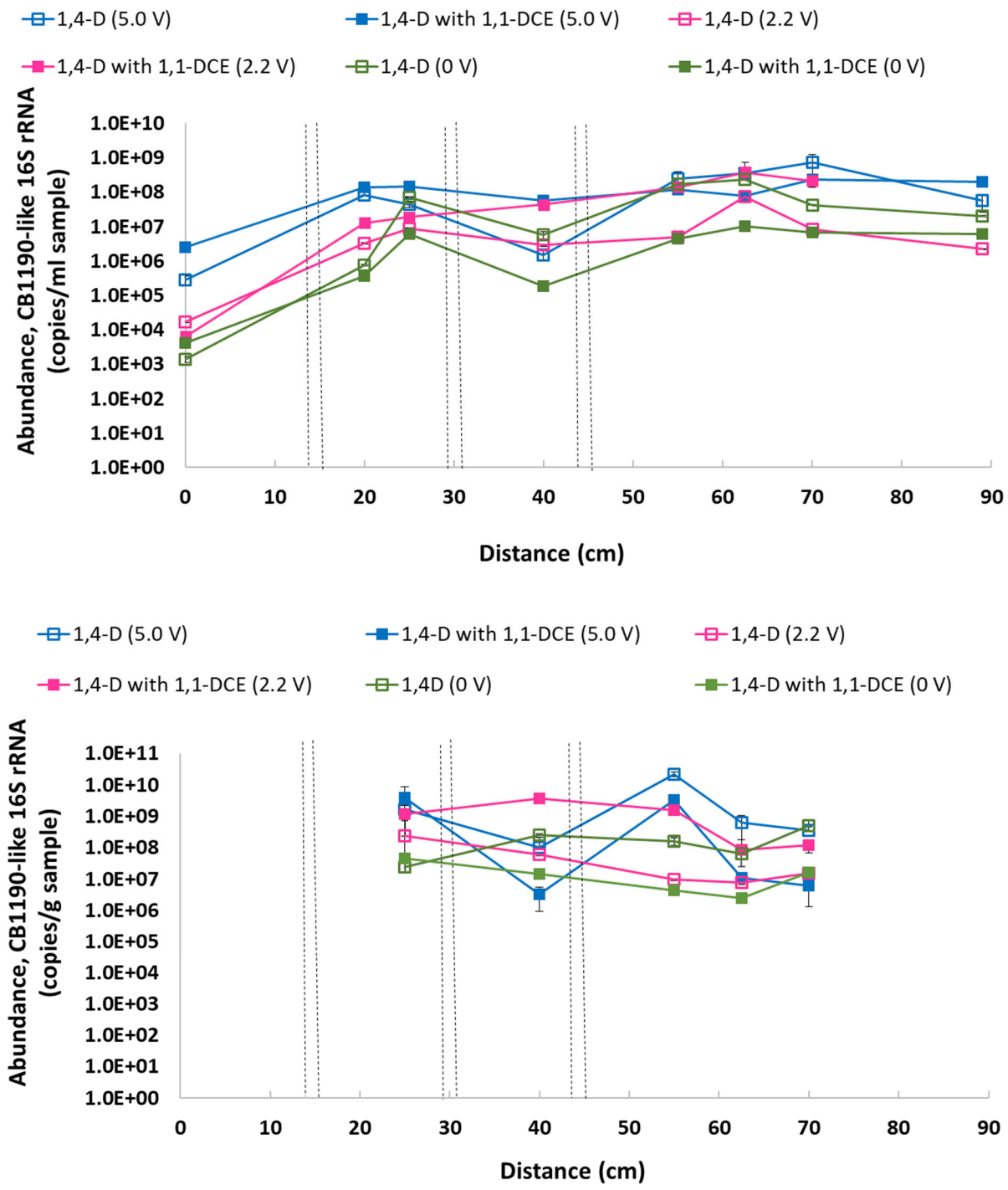

Figure 11: Planktonic (top) and sessile (bottom) qPCR results throughout the six bioaugmented reactors at 2.2 V (pink), 5.0 V (blue), and in the biological control (green). The vertical dashed lines indicate the location of anodes electrodes.

The bacterial abundance (quantified based on CB-1190-like 16S rRNA as proxy) in both suspended and solid states and in the absence of co-contaminant was highest at 5.0 V, supporting the higher 1,4-dioxane degradation kinetics observed at this potential. At 2.2 V, the abundance of biofilm cells was higher than in the biological control at 0 V as expected based on a higher 1,4-dioxane degradation rate; however, the aqueous abundance was higher at 0 V than at 2.2 V. The latter observation may be due to the fact that the remaining DO in the degassed influent (<2.0 mg/L) was not low enough and/or the multi-week experimental runs were still not long enough to reflect long-term effects caused by a lack of electron acceptor.

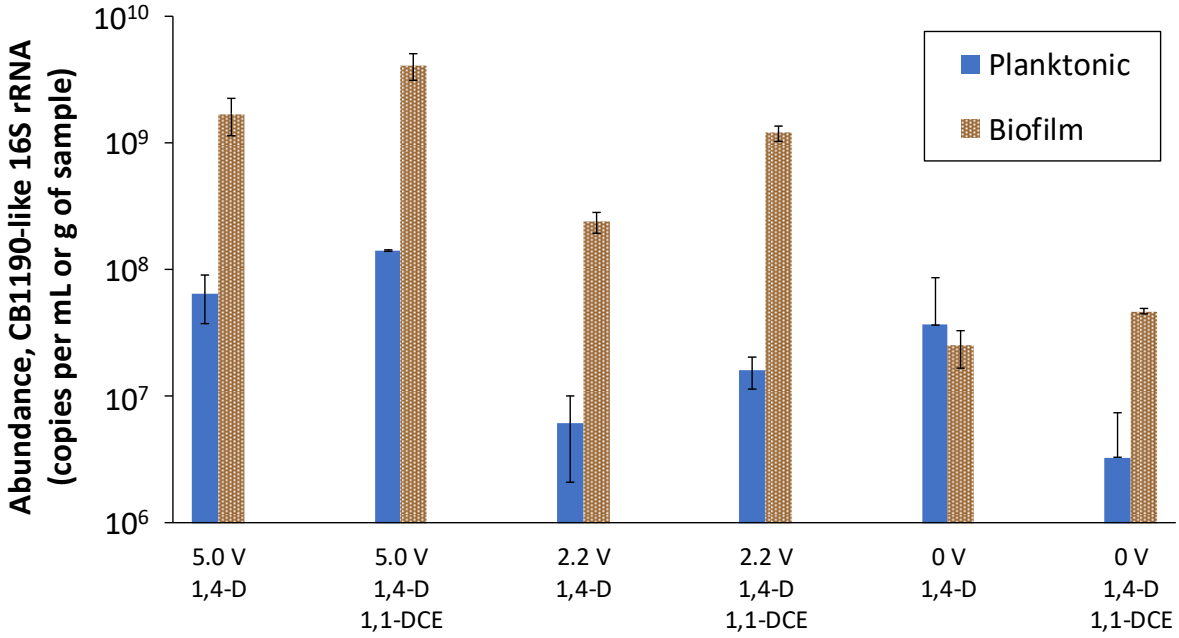

Figure 12: Planktonic (blue) and sessile (brown) qPCR results between the first and second electrode pairs (15-30 cm) at 5.0 V, 2.2 V, and in the biological control (0 V).

With one exception (planktonic count at 0 V), CB1190 abundances generally increased in the presence of 1,1-DCE, which may be due to increased biofilm formation as a stress response by CB1190 and subsequent cell release into the aqueous phase,[31,59] or the electrochemically degraded 1,1-DCE provided more bioavailable intermediates for CB1190. Under these conditions, the trends in bacterial abundance in both planktonic and sessile states of 5.0 V > 2.2 V > 0 V was aligned with the observed 1,4-dioxane degradation rates, suggesting higher biological activity as one of the causes for increasing bioelectrochemical treatment performance.

3.3.5 Fate of chlorine

Untargeted oxidation of naturally occurring reduced water solutes such as chlorine may lead to DBP generation, a general concern associated with all advanced oxidation processes.[60-62] No organic DBPs were detected under any of the experimental conditions (Figure 13 through Figure 15). At 2.2 V, no perchlorate was detected but effluent chlorate concentrations of 71 µmol/L and

5.0 µmol/L were observed in abiotic and biotic electrochemical oxidation systems, respectively. At the higher anode potential of 5.0 V, chlorate concentrations of 252 µmol/L and 112 µmol/L were observed in the effluent of the non-augmented and bioaugmented column reactors, respectively. In contrast to the lower potential of 2.2 V, some chlorate was further oxidized to perchlorate, reaching effluent concentrations of 0.27 µmol/L (abiotic) and 0.60 µmol/L (biotic).

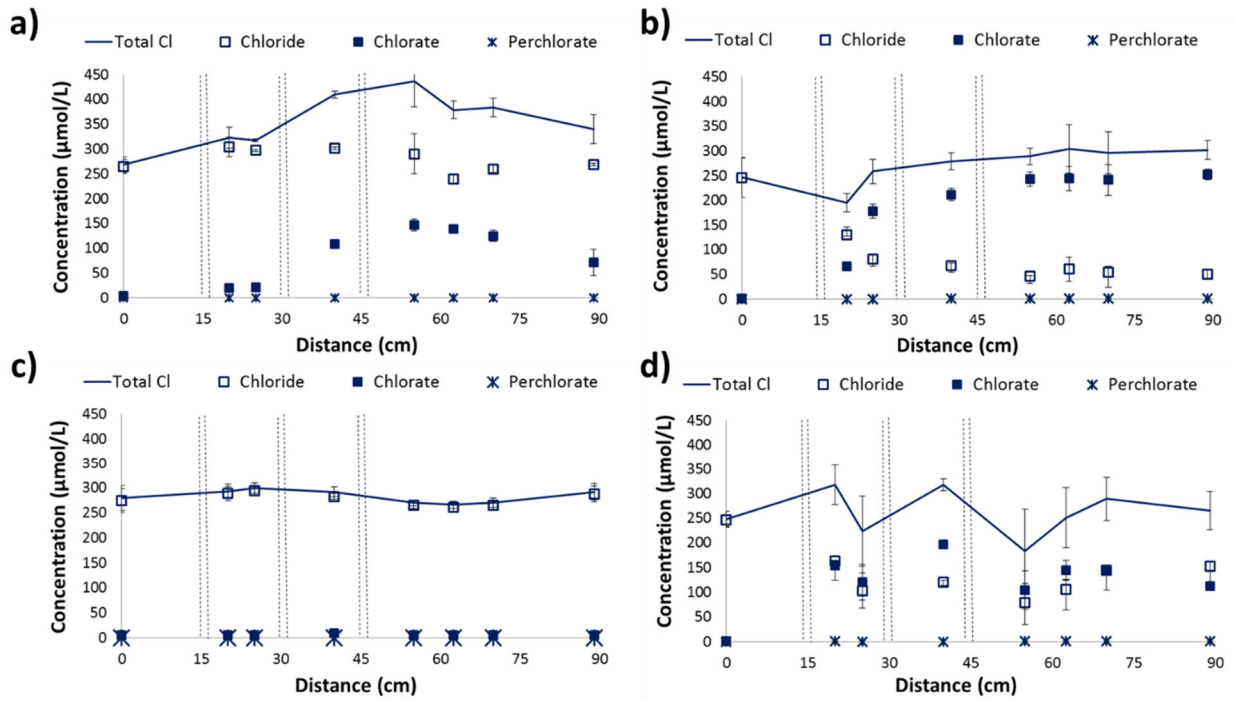

Figure 13: Chlorine mass balance (solid line) and speciation throughout the reactors during a) 2.2 V electrochemical treatment, b) 5.0 V electrochemical treatment, c) 2.2 V bioelectrochemical treatment, and d) 5.0 V bioelectrochemical treatment in the absence of 1,1-DCE. The vertical dashed lines indicate the location of (leading) anode and (trailing) cathode pairs.

As the total chlorine mass balances were approximately complete for all 10 experimental conditions, it can be concluded that no other major chlorine species had been overlooked. In conclusion, more rapid (bio)electrochemical oxidation comes at the cost of increasing DBP generation, either through higher applied potentials or more reactive anode materials.[28] However, DBP formation can be minimized through the use of bioelectrochemical processes based on lower applied voltage requirements to achieve the same 1,4-dioxane removal efficiency. Nevertheless, post-treatment strategies for chlorate and perchlorate need to be considered, for instance through biological treatment.[63]

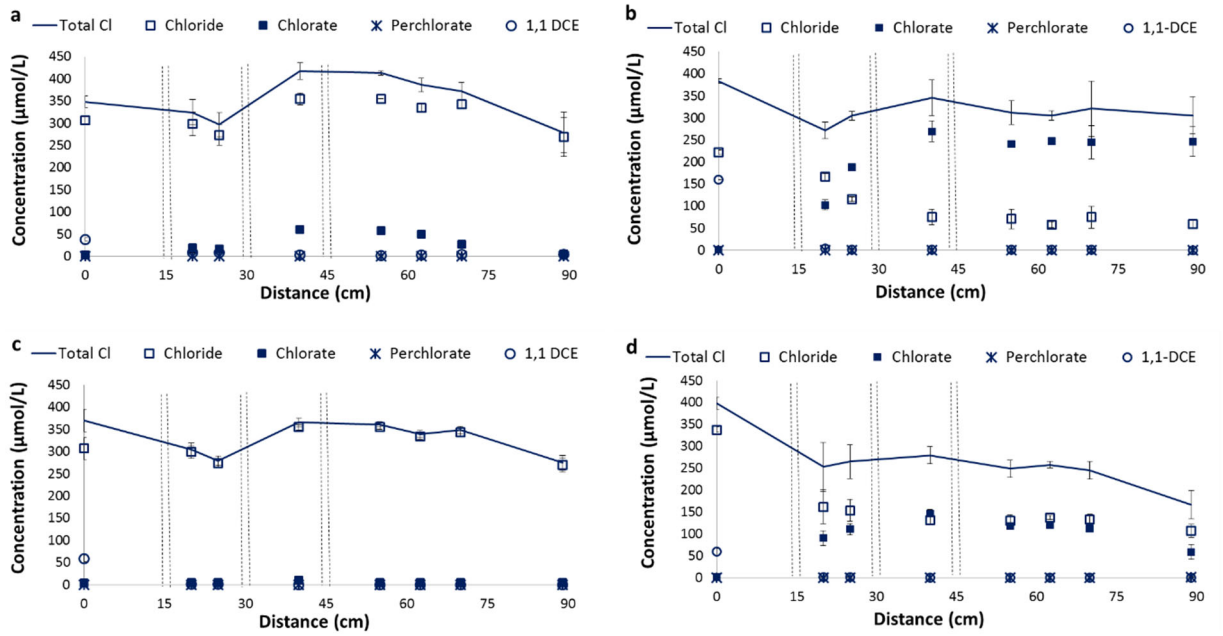

Figure 14: Chlorine speciation and mass balance throughout the reactors at 2.2 V electrochemical treatment (a), 5.0 V electrochemical treatment (b), 2.2 V bioelectrochemical treatment (c), and 5.0 V bioelectrochemical treatment (d) in the presence of 1,1-DCE. The vertical dashed lines indicate the location of anodes and cathodes.

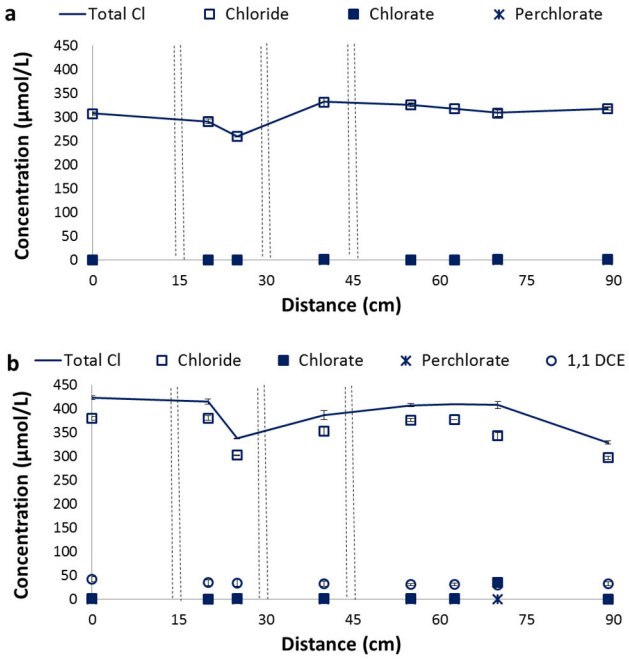

Figure 15: Chlorine speciation and mass balance throughout the biological control experiment (0 V) when no co-contaminant was present (a) and when the co-contaminant 1,1-DCE was present (b). The vertical dashed lines indicate the location of anodes and cathodes.

3.3.6 Cytotoxicity and effluent evaluation

Cytotoxicity of the column effluent samples (Figure 16) was determined via luminescence in relative light units (RLU) from enzymatic reactions with ATP. Luminescence displays a negative correlation with cytotoxicity. When comparing the columns with the same treatment strategy (e.g., electrochemical or bioelectrochemical), the addition of 1,1-DCE clearly increased the toxic effects. A larger difference in toxicity was seen between columns that include electrochemical treatment with or without bioaugmentation, which could be attributed to the strong and non-selective effects of voltage and the generation of DBPs. In the columns that were operated at the same anode potential (2.2 V or 5.0 V) with 1,1-DCE, the sample from the electrochemical only treatment was affected to a greater extent than that from the bioelectrochemical treatment. The opposite trend was observed in the absence of 1,1-DCE, where the samples from bioelectrochemical treatment had lower luminescence than those discharged from the electrochemical only treatment. Lastly, the highest anode potential (5.0 V) generated the highest cytotoxicity when comparing columns with the same treatment approach and contaminant mixtures.

To unravel the relationships among effluent factors in this study, including 1,4-dioxane, 1,1-DCE, ATP, DBPs and applied potential, we applied multivariate principal component analysis (PCA). Applied potential as the only operational factor on the PCA biplot mainly contributed to the first dimension, which accounted for most of the variability (56.6%) and grouped samples in terms of voltages (Figure 16). The applied potentials showed negative correlations with ATP as well as with 1,4-dioxane and 1,1-DCE concentrations in the effluent, indicating that the higher voltages may not only reduce the contaminant concentrations, but also increase the cytotoxicity. However, the separation of the vectors indicated that 1,1-DCE also generated inhibitory impacts on ATP production, and to a larger extent than 1,4-dioxane. Consequently, optimizing applied potentials to balance electrochemical oxidation efficiency and toxicity needs to be carefully considered during the remediation planning stage.

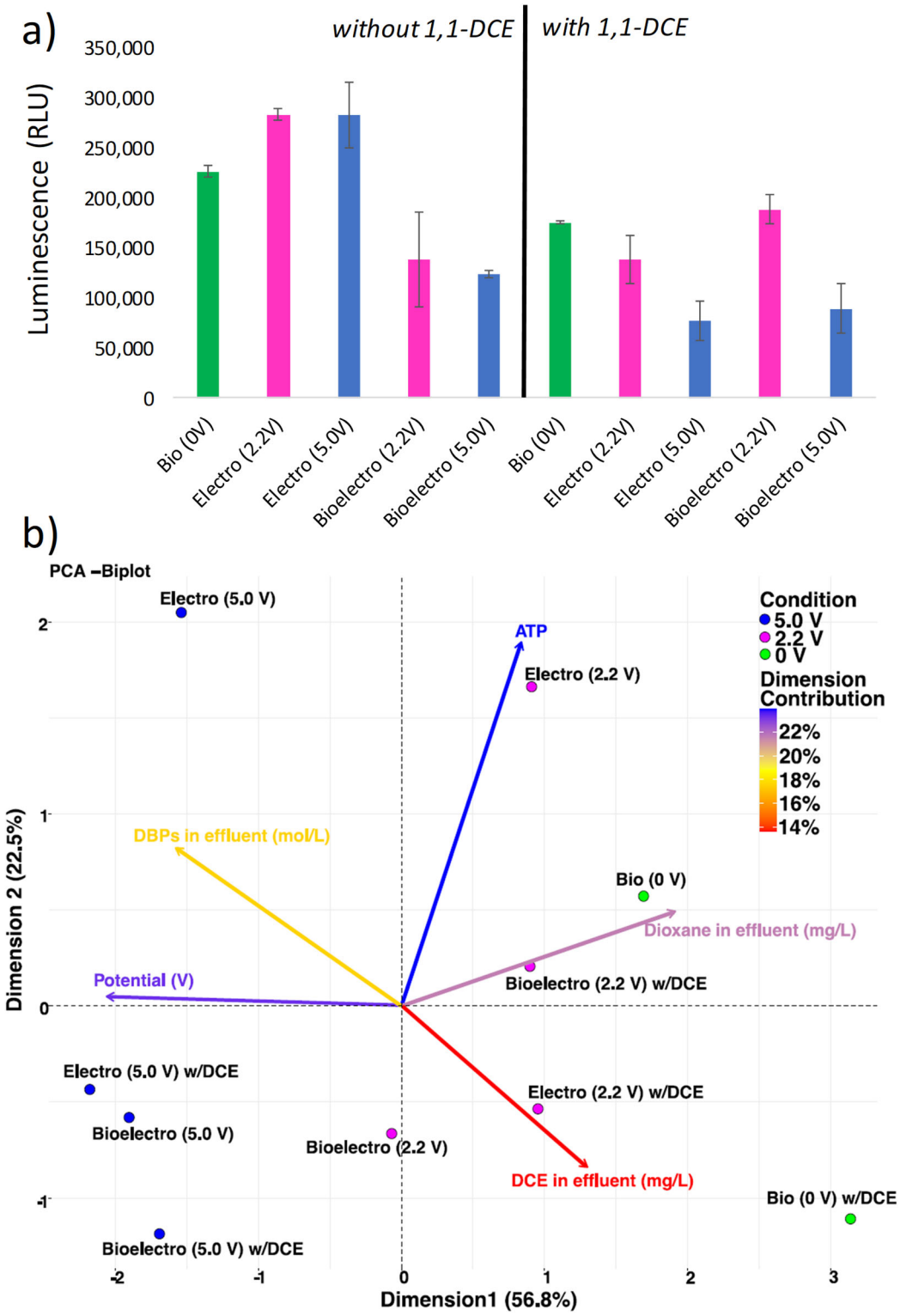

Figure 16: ATP production in CB1190 after incubating with column reactor effluents from different treatment conditions (a). Principal component analysis showing the relationship between treatment conditions and ATP production (b).

3.3.7 Sustainability considerations

Figure 17 compares the anode surface area per order of 1,4-dioxane removed (ASA_O, major capital cost driver) for electrochemical and bioelectrochemical oxidation. The higher removal kinetics at 5.0 V compared to 2.2 V led to a significant reduction in the required electrode area of 93% for electrochemical oxidation and 94% for bioelectrochemical oxidation. Material usage and cost savings associated with the electrodes further decreased when biological and electrochemical oxidation were combined. Compared to the abiotic electrochemical process, bioelectrochemical treatment led to decreases in ASA_O of 87% at 2.2 V and 90% at 5.0 V applied, achieving 87 $m^2 \cdot h \cdot m^{-3}$ in the latter case.

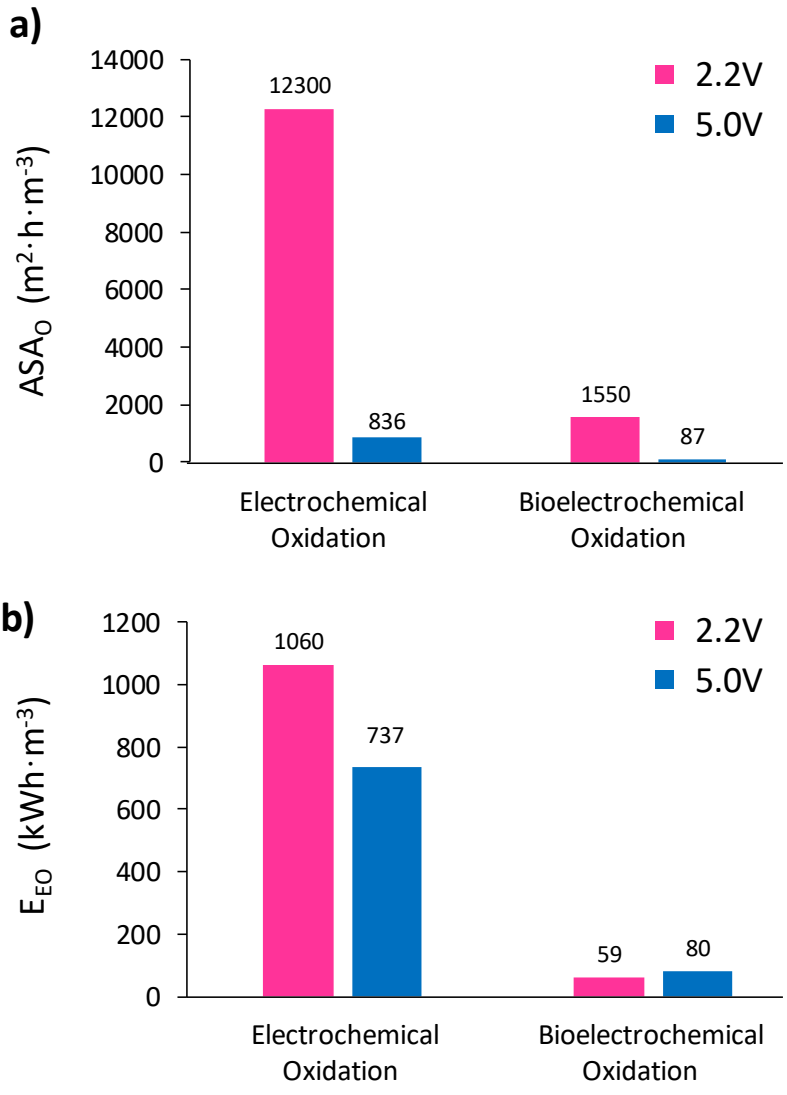

Figure 17: a) Required anode surface area and b) electric energy per order of magnitude of 1,4-dioxane removed for electrochemical versus bioelectrochemical treatment of 1,4-dioxane at anode potentials of 2.2 V and 5.0 V.

Figure 17 also illustrates the electric energy per order of magnitude of 1,4-dioxane removed (E_{EO}, major operational cost driver). During electrochemical oxidation, the energy consumption was higher at 2.2 V (1060 kWh·m^{-3}) than at 5.0 V (737 kWh·m^{-3}) due to the poor overall 1,4-dioxane removal at the lower applied potential. The coupling of biological with electrochemical oxidation achieved significant reductions in E_{EO} by 94% at 2.2 V and 89% at 5.0 V, substantially lowering the technology's carbon footprint. Energy efficiency per unit of contaminant removed was only slightly higher at the lower applied potential of 2.2 V (59 kWh·m^{-3}) than at 5.0 V (80 kWh·m^{-3}). These E_{EO} values are higher than those previously reported for UV-based technologies, which can achieve 1,4-dioxane treatment at single digit kWh·m^{-3} or in the case of vacuum ultraviolet (VUV) treatment even below.[23,25-27] However, commonly occurring inorganic ions[23] and organic co-contaminants[26] may increase power consumption, and the addition of oxidants during ozone- or H_2O_2-based UV treatment needs to be considered.[25,64] The comparatively higher energy consumption for (bio)electrochemical 1,4-dioxane oxidation in our experiments is at least partly due to the fact that this parameter was not determined in a reactor optimized for mass transfer, but at seepage velocities representative of groundwater, where mass transfer solely relied on slow diffusion processes. High-flow pumping in *ex situ* reactors is expected to increase mass transfer and consequently to decrease energy consumption.[65]

The optimized process design in combination with the more reactive Ti/SnO_2-X anodes achieved a 70% lower energy consumption and 96% reduction in required electrode material compared to our initial proof-of-concept study.[31] Overall, our techno-economic assessment suggests lower bioelectrochemical costs at the higher applied potential, though at the expense of higher DBP formation. Consequently, site-specific scale-up efforts should include the determination of an ideal energy-optimized current density at which the applied current density is equal to the limiting current density.[55]

3.3.8 Long-term stability of the anode

A service life test based on ref. 67 was carried out in a batch electrochemical reactor under potentiostatic conditions at 4.0 V applied to test the longevity of the doped tin oxide anode. The current relative to an Ag/AgCl reference electrode was monitored and logged during the service life test (Figure 18). Throughout the entire 14-day experiment, the current density did not substantially decrease and, at an average of 67.6 mA/cm^2, remained well above that of the pure Ti substrate (0.052 mA/cm^2 on average, data not shown). Considering the current densities during the (bio)electrochemical experiments (1.95 mA/cm^2 at 2.2 V; 15.4 mA/cm^2 at 5.0 V), these data suggest an anode service life of at least > one year for the lower potential and at least several months for the higher potential.

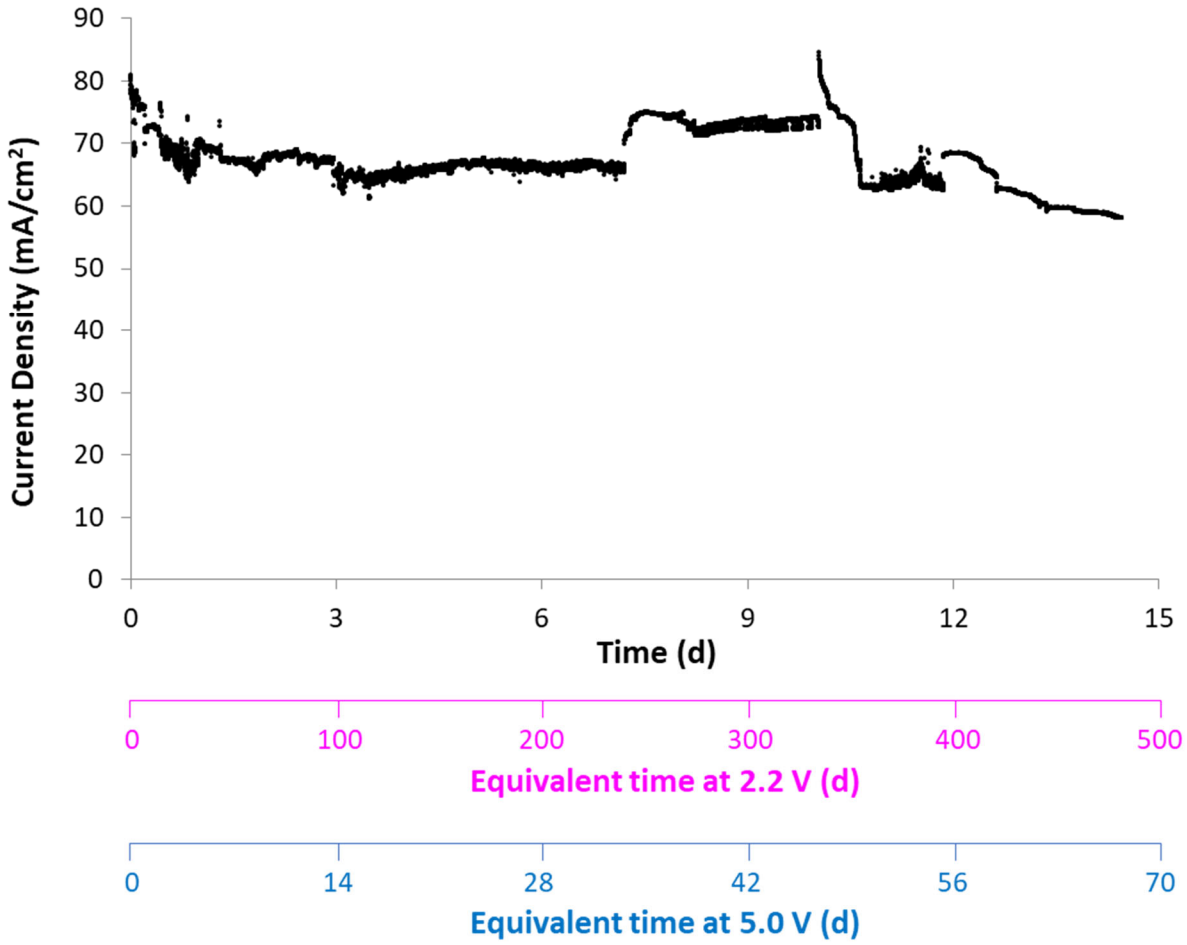

Figure 18: Accelerated service life test for the doped tin oxide anode material under potentiostatic conditions (4.0 V applied). 1 M H_2SO_4 was used as electrolyte at ambient temperature.

Furthermore, the electrodes were recovered from the reactors at the end of the bioelectrochemical experiments, rinsed with tap water, air-dried, and visually inspected (Figure 19). The circular mesh anode looked practically unchanged in comparison to the original doped tin oxide anode material, showing no signs of coating loss compared to the underlying pure Ti mesh substrate.

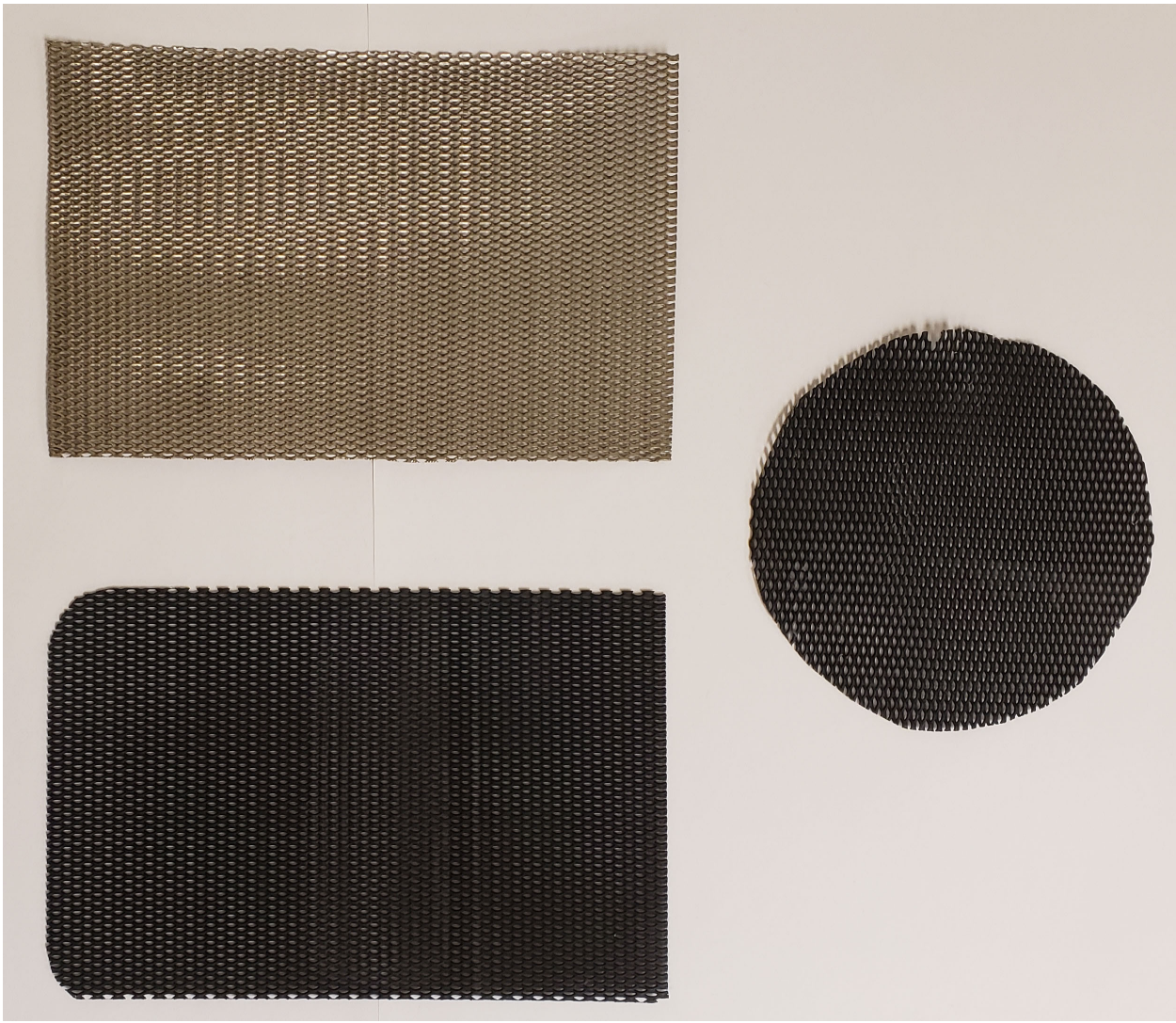

Figure 19: The circular mesh anode (right, 10 cm diameter) at the end of the (bio)electrochemical oxidation experiments looks practically unchanged in comparison to the original doped tin oxide anode material (bottom left, 10 x 15 cm), showing no signs of coating loss compared to the underlying pure Ti mesh substrate (top left, 10 x 15 cm).

3.4 Conclusions

Electrochemical oxidation is a capable water treatment technology that can mineralize even the most refractory organic pollutants. However, high capital costs driven by the electrode material have delayed scale-up for field applications. Furthermore, electric energy consumption can be significant and is largely wasted in untargeted side reactions such as water electrolysis into O_2 and H_2.[31,66] Our findings demonstrate that the synergistic effects from chemical and biological oxidation may lower both material usage and energy consumption by more than one order of magnitude. Consequently, bioelectrochemical treatment of refractory organic water contaminants is substantially more cost-effective and sustainable than electrochemical water treatment alone.

We note that at the end of the multi-month experiments neither a visual deterioration of the electrodes nor a decline in 1,4-dioxane removal were observed. In addition, the results of accelerated service life testing[67] supported the viability of the dimensionally stable electrodes for longer-term field applications.

Furthermore, we showed that bioelectrochemical treatment with *P. dioxanivorans* CB 1190 can reduce 1,4-dioxane concentrations by several orders of magnitude from more than 100 mg/L to less than our detection limit of 3 µg/L. Once implemented in the field and run over longer treatment periods, it appears possible that other native microorganisms may eventually co-exist with and/or even outperform CB1190 depending on water quality and treatment conditions. As both metabolic and co-metabolic bioremediation approaches are challenged at low- or sub-ppb 1,4-dioxane concentrations, our findings highlight the potential capability of this technology to achieve effluent concentrations below the strict regulatory limits in the U.S. It appears likely that bioelectrochemical oxidation can be applied with other types of bacteria including co-metabolic strains and mixed cultures,[68] highlighting the potential for further improvement in treatment efficiency.

Our current research is focusing on scaling up bioelectrochemical treatment of 1,4-dioxane in the presence of CVOCs to the pilot scale at a contaminated field site. Pilot-scale performance testing prior to full-scale implementation is critical in that site-specific parameters such as water quality, contaminant concentrations, flow rate and potential infrastructural limitations can inform final reactor design and operational parameters such as optimal voltage, number of electrode pairs, reactor geometry, and frequency of polarity reversals to minimize cathodic scale formation. Within this upcoming demonstration, we are also determined to address the remaining challenge of DBP formation through harnessing reductive microbial processes that can take advantage of thus far unutilized cathodic processes.

3.5 Literature References

1) Adamson, D. T.; Mahendra, S.; Walker, K. L.; Rauch, S. R.; Sengupta, S.; Newell, C. J. A. Multisite Survey to Identify the Scale of the 1,4-dioxane Problem at Contaminated Groundwater Sites. *Environ. Sci. Technol. Lett.* 2014, *1*, 254-258, DOI: 10.1021/ez500092u.

2) U.S. Environmental Protection. 1,4-Dioxane (CASRN 123-91-1). Integrated Risk Information System (IRIS), National Center for Environmental Assessment, Office of Research and Development, Washington, DC, 2013. cfpub.epa.gov/ncea/iris2/chemicalLanding.cfm?substance_nmbr=326

3) Broughton, A.; Sepulveda, A.; Foster, K.; Kruk, T.; Nickelsen, M. G.; Gillan, M.; Mohr, T. K. G. 1,4-Dioxane: Emerging technologies for an emerging contaminant. *Remediation* 2019, *29*, 49-63.

4) Blotevogel, J.; Pijls, C.; Scheffer, B.; de Waele, J.P.; Lee, A.; van Poecke, R.; van Belzen, N.; Staal, W. Pilot-Scale Electrochemical Treatment of a 1,4-Dioxane Source Zone. *Groundwater Monitoring & Remediation*. 2019, *39*, 36-42.

5) Han, T. H.; Han, J. S.; So, M. H.; Seo, J. W.; Ahn, C. M.; Min, D. H.; Yoo, Y. S.; Cha, D. K.; Kim, C. G. The Removal of 1,4-dioxane From Polyester Manufacturing Process Wastewater Using an Up-Flow Biological Aerated Filter (UBAF) Packed With Tire Chips. *J. Environ. Sci. Health, Part A: Toxic/Hazard. Subst. Environ. Eng.* 2012, *47*, 117– 129, DOI: 10.1080/10934529.2012.630291.

6) Isaka, K.; Udagawa, M.; Sei, K.; Ike, M. Pilot Test of Biological Removal of 1,4-dioxane From a Chemical Factory Wastewater by Gel Carrier Entrapping Afipia sp. Strain d1. *J. Hazard. Mater.* 2016, *304*, 251– 258, DOI: 10.1016/j.jhazmat.2015.10.066.

7) Zenker, M. J.; Borden, R. C.; Barlaz, M. A. Occurrence and Treatment of 1,4-dioxane in Aqueous Environments. *Environmental Engineering Science*. 2003, *20*, 423– 432, DOI: 10.1089/109287503768335913.

8) DiGuiseppi, W.; Walecka-Hutchison, C.; Hatton, J. 1,4-Dioxane Treatment Technologies. *Remediation Journal*. 2016, 27, 71-92.

9) DiGuiseppi, W.; Whitesides, C. Treatment Options for Remediation of 1,4-dioxane in Groundwater. *Environ. Eng. Appl. Res. Pract*. 2007, *2*, 1-7.

10) Barndõk, H.; Cortijo, L.; Hermosilla, D.; Negro, C.; Blanco, Á. Removal of 1,4-dioxane From Industrial Wastewaters: Routes of Decomposition Under Different Operational Conditions to Determine the Ozone Oxidation Capacity. *J. Hazard. Mater*. 2014, *280*, 340–347, https://doi.org/10.1016/j.jhazmat.2014.07.077.

11) Guan, Y.H.; Ma, J.; Li, X.C.; Fang, J.Y.; Chen, L.W. Influence of pH on the Formation of Sulfate and Hydroxyl Radicals in the UV/Peroxymonosulfate System. *Environ. Sci. Technol*. 2011, *45*, 9308-9314.

12) Khan, N.A.; Johnson, M.D.; Kubicki, J.D.; Holguin, F.O.; Dungan, B.; Carroll, K.C. Cyclodextrin-Enhanced 1, 4-dioxane Treatment Kinetics With TCE and 1,1,1-TCA Using Aqueous Ozone. *Chemosphere.* 2019, *219*, 335-344.

13) Kishimoto, N.; Nakagawa, T.; Asano, M.; Abe, M.; Yamada, M.; Ono, Y. Ozonation Combined With Electrolysis of 1,4-dioxane Using a Two-Compartment Electrolytic Flow Cell with Solid Electrolyte. *Water Res.* 2008, *42*, 379-385.

14) Miao, Y.; Johnson, N. W.; Gedalanga, P. B.; Adamson, D.; Newell, C.; Mahendra, S. Response and recovery of microbial communities subjected to oxidative and biological treatments of 1,4-dioxane and co-contaminants. *Water Res.* 2019, 149, 74-85.

15) Miao, Y.; Johnson, N. W.; Heck, K.; Guo, S.; Powell, C. D.; Phan, T.; Gedalanga, P. B.; Adamson, D. T.; Newell, C. J.; Wong, M. S.; Mahendra, S. Microbial responses to combined oxidation and catalysis treatment of 1,4-dioxane and co-contaminants in groundwater and soil. *Front. Environ. Sci. Eng.* 2018, 12, 2.

16) Mohr, T.K.; Stickney, J.A.; DiGuiseppi, W.H. Environmental Investigation and Remediation: 1, 4-Dioxane and Other Solvent Stabilizers. *CRC Press*. 2010.

17) Shen, W.; Wang, Y.; Zhan, J.; Wang, B.; Huang, J.; Deng, S.; Yu, G. Kinetics and Operational Parameters for 1,4-dioxane Degradation by the Photoelectro-Peroxone Process. *Chem. Eng. J*. 2017, *310*, 249–258, https://doi.org/10.1016/j.cej.2016.10.111.

18) Son, H.S.; Choi, S.B.; Khan, E.; Zoh, K.D. Removal of 1,4-dioxane From Water Using Sonication: Effect of Adding Oxidants on the Degradation Kinetics. *Water Res*. 2006, 692–698, https://doi.org/10.1016/j.watres.2005.11.046.

19) Stefan, M.I.; Bolton, J.R. Mechanism of the degradation of 1, 4-dioxane in dilute aqueous solution using the UV/hydrogen peroxide process. *Environ. Sci. Technol*. 1998, *40*, 1588–1595, https://doi.org/10.1021/es970633m.

20) Xiong, Y.; Zhang, Q.; Wandell, R.; Bresch, S.; Wang, H.; Locke, B.R.; Tang, Y. Synergistic 1, 4-dioxane Removal by Non-Thermal Plasma Followed by Biodegradation. *Chem. Eng. J.* 2019, *361*, 519-527.

21) Vatankhah, H.; Szczuka, A.; Mitch, W.A.; Almaraz, N.; Brannum, J.; Bellona, C. Evaluation of Enhanced Ozone–Biologically Active Filtration Treatment for the Removal of 1,4-Dioxane and Disinfection Byproduct Precursors from Wastewater Effluent. *Environ. Sci. Technol.* 2019, 53, 5, 2720–2730

22) Zhang, Z.; Chuang, Y.-H.; Szczuka, A.; Ishida, K.P.; Roback, S.; Plumlee, M.H.; Mitch, W.A. Pilot-scale evaluation of oxidant speciation, 1,4-dioxane degradation and disinfection byproduct formation during UV/hydrogen peroxide, UV/free chlorine and UV/chloramines advanced oxidation process treatment for potable reuse. *Water Research* 2019, 164, 114939

23) Nomura, Y.; Fukahori, S.; Fujiwara, T. Removal of 1,4-dioxane from landfill leachate by a rotating advanced oxidation contactor equipped with activated carbon/TiO_2 composite sheets. *J. Haz. Mat*. 2020, 383, 121005.

24) Ouyang, D.; Chen, Y.; Yan, J.; Qian, L.; Han, L.; Chen, M. Activation mechanism of peroxymonosulfate by biochar for catalytic degradation of 1,4-dioxane: Important role of biochar defect structures. *Chem. Eng. J.* 2019, 370, 614-624.

25) Matsushita, T.; Hirai, S.; Ishikawa, T.; Matsui, Y.; Shirasaki, N. Decomposition of 1,4-dioxane by vacuum ultraviolet irradiation: Study of economic feasibility and by-product formation. *Process. Saf. Environ. Prot*. 2015, 94, 528-541.

26) Matsushita, T.; Sugita, W.; Ishikawa, T.; Shi, G.; Nishizawa, S.; Matsui, Y.; Shirasaki, N. Prediction of 1,4-dioxane decomposition during VUV treatment by model simulation taking into account effects of coexisting inorganic ions. *Water Research* 2019, 164, 114918.

27) Martijn, B.J.; Fuller, A.L.; Malley, J.P.; Kruithof, J.C. Impact of IX-UF Pretreatment on the Feasibility of UV/H2O2 Treatment for Degradation of NDMA and 1,4-Dioxane. *Ozone: Science & Engineering* 2010, 32, 383–390.

28) Bagastyo, A.Y.; Batstone, D.J.; Rabaey, K.; Radjenovic, J. Electrochemical Oxidation of Electrodialysed Reverse Osmosis Concentrate on Ti/Pt–IrO2, Ti/SnO2–Sb and Boron-Doped Diamond Electrodes. *Water Res.* 2013, *47*, 242-250.

29) Farhat, A.; Keller, J.; Tait, S.; Radjenovic, J. Removal of Persistent Organic Contaminants by Electrochemically Activated Sulfate. *Environ. Sci. Technol.* 2015, *49*, 14326-14333.

30) Jasmann, J. R.; Borch, T.; Sale, T. C.; Blotevogel, J. Advanced Electrochemical Oxidation of 1,4-dioxane via Dark Catalysis by Novel Titanium Dioxide (TiO_2) Pellets. *Environ. Sci. Technol*. 2016, *50*, 8817– 8826, DOI: 10.1021/acs.est.6b02183.

31) Jasmann, J.R.; Gedalanga, P.B.; Borch, T.; Mahendra, S.; Blotevogel, J. Synergistic Treatment of Mixed 1, 4-dioxane and Chlorinated Solvent Contaminations by Coupling Electrochemical Oxidation With Aerobic Biodegradation. *Environ. Sci. Technol.* 2017, *51*, 12619-12629.

32) Radjenovic, J.; Sedlak, D. L. Challenges and Opportunities for Electrochemical Processes as Next-Generation Technologies for the Treatment of Contaminated Water. *Environ. Sci. Technol.* 2015, *49*, 11292-11302.

33) Canizares, P.; Paz, R.; Saez, C.; Rodrigo, M. A. Costs of the Electrochemical Oxidation of Wastewaters: A Comparison with Ozonation and Fenton Oxidation Processes. *J. Environ. Manage.* 2009, *90*, 410-420.

34) Petersen, M. A.; Sale, T. C.; Reardon, K. F. Electrolytic Trichloroethene Degradation Using Mixed Metal Oxide Coated Titanium Mesh Electrodes. *Chemosphere*. 2007, *67*, 1573– 1581, DOI: 10.1016/j.chemosphere.2006.11.056.

35) Sale, T.; Petersen, M.; Gilbert, D. Electrically Induced Redox Barriers for Treatment of Groundwater, ESTCP Final Report CU-0112; U.S. Department of Defense, 2005.

36) Chaplin, B. P. Critical review of electrochemical advanced oxidation processes for water treatment applications. *Environ. Sci.: Processes Impacts* 2014, *16,* 1182-1203.

37) Gedalanga, P.B.; Pornwongthong, P.; Mora, R.; Chiang, S.; Baldwin, B.; Ogles, D.; Mahendra, S. Identification of Biomarker Genes to Predict Biodegradation of 1,4-dioxane. *Appl. Environ. Microbiol*. 2014, *80*, 3209–3218.

38) Grostern, A.; Sales, C.M.; Zhuang, W.Q.; Erbilgin, O.; Alvarez-Cohen, L. Glyoxylate Metabolism is a Key Feature of the Metabolic Degradation of 1,4-dioxane by Pseudonocardia Dioxanivorans Strain CB1190. *Appl. Environ. Microbiol*. 2012, *78*, 3298–3308.

39) Hand, S.; Wang, B.; Chu, K.H. Biodegradation of 1, 4-dioxane: Effects of Enzyme Inducers and Trichloroethylene. *Science of the Total Environment*. 2015, *520*, 154-159.

40) Kim, Y.M.; Jeon, J.R.; Murugesan, K.; Kim, E.J.; Chang, Y.S. 2009. Biodegradation of 1,4-dioxane and Transformation of Related Cyclic Compounds by a Newly Isolated Mycobacterium sp. PH-06. *Biodegradation*. 2009, *20*, 511–519.

41) Lan, R.S.; Smith, C.A.; Hyman, M.R. Oxidation of Cyclic Ethers by Alkane-Grown Mycobacterium Vaccae JOB5. *Remediation Journal.* 2013, *23*, 23–42.

42) Lippincott, D.; Streger, S.H.; Schaefer, C.E.; Hinkle, J.; Stormo, J.; Steffan, R.J. Bioaugmentation and Propane Biosparging for in Situ Biodegradation of 1,4-dioxane. *Groundwater Monitoring Remediation*. 2015, *35*, 81–92.

43) Mahendra, S.; Petzold, C. J.; Baidoo, E. E.; Keasling, J. D.; Alvarez-Cohen, L. Identification of the Intermediates of in Vivo Oxidation of 1,4-Dioxane by Monooxygenase-Containing Bacteria. *Environ. Sci. Technol*. 2006, *40*, 5435–5442, https://doi.org/10.1021/es060714v.

44) Parales, R.E.; Adamus, J.E.; White, N.; May, H.D. Degradation of 1,4-dioxane by an Actinomycete in Pure Culture. *Appl. Environ. Microbiol*. 1994, *60*, 4527–4530.

45) Vainberg, S.; McClay, K.; Masuda, H.; Root, D.; Condee, C.; Zylstra, G.J.; Steffan, R.J. Biodegradation of Ether Pollutants by Pseudonocardia sp. Strain ENV478. *Appl. Environ. Microbiol.* 2006, *72*, 5218–5224, https://doi.org/10.1128/AEM.00160-06.

46) Zhang, S.; Gedalanga, P. B.; Mahendra, S. Biodegradation kinetics of 1,4-dioxane in chlorinated solvent mixtures. *Environ. Sci. Technol.* **2016**, *50*, 9599-9607.

47) Barajas-Rodriguez, F. J.; Freedman, D. L. Aerobic biodegradation kinetics for 1,4-dioxane under metabolic and cometabolic conditions. *J. Haz. Mat.* 2018, 350, 180-188.

48) Suthersan, S.; Quinnan, J.; Horst, J.; Ross, I.; Kalve, E.; Bell, C.; Pancras, T. Making Strides in the Management of "Emerging Contaminants". *Groundwater Monitoring Remediation*. 2016, *36*, 15–25.

49) Liu, Y.; Johnson, N.W.; Liu, C.; Chen, R.; Zhong, M.; Dong, Y.; Mahendra, S. Mechanisms of 1,4-Dioxane Biodegradation and Adsorption by Bio-zeolite in the Presence of Chlorinated Solvents: Experimental and Molecular Dynamics Simulation Studies. *Environmental Science & Technology* 2019, *53*, 14538-14547.

50) Matyasovszky, N.; Tian, M.; Chen, A. Kinetic Study of the Electrochemical Oxidation of Salicylic Acid and Salicylaldehyde Using UV/vis Spectroscopy and Multivariate Calibration. *J. Phys. Chem. A* 2009, *113*, 9348-9353.

51) Zhuo, Q.F.; Dent, S.B.; Yang, B.; Huang, J.; Yu, G. Efficient Electrochemical Oxidation of Perfluorooctanoate Using a Ti/SnO_2-Sb-Bi anode. *Environ. Sci. Technol.* 2011, *45*, 2973-2979

52) Anderson, R.H.; Anderson, J.K.; Bower, P.A. Co-Occurrence of 1,4-Dioxane with Trichloroethylene in Chlorinated Solvent Groundwater Plumes at US Air Force Installations: Fact or Fiction. *Integr. Environ. Assess. Manag*. 2012, 8, 731-737.

53) Pica, N.E.; Funkhouser, J.; Yin, Y.; Zhang, Z.; Ceres, D.; Tong, T.; Blotevogel, J. Electrochemical Oxidation of Hexafluoropropylene Oxide Dimer Acid (GenX): Mechanistic Insights and Efficient Treatment Train with Nanofiltration. *Environ. Sci. Technol.* 2019, *53*, 12602-12609.

54) Mahendra, S.; Alvarez-Cohen, L. Kinetics of 1,4-dioxane Biodegradation by Monooxygenase-Expressing Bacteria. *Environ. Sci. Technol*. 2007, *41*, 7330-7336.

55) Comninellis, C.; Chen, G. Electrochemistry for the Environment; Springer: New York, NY, 2010.

56) Lin, H.; Niu, J.; Ding, S.; Zhang, L. Electrochemical degradation of perfluorooctanoic acid (PFOA) by Ti/SnO_2-Sb, Ti/SnO_2-Sb/PbO_2 and Ti/SnO_2-Sb/MnO_2 anodes. *Water Research* **2012**, *46*, 2281-2289.

57) Dalle, A.A.; Domergue, L.; Fourcade, F.; Assadi, A.A.; Djelal, J.; Lendormi, T.; Soutrel, I.; Taha, S.; Amrane, A. Efficiency of DMSO as hydroxyl radical probe in an Electrochemical Advanced Oxidation Process − Reactive oxygen species monitoring and impact of the current density. *Electrochimica Acta* 2017, 246, 1-8.

58) Cabiscol, E.; Tamarit, J.; Ros, J. Oxidative stress in bacteria and protein damage by reactive oxygen species. *J. Biol. Chem.* 2010, *3*, 3-8.

59) LaFleur, M. D.; Kumamoto, C. A.; Lewis, K. *Candida albicans* biofilms produce antifungal-tolerant persister cells. *Antimicrob. Agents Chemother.* 2006, *50*, 3839-3846.

60) Jo, C.H.; Dietrich, A.M.; Tanko, J.M. Simultaneous Degradation of Disinfection By-Products and Earthy-Musty Odorants by the UV/H2O2 Advanced Oxidation Process. *Water Res.* 2011, *45*, 2507-2516.

61) Miklos, D.B.; Remy, C.; Jekel, M.; Linden, K.G.; Drewes, J.E.; Hübner, U. Evaluation of advanced oxidation processes for water and wastewater treatment – A critical review. *Water Research* 2018, *139*, 118-131.

62) Zöllig, H.; Remmele, A.; Fritzsche, C.; Morgenroth, E.; Udert, K.M. 2015. Formation of Chlorination Byproducts and Their Emission Pathways in Chlorine Mediated Electro-Oxidation of Urine on Active and Nonactive Type Anodes. *Environ. Sci. Technol.* 2015, *49*, 11062-11069.

63) Schaefer, C.E.; Andaya, C.; Burant, A.; Condee, C.W.; Urtiaga, A.; Strathmann, T.J.; Higgins, C.P. Electrochemical treatment of perfluorooctanoic acid and perfluorooctane sulfonate: Insights into mechanisms and application to groundwater treatment. *Chemical Engineering Journal* 2017, *317*, 424-432.

64) Müller, J.-P.; Jekel, M. Comparison of advanced oxidation processes in flow-through pilot plants (Part I). *Water Sci. Technol.* 2001, 44, 303-309.

65) Martínez-Huitle, C. A.; Rodrigo, M. A.; Sirés, I.; Scialdone, O. Single and Coupled Electrochemical Processes and Reactors for the Abatement of Organic Water Pollutants: A Critical Review. *Chem. Rev.* 2015, 115, 13362-13407.

66) Schaefer, C.E.; Choyke, S.; Ferguson, P.L.; Andaya, C.; Burant, A.; Maizel, A.; Strathmann, T.J.; Higgins, C.P. Electrochemical Transformations of Perfluoroalkyl Acid (PFAA) Precursors and PFAAs in Groundwater Impacted with Aqueous Film Forming Foams. *Environ. Sci. Technol.* 2018, *52*, 10689-10697.

67) Correa-Lozano, B.; Comninellis, C.; De Battisti, A. Service life of Ti/SnO_2-Sb_2O_5 anodes. *J. Appl. Electrochem.* 1997, 27, 970-974.

68) Polasko, A.L.; Zulli, A.; Gedalanga, P.B.; Pornwongthong, P.; Mahendra, S. A Mixed Microbial Community for the Biodegradation of Chlorinated Ethenes and 1, 4-Dioxane. *Environ. Sci. Technol. Lett.* 2019, *6*, 49-54.

4 FLOW-THROUGH ELECTROCHEMICAL TREATMENT OF PFASs UNDER SIMULATED *IN SITU* CONDITIONS

4.1 Introduction

Per- and polyfluoroalkyl substances (PFASs) are a family of emerging contaminants that have been synthesized for use in various applications and products since the mid-20th century [1,2]. Their widespread use has inadvertently led to global contamination of groundwater, surface water, and drinking water [3–7], raising concerns about adverse health effects [8]. Two of the most produced and studied compounds are perfluorooctane sulfonate (PFOS), a perfluoroalkane sulfonic acid (PFSA), and perfluorooctanoate (PFOA), a perfluoroalkyl carboxylic acid (PFCA) [9]. The United States Environmental Protection Agency (U.S. EPA) recently determined health advisory levels (HALs) for PFOS and PFOA in drinking water at 0.07 μg/L, both separately and combined [10]. In addition, many states and countries have developed their own water guideline levels.

Treatment technologies such as adsorption to activated carbon, ion exchange, and membrane filtration have been successfully used to remove PFASs from impacted water [11–13]. However, these removal processes generate concentrated PFAS waste streams that are often disposed of in landfills, simply transferring these persistent organic pollutants to a different environmental compartment [14]. Clearly, destructive treatment of PFAS-impacted media is desirable. However, Fenton-based advanced oxidation processes (AOPs) are ineffective for the degradation of perfluoroalkyl acids (PFAAs) such as PFSAs and PFCAs [15]. Technologies that have been shown to mineralize PFAAs include incineration [16], sonolysis [17], plasma treatment [18], reductive defluorination with hydrated electrons [19], and hydrothermal alkaline treatment [20]. Unfortunately, these technologies are difficult to impossible to install *in situ* for groundwater remediation. Yet, *in situ* treatment is often desirable for several potential reasons, such as lower costs, less surface infrastructure disruption, lower environmental footprint compared to *ex situ* approaches, and partial treatment of groundwater contaminants without the need to meet regulatory (discharge) limits.

In recent years, the interest in electrochemical oxidation (EO) has been growing due to its energy efficiency, operational simplicity, adaptability, and its capability in mineralizing the most recalcitrant organic pollutants including PFASs [21–25]. Using mesh electrodes, electrochemical water treatment can be implemented *in situ*, for instance as a permeable reactive barrier (PRB) without active pumping, using the natural hydraulic gradient of the groundwater [26–28]. However, several knowledge gaps exist that must be addressed before considering the *in situ* electrochemical oxidation of PFASs. First, previous studies on passive-flow EO systems have only investigated environmental contaminants that are susceptible to indirect electrochemical oxidation processes involving reactive oxygen species (ROS). In contrast, PFAA mineralization requires direct electron transfer (DET) at the very surface of the anode. DET is considered the rate-limiting step for electrochemical PFAS oxidation, and its notorious mass transfer limitations are typically overcome by pumping at high flow rates [23]. Second, no information is available about the

performance of different mesh anode materials and the impacts of process parameters regarding the electrochemical oxidation of PFAAs in slow passive-flow systems. Efficient DET processes require anode materials with a high oxidation evolution potential and stability. Three common anode materials that have been shown to effectively mineralize PFAAs, listed in the order of decreasing cost [27,29], are boron-doped diamond (BDD) [30,31], Magnéli-phase titanium suboxides Ti_nO_{2n-1} [22,32], and metal oxides such as RuO_2 [33]. Third, critical questions remain as to the fate of PFAA breakdown products in electrochemical systems, especially related to the generation of volatile species and shorter-chain PFAA intermediates [2,23,30,34,35]. This is a particularly critical knowledge gap to address for *in situ* remediation, where the treated water is not discharged to a treatment plant but remains in the aquifer.

Consequently, to explore the potential of EO for the *in situ* treatment of PFAS-impacted groundwater, we compared the performance of Magnéli-phase Ti_nO_{2n-1}, Ti/IrO_2-Ta_2O_5, and boron-doped ultrananocrystalline diamond (UNCD) mesh anodes in a bench-scale flow-through reactor and evaluated the potential for oxidation by-product formation as well as the sustainability parameters energy consumption and material usage [28]. The effects of key parameters such as current density, seepage velocity, and both electrolyte and PFAS concentrations on the PFAS degradation rates were investigated. Furthermore, we tracked the fate of fluorine in the various phases under slow flow conditions representative of groundwater. Finally, we assessed the electrochemical oxidation rates of several PFSAs and PFCAs as a function of chain length and branching.

4.2 Materials and Methods

4.2.1 Chemicals

PFOS was supplied from Sigma-Aldrich (>98% purity, mixture of branched and linear isomers, St. Louis, MO, USA). All other native PFAAs and corresponding heavy isotope-labeled species to be used as internal standards were purchased from Wellington Laboratories Inc. (Guelph, ON, Canada) with a purity of >99%. Na_2SO_4, NaCl, HCl, and NaOH (>99% purity) were used as received from various chemical suppliers. All solutions were prepared with Milli-Q water (18.2 MΩ cm^{-1} resistivity, 25 °C) from a Nanopure Barnstead Diamond^{TM} purification system (Thermo Scientific, Waltham, MA, USA).

4.2.2 Flow-through electrochemical reactor

EO experiments were carried out in a flow-through reactor (poly (methyl methacrylate)) with a volume of 100 mL (Figure 20). This electrochemical cell held two mesh electrodes (1.0 mm thick with 11 cm in height and length, and approximately 1 x 3 mm diamond-shaped openings) separated at 4 mm by a rubber gasket. Ti/IrO_2-Ta_2O_5 mesh electrodes (Corrpro Companies Inc., Medina, OH, USA) served as cathode [36]. Three materials were tested as mesh anodes: (1) BDD-type UNCD on a niobium substrate (Advanced Diamond Technologies Inc., Romeoville, IL, USA), (2) titanium mesh coated with Magnéli-phase titanium suboxides Ti_nO_{2n-1} (Magneli Materials, LLC, New Canaan, CT, USA), and (3) the commercially available mixed metal oxide Ti/IrO_2-Ta_2O_5, which to the best of our knowledge is tested here for anodic PFAS oxidation for the first time. The

interior dimensions of the flow-through electrochemical reactor mimicked those of a commercially available electrochemical parallel plate reactor with a UNCD anode that is operated at high flow rates (Advanced Diamond Technologies Inc., Romeoville, IL, USA) [37].

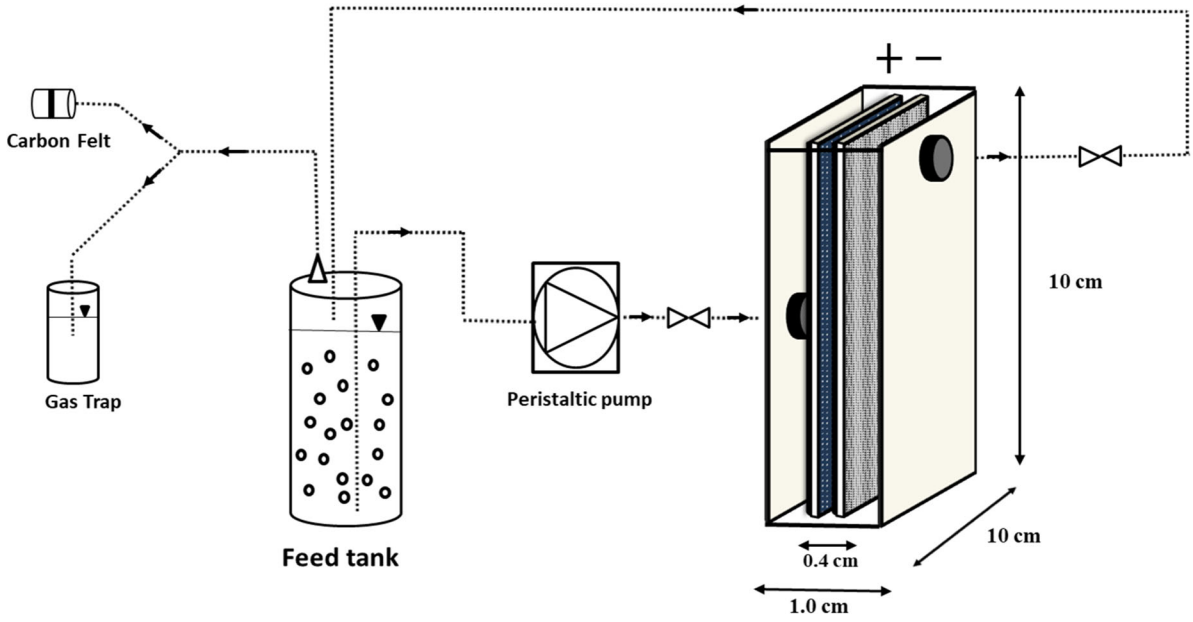

Figure 20: Schematic of the flow-through electrochemical reactor system showing the interior dimensions of the reactor and the 0.4 cm electrode spacing. While the influent was at the center of one side, the effluent was at the top of the opposite side to ensure that the reactor was completely filled with aqueous solution. The gas vent of the feed tank could be connected either to a base trap or to a carbon felt. The system could be operated in recirculation mode or in flow-through mode when the effluent was connected to a waste container.

A 1-L polypropylene feed tank held 250 mL of influent PFAS solution, which was pumped through or recirculated within the electrochemical reactor system. Both reactor inlet and outlet lines (high-density polyethylene) were equipped with two liquid sampling ports to collect samples over time. The closed feed tank's gas vent could be connected either to a carbon felt cartridge or to a 0.1 M NaOH gas trap to capture volatile organofluorine compounds and HF [37].

4.2.3 Electrochemical oxidation experiments

EO experiments were performed using a bench-top direct current (DC) power supply (GW Instek® GPS-3030D, Montclair, CA, USA) in potentiostatic or galvanostatic mode. Like previous studies on the electrochemical oxidation of PFASs, Na_2SO_4 and NaCl were chosen as supporting electrolytes in synthetic groundwater [21,37]. While Na_2SO_4 concentrations were varied in the experiments, a constant concentration of 10 mg/L NaCl served the purpose of investigating the formation of the suspected oxidation by-products chlorate and perchlorate [21,38].

Aqueous samples (100 µL for PFAS analysis and 600 µL for fluoride analysis) were obtained from the feed tank in recirculation mode and from the outlet sampling port in flow-through mode after shutting down the EO system. Samples for PFAS analysis were immediately diluted 1:1 with methanol (UHPLC Plus, Sigma-Aldrich, St. Louis, MO, USA) including isotope-labeled internal standards in 2-mL LC vials holding 250-µL polypropylene vial inserts (Restek, Bellefonte, PA, USA) with polypropylene caps (Phenomenex, Torrance, CA, USA). PFAS samples were stored at ambient temperature and analyzed within three days after the final sample was taken. Fluoride samples were analyzed immediately.

To assess the energy requirements of the EO treatment, the electric energy per order of PFOS removed (E_{EO}) was calculated by the following (Eq.1):

$$E_{EO}\left(\frac{kWh}{m^3}\right) = \frac{P\,t}{V\,log\left(\frac{C_0}{C_t}\right)} \quad \text{(Eq.1)}$$

where P is power (kW), t is treatment time (h), V is the treated water volume (m^3), and C_0 and C_t are initial and final PFOS concentrations, respectively. Alternatively, the electric energy per order of PFOS-bonded fluorine removed ($E_{EO,F}$) was determined as a more accurate descriptor of fully mineralizing PFOS by one order of magnitude in a unit volume of contaminated water.

As major capital cost driver, the anode surface area per order of contaminant removed (ASA_O) or per order of PFOS-bonded fluorine removed was calculated using [37]:

$$ASA_O\left(\frac{m^2h}{m^3}\right) = \frac{A\,t}{V\,log\left(\frac{C_0}{C_t}\right)} \quad \text{(Eq.2)}$$

where A is the apparent anode area (m^2).

The reactor was thoroughly cleaned between experiments by extensive flushing with PFAS-free electrolyte solution and with methanol, both with and without applied voltage, until effluent samples showed no background contamination.

4.2.4 Chemical analyses

PFASs were analyzed on an Agilent 1290 liquid chromatograph coupled to an Agilent 6460 triple quadrupole mass spectrometer (LC/QqQ-MS) equipped with an electrospray ionization (ESI) source (Agilent, Santa Clara, CA). The analytes were separated on an Agilent Poroshell C18 column (2.1 mm x 100 mm, 2.7 µm particle size) at 40 °C. A sample volume of 15 µL was injected into a binary mixture of 5 mM ammonium acetate in water (A) and 5 mM ammonium acetate in methanol (B) at a flow rate of 0.4 mL/min. The gradient used was 20% B for 1 minute, increasing to 45% B at 2 min, and finally increasing to 100% B at 5 min. Analytes were identified by comparison of retention times with analytical standards, individual multiple reaction monitoring mass transitions, and with MS/MS ion ratios. To minimize system-related interferences or background, an Agilent Eclipse Plus C18 column (4.6 mm x 50 mm, 5 µm particle size) was installed as a delay column. Five injections of pure methanol were made prior to sample analysis

to ensure that no system background analytes were present. Further details of our analytical method can be found in Singh Kalra et al. (2021) [17].

Ion chromatography on a Dionex Integrion HPIC (Thermo Fisher Scientific, USA) with a conductivity detector was used to quantify fluoride, chloride, chlorate, and perchlorate. The columns were a Dionex™ IonPac™ AG20 Guard Column (4 x 50 mm) and a Dionex™ IonPac™ AS20 Analytical Column (4 x 250 mm) operated at 30 °C. Chromatographic separation of anions, including verified baseline separation of fluoride and formate, was achieved using an aqueous hydroxide mobile phase gradient ramping from 0.5 mM to 55 mM at a flow rate of 1 mL/min for a total run time of 35 min plus 10 min of equilibration time between runs. The quantification limit for all four anions was 7.0 μg/L.

Particle-induced gamma-ray emission (PIGE) spectroscopy was conducted at the University of Notre Dame according to previous publications.

4.2.5 Quantum chemical calculations

Density functional theory calculations were carried out at the unrestricted ωB97-XD/6-311+G(2d,2p) level of theory with the Polarizable Continuum Model (PCM) for implicit water solvation using Gaussian 09, Revision B.01, to determine free energies of activation for DET. The crossing points between potential energy surfaces along a linearized reaction coordinate for the neutral parent compound and the one-electron oxidation product were calculated as a function of anode potential. The details of our computational approach are documented in Pica et al. (2019) [37]. The ωB97-XD functional was chosen because standard DFT approaches such as B3LYP significantly overestimate the impact of long-range charge transfer by underestimating the non-local nature of electron exchange [39]. This level of theory has previously been successfully applied to investigate the reductive dehalogenation of PFASs [40].

4.3 Results and Discussion

4.3.1 Performance comparison of mesh anode materials

The choice of anode material affects the efficiency of the electrochemical treatment processes as well as the formation of potentially problematic oxidation by-products. To determine the performance of the three tested mesh anodes, we evaluated the electrochemical oxidation of PFOS at a high concentration of 5000 μg/L in recirculation mode at a constant current density of 60 mA/cm^2, a seepage velocity of 60 cm/d (i.e., one reactor volume exchange per 0.4 h), and Na_2SO_4 and NaCl concentrations of 500 mg/L and 10 mg/L, respectively. The pseudo-first order PFOS oxidation half-life $t_{1/2}$ (2.2 h) and the electric energy per order of PFOS removed E_{EO} (4000 kWh/m^3) were lowest with the Magnéli-phase Ti_nO_{2n-1} anode (Figure 21), followed by IrO_2-Ta_2O_5 (3.3 h and 4500 kWh/m^3) and UNCD (5.5 h and 9600 kWh/m^3). Porous Ti_nO_{2n-1} is known to have a high electro-active surface area, favoring high contaminant oxidation rates and low energy consumption [41]. The higher degradation rate of the "active" IrO_2-Ta_2O_5 mesh anode compared to the "non-active" UNCD mesh anode was unexpected given the higher oxygen evolution potential (OEP) and thus reactivity towards organic solutes of the BDD material [27,42]. The

energy consumption was roughly two orders of magnitude higher than what previous studies on electrochemical PFAS degradation have achieved in high-flow electrochemical reactors [43]. As alluded to previously, our flow-through reactor was designed with the same geometry as a commercial parallel plate reactor with a UNCD anode [37], albeit with one minor difference being that the commercial cell uses a stainless steel cathode instead of Ti/IrO_2-Ta_2O_5. Using a high flow rate of 3 L/min under otherwise comparable conditions, we achieved an E_{EO} of 94 kWh/m^3 for PFOS treatment in the commercial cell, roughly 100 times lower than the 9600 kWh/m^3 obtained in the low-flow reactor at 0.004 L/min simulating *in situ* groundwater conditions. Consequently, mass transfer significantly impacts the efficiency of electrochemical PFOS treatment using mesh electrodes, as frequently observed in previous electrochemical treatment studies [44].

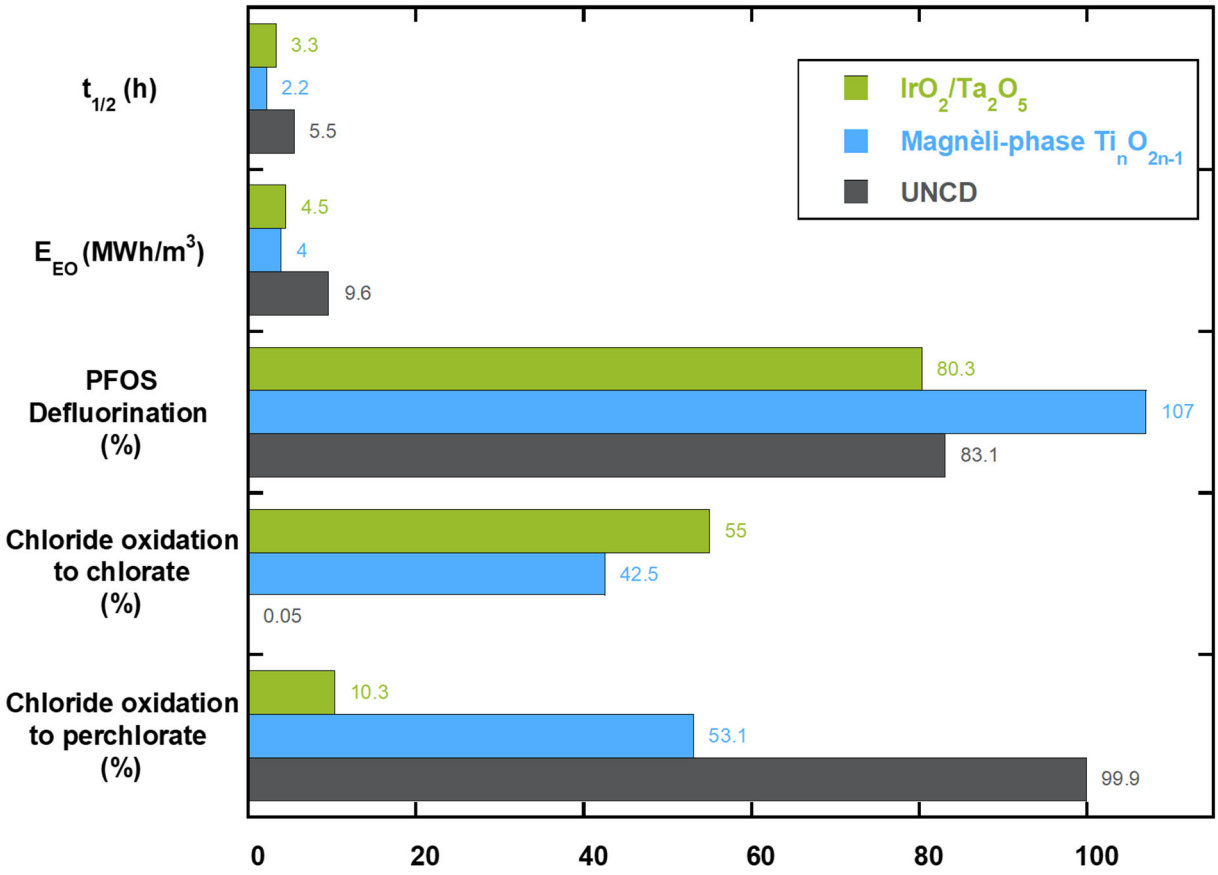

Figure 21: Comparison of mesh anode materials for electrochemical PFOS oxidation based on half-life ($t_{1/2}$), electric energy per order (E_{EO}), PFOS defluorination (%), and both chlorate and perchlorate generation (%). Experimental conditions: current density 60 mA/cm^2, seepage velocity 60 cm/d, PFOS concentration 5000 µg/L, Na_2SO_4 concentration 500 mg/L, NaCl concentration 10 mg/L.

The PFOS defluorination efficiency was highest (and complete) for the Magnéli-phase Ti_nO_{2n-1} (107%), indicating a low potential for the formation of organofluorine intermediates, while only

some 80% of the fluorine in the degraded PFOS was recovered when IrO_2-Ta_2O_5 and UNCD mesh anodes were used.

The oxidation by-products chlorate and perchlorate were produced by all three materials; however, the extent of chloride oxidation was the lowest using Ti/IrO_2-Ta_2O_5 (55.0% chlorate and 10.3% perchlorate within 6 hours). The lower generation of chlorine oxyanions on this mixed metal oxide is due to its lower OEP of 1.5-1.8 V vs. standard hydrogen electrode (SHE). Ti_nO_{2n-1} and BDD have a higher OEP around 2.6 V vs. SHE [45,46], resulting in a higher degree of chloride oxidation on Ti_nO_{2n-1} (42.5% chlorate, 53.1% perchlorate) and near-complete oxidation on UNCD (0.05% chlorate, 99.9% perchlorate). This finding is in agreement with preview studies, which have observed total conversion of Cl^- to ClO_4^- during electrochemical treatment operating with a BDD anode [21,47].

Based on faster oxidation kinetics, higher defluorination rate, and lower energy consumption, the Magnéli-phase Ti_nO_{2n-1} mesh anode was chosen for further testing in subsequent experiments. Even though the higher generation of chlorine oxyanions using the Magnéli-phase Ti_nO_{2n-1} mesh anode compared to the Ti/IrO_2-Ta_2O_5 mesh anode was considered a minor disadvantage, both the use of either material would require a secondary treatment step and microbial reduction of chlorate and perchlorate can be readily achieved [21]. We note that while PFOS oxidation kinetics were relatively rapid at a current density of 60 mA/cm^2, we observed high water temperatures and steam generation in the feed tank. Thus, current densities above 50 mA/cm^2 were avoided in the following experiments.

4.3.2 Impacts of varying process parameters on PFOS mineralization

To test the impact of process parameters on the efficiency of electrochemical PFOS mineralization, we determined pseudo-first order half-lives, electric energy per order ($E_{EO,F}$) and anode surface area per order ($ASA_{O,F}$) of fluoride released as a function of current density, electrolyte concentration, seepage velocity, and initial PFOS concentration (Figure 22). The EO experiments were carried out in flow-through mode using the Magnéli-phase Ti_nO_{2n-1} anode. The baseline conditions from which the individual parameters were varied included a current density of 50 mA/cm^2, a seepage velocity of 60 cm/d, a PFOS concentration of 1000 μg/L, and a Na_2SO_4 concentration of 500 mg/L.

Both the kinetic parameter $t_{1/2}$ and the two sustainability indicators showed a clear improvement (i.e., a decrease) when the current was increased from 30 mA/cm^2 to 40 mA/cm^2, but only a minor improvement when further increasing to 50 mA/cm^2 (Figure 22A), suggesting current-limited conditions occurred below 40 mA/cm^2 [48,49].

By increasing the electrolyte concentration, $t_{1/2}$ values increased from 1.4 h to 2.0 h and 3.2 h operating at 250, 500, 1000 mg/L Na_2SO_4, respectively (Figure 22B). In contrast, only slight increases in $E_{EO,F}$ and $ASA_{O,F}$ values were obtained under the same electrolyte conditions, likely due to less electrical resistivity at higher electrolyte concentrations. The increasing PFOS half-life with increasing Na_2SO_4 concentration may be due to competition for DET under current-limiting conditions given that sulfate can be electrochemically activated/oxidized [37,50] and was about

three orders of magnitude more abundant than PFOS. Yet, the generated sulfate radicals are known to be unreactive towards PFSAs [51], thus not facilitating PFOS degradation in EO systems.

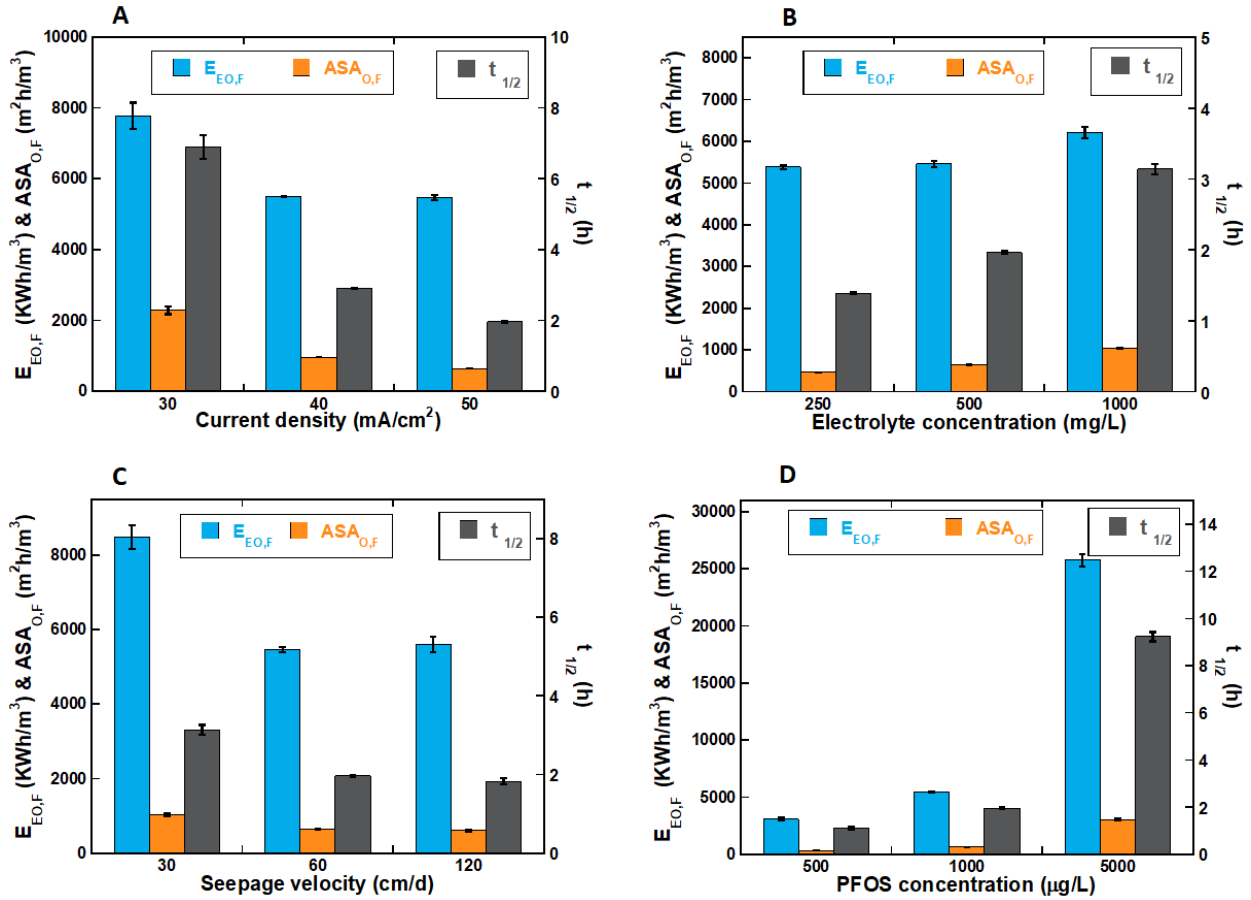

Figure 22: Impacts of current density (A), Na_2SO_4 electrolyte concentration (B), seepage velocity (C) and initial PFOS concentration (D) on the PFOS oxidation half-life ($t_{1/2}$), electric energy per order ($E_{EO,F}$) and required anode surface area per order ($ASA_{O,F}$) of fluorine released as aqueous fluoride. The EO experiments were completed in flow-through mode using Magnéli-phase Ti_nO_{2n-1} and Ti/IrO_2-Ta_2O_5 as anode and cathode, respectively.

Variations in seepage velocities showed a decreasing PFOS half-life, $E_{EO,F}$, and $ASA_{O,F}$ with an increase from 30 cm/d to 120 cm/d (Figure 22C). At higher flow rate, better removal of O_2 gas generated from water electrolysis likely increased mass transfer through enhanced wetting of the anode surface [36].

With increasing initial PFOS concentrations, all three parameters $E_{EO,F}$, $ASA_{O,F}$ and $t_{1/2}$ increased (Figure 22D). As reported in previous studies, a high initial contaminant concentration may lead to a higher concentration of transient intermediates which compete for DET with the parent contaminant on the anode surface, reducing the observed degradation efficiency [52]. The apparent concentration-dependence suggests current limitations in addition to mass transfer limitations under these treatment conditions [53].

4.3.3 Fate of fluorine during anodic PFOS oxidation

Many previous electrochemical studies have reported incomplete fluorine mass balances, impeding a reliable assessment regarding the potential formation of problematic intermediates. A critical knowledge gap concerns the formation of volatile species that may escape into the atmosphere [23]. Consequently, we performed an experiment with an initial PFOS concentration of ~200 µg/L in recirculation mode to track the fate of fluorine in our system. The current density was 50 mA/cm^2, the seepage velocity was 120 cm/d, and the Na_2SO_4 and NaCl concentrations were 500 mg/L and 10 mg/L, respectively.

Figure 23A shows that after a short lag time in the system, the concentration of PFOS-bonded fluorine dropped continuously from 121 µg/L to 0.36 µg/L after 74 h of treatment, equivalent to 99.7% of PFOS removal. In addition, 83.5% of the fluorine originating from PFOS, equivalent to an aqueous concentration of 101 µg/L, was recovered as aqueous fluoride, indicating that cleavage of the carbon-fluorine bond had been achieved as a result of electrochemical oxidation. Several previous studies have reported transient electrochemical transformation of PFOS to PFOA and successively shorter-chain PFCAs [35,48,54]. However, our sensitive LC/QqQ-MS analysis did not detect any aqueous PFCAs at a quantification limit of 5 µg/L (i.e., ~2.5% of the initial PFOS concentration). Consequently, at the end of this experiment, >15% of the initial fluorine in PFOS was not accounted for in the aqueous phase.

In an effort to close the fluorine mass balance, we analyzed the effluent gas generated during the electrolysis of water. The IC analyses of fluoride recovered in the gas trap showed that 2.0% of the initial PFOS-bonded fluorine had been volatilized from the feed tank as HF. Additional fluorine was detected via PIGE, equivalent to 2.2 µg/L or 1.8% of the initial PFOS-bonded F. A control experiment in which HF gas was equilibrated with the carbon felt showed that even full conversion of the 200 µg/L PFOS to HF would not have been detectable by PIGE due to poor adsorption of HF to the carbon felt. Consequently, the 1.8% of fluorine detected by PIGE was likely volatile organofluorine compounds.

Despite our best efforts to close the fluorine mass balance, 12.4% of fluorine remained unaccounted for in the EO system (Figure 23B). Other loss mechanisms for fluorine exist that would have escaped our analytical techniques. For instance, at high anodic potentials, fluoride may be oxidized to F_2 gas [23]. Transient organic intermediate products other than PFCAs may have been formed, whose identification through non-targeted high-resolution mass spectrometry and quantification, however, would have been severely challenged by low concentrations and availability of reference standards, respectively. Furthermore, sorptive losses to the reactor materials may have occurred as supported by the decline in total aqueous fluorine within the initial period of the experiment (Figure 23A) as well as by the findings of the experiment reported below.

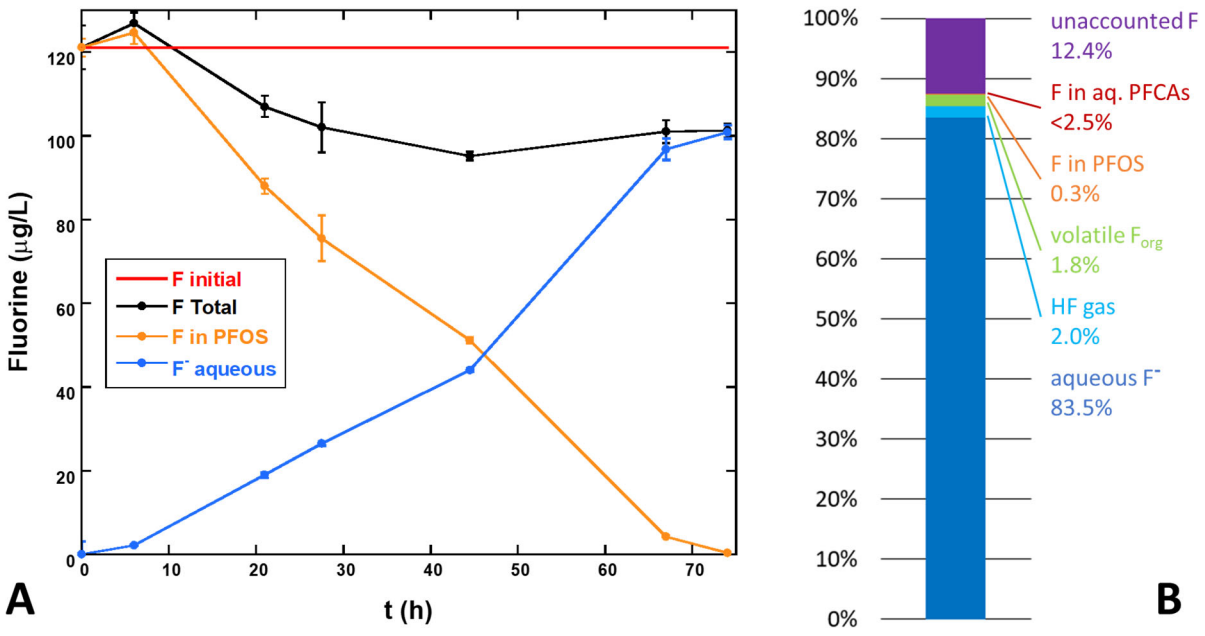

Figure 23: A) Aqueous fluorine mass balance for the electrochemical oxidation of ~200 µg/L PFOS at a Magnéli-phase Ti_nO2_{n-1} mesh anode, showing the time-dependent concentrations of F bonded in the parent PFOS (orange), generated fluoride in aqueous solution (blue) and the sum of these two species as total F (black). The red line indicates F concentration in the system at the start of the experiment. B) Total fluorine mass balance at the end of the 74-hour experiment.

A specific knowledge gap that has not been sufficiently addressed is whether fluorination of the anode during electrochemical PFAS oxidation may occur [55]. Consequently, we used PIGE spectroscopy to probe the extent and nature of PFOS adsorption to the mesh anode. Due to the low PFOS concentrations in our experiments, we recovered the used Ti_nO_{2n-1} anode after multiple experiments (Figure 22 and Figure 23) to enable sufficient accumulation of fluorine, and thus acknowledge that our PIGE analysis is not quantitative with respect to the fluorine mass balance shown in Figure 23B. After rinsing with DI water and air-drying, the used anode showed a significantly higher signal of 482 ± 35 counts/µC compared to an unused mesh anode (180 ± 22 counts/µC), indicating that fluorine had accumulated at the anode surface during treatment. When the used anode was subsequently extracted with pure methanol for 30 minutes, the PIGE signal dropped to 214 ± 22 counts/µC, not significantly higher than for the unused mesh anode. This observation implies that the association of fluorine and/or fluorine-bearing organic species to the Magnéli-phase Ti_nO_{2n-1} anode were due to physisorption rather than through formation of covalent bonds at the surface.

Finally, we tracked the fate of chlorine throughout the 74-h treatment experiment (Figure 24) to further evaluate the generation of oxidation by-products. Specifically, 87% of the initial chloride was oxidized within the first 6 hours of treatment, leading to rapid generation of chlorate and

subsequent slower oxidation to perchlorate. A ~25% deficit in the aqueous chlorine mole balance was observed during the initial period of maximum chloride oxidation to chlorate, likely due to the intermediate generation and (partial) volatilization of Cl_2 and HOCl gasses [38].

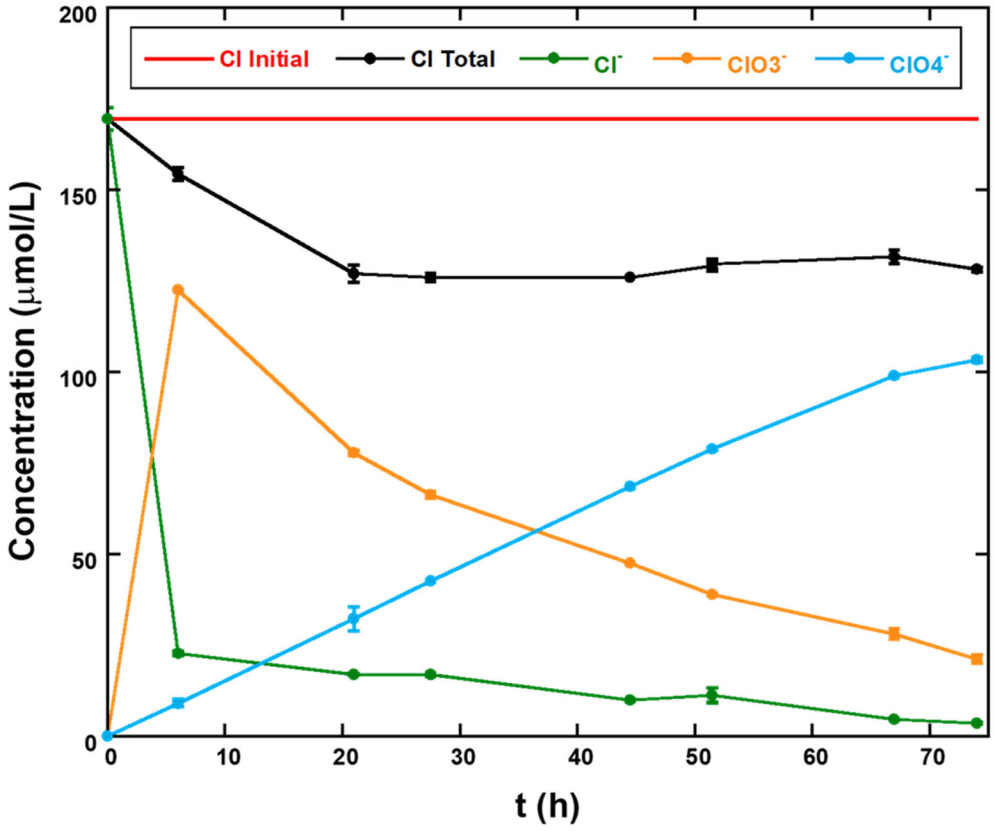

Figure 24: Chlorine mole balance for the PFOS degradation experiment illustrated in Figure 4 of the main manuscript, showing aqueous chloride (green), chlorate (orange), and perchlorate (blue) concentrations as well as the sum of these three species as total chlorine (black) as a function of electrochemical oxidation time. The red line indicates the initial chlorine concentration in the reactor system at the start of the experiment.

4.3.4 Comparison of electrochemical oxidation kinetics for PFCAs and PFSAs

Previous studies have reported contradictory results regarding the EO kinetics of PFSAs compared to PFCAs. While most studies have observed faster degradation of PFCAs, Wang and co-workers (2020) witnessed faster PFSA oxidation at a Ti_4O_7 anode [23,25]. To investigate the EO kinetics as a function of chain length and terminal functional group at the Magnéli-phase Ti_nO_{2n-1} mesh anode, we tested the simultaneous degradation of various PFAAs under similar conditions as in Section 3.3, i.e., a seepage velocity of 120 cm/d and Na_2SO_4 and NaCl concentrations of 500 mg/L and 10 mg/L, respectively. The current density was slightly lower at 45 mA/cm^2, with negligible differences expected compared to 50 mA/cm^2 based on the observations in Figure 22C. The

concentrations of the species was ~25 µg/L each, approximately one order of magnitude below the PFOS concentration used in the experiment above and sufficiently dilute so that competition between PFASs for active anode adsorption sites can be neglected [25]. However, before applying a potential to the electrodes, the synthetic groundwater solution was circulated in the reactor system for two hours to assess adsorption losses. As Figure 25 shows, adsorption was negligible for PFCAs with ≤8 carbon atoms, while losses of 37 ± 6% and 73 ± 3% were observed for the long-chain species perfluorononanoate (PFNA) and perfluorodecanoate (PFDA). Among the more hydrophobic PFSAs, losses in perfluorobutane sulfonate (PFBS) and perfluorohexane sulfonate (PFHxS) were negligible, while the PFOS concentration decreased by 24 ± 7%.

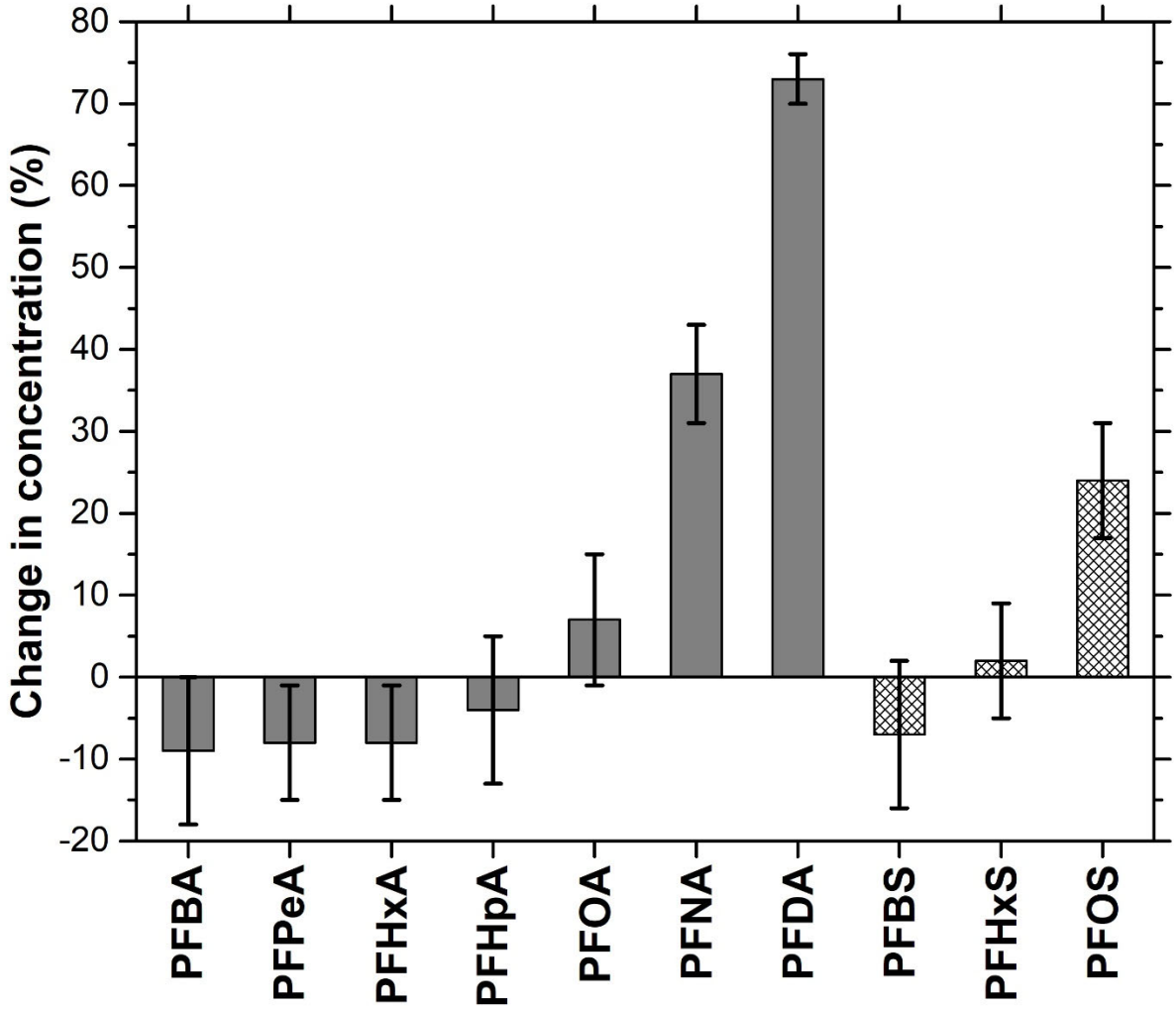

Figure 25: Change in PFAS species concentration (%) during the two hours in the reactor system prior to applying a potential, indicating sorption losses.

During electrochemical treatment, two general reactivity trends were observed (Figure 26): (1) PFCAs ($0.0182 \pm 0.0003 – 0.0389 \pm 0.0041$ h^{-1}) were removed faster than PFSAs ($0.0047 \pm 0.0005 – 0.0242 \pm 0.0024$ h^{-1}) with the same number of fluorinated carbon atoms; and (2) first-order rate constants increased with increasing chain length (Figure A 1 in Appendix A). The only exception to the latter observation was PFDA, whose concentration had substantially decreased upon adsorption within the first two hours prior to applying a potential. Further losses in the fluorine mass balance during the first few hours of the experiments suggested ongoing PFAS adsorption (Figure 27). A final fluorine recovery of 85% in the aqueous phase calculated from the sum of PFAS-bonded F and aqueous F^- suggested a similar fate of fluorine as determined in Figure 23B.

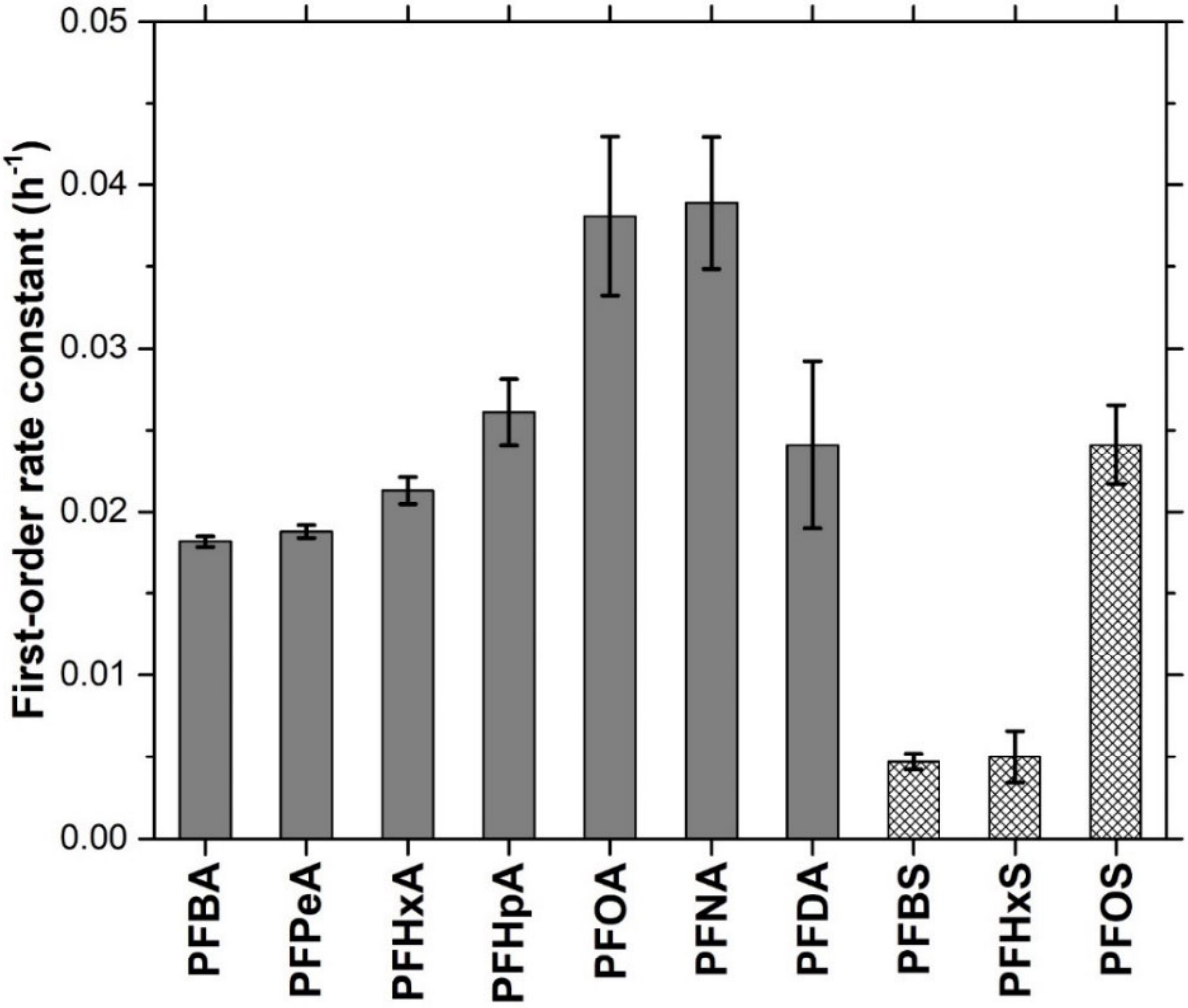

Figure 26: Observed pseudo-first-order rate constants for seven PFCAs (solid) and three PFSAs (shaded) undergoing oxidation at a Magnéli-phase Ti_nO_{2n-1} mesh anode.

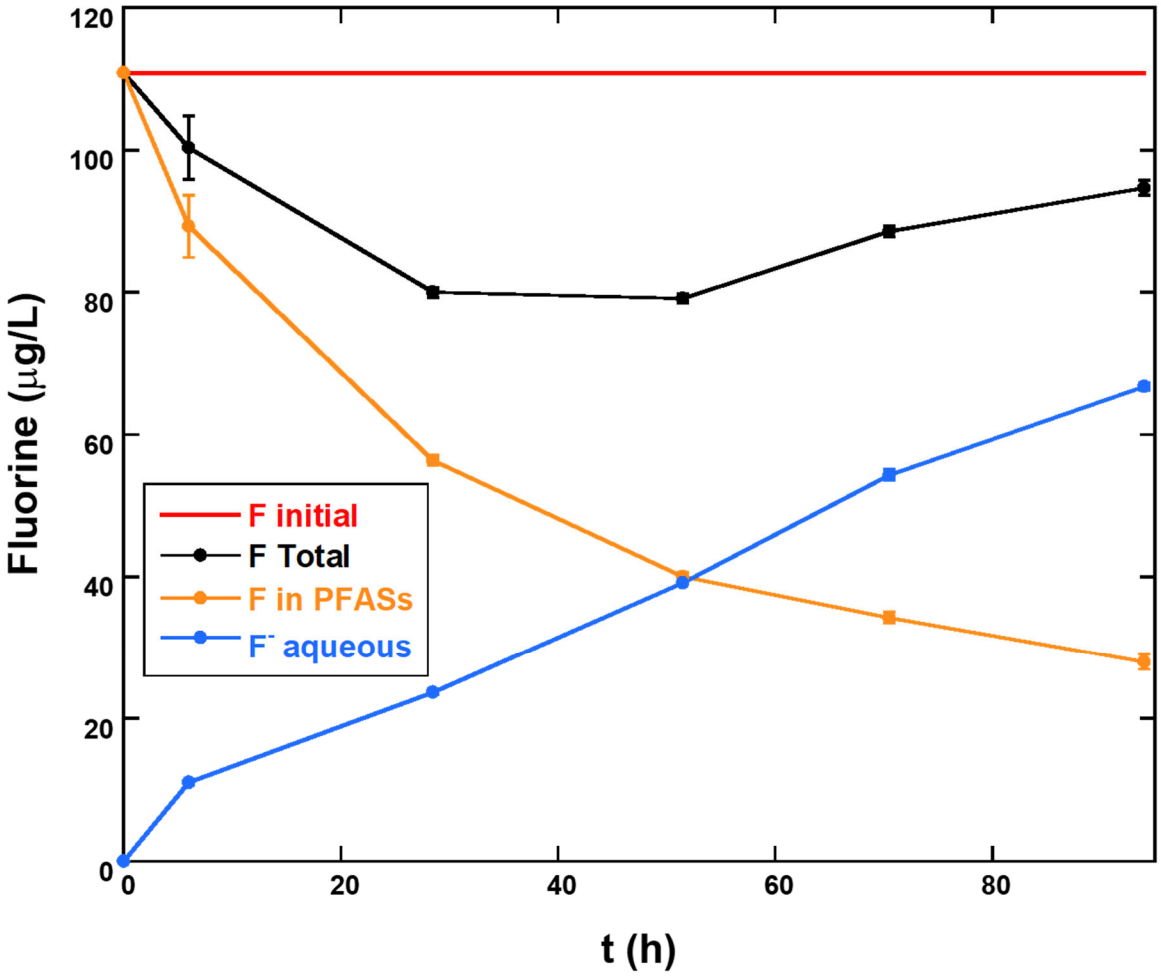

Figure 27: Fluorine mass balance for the simultaneous electrochemical oxidation of 10 perfluoroalkyl acids, showing fluorine concentrations in PFASs (orange), in aqueous solution (as fluoride, blue), and the sum of these two species as total fluorine (black) as a function of electrochemical oxidation time. The red line indicates the fluorine concentration in the system at the start of the experiment, corrected for adsorption losses observed in the first two hours prior to applying a potential (Figure 25).

Differences in EO kinetics can in theory be caused by several compound-specific factors, such as diffusivity, activation barrier, hydrophobicity, and reactivity towards co-occurring chemical species. Despite the observed mass transfer limitations, diffusivity did not appear to be a governing factor as diffusion coefficients decrease with increasing chain length, favoring short-chain PFASs [56]. Our DFT calculations in Figure 28A showed that there were no considerable differences in chain length-dependent activation free energies for DET among PFCAs (PFBA, PFHxA, PFOA) and PFSAs (PFBS, PFHxS, PFOS). This finding is in agreement with standard reduction potentials E^0 predicted by Radjenovic and co-workers (2020) [23], but contrasts findings by Li et al. (2021), who reported a low DET activation barrier for PFBS but subsequent C-S bond breakage being the

rate-limiting step [57]. Furthermore, perfluoroalkyl chain branching, which may impact electrochemical oxidation kinetics but has not been sufficiently studied to date [23,58], did not affect the dependence of anode potential on the free energy of activation (Figure 28B). Yet, PFSAs were found to require slightly higher anode potentials than PFCAs (Figure 28A); while DET becomes barrierless for PFCAs at an anode potential versus standard hydrogen electrode E_{SHE} of 3.1 V, PFSAs require an E_{SHE} of 3.3 V. The calculated potential for PFCAs here was slightly higher than the E^0 of 2.9-3.0 V predicted by Radjenovic et al. (2020) [23] and for PFSAs lower than the 3.7 V predicted by Radjenovic et al. (2020) [23] and Shi et al. (2019) [35]. We note, however, that the ωB97-XD functional used in this study more accurately treats the non-local nature of electron exchange than previously used functionals [39]. Nevertheless, the relatively minor differences in potential-driven activation free energies for DET between PFCAs and PFSAs cannot explain the observed differences in electrochemical oxidation kinetics as the anode potential was higher than required for barrierless DET at the applied potential of ~20 V (Figure 29).

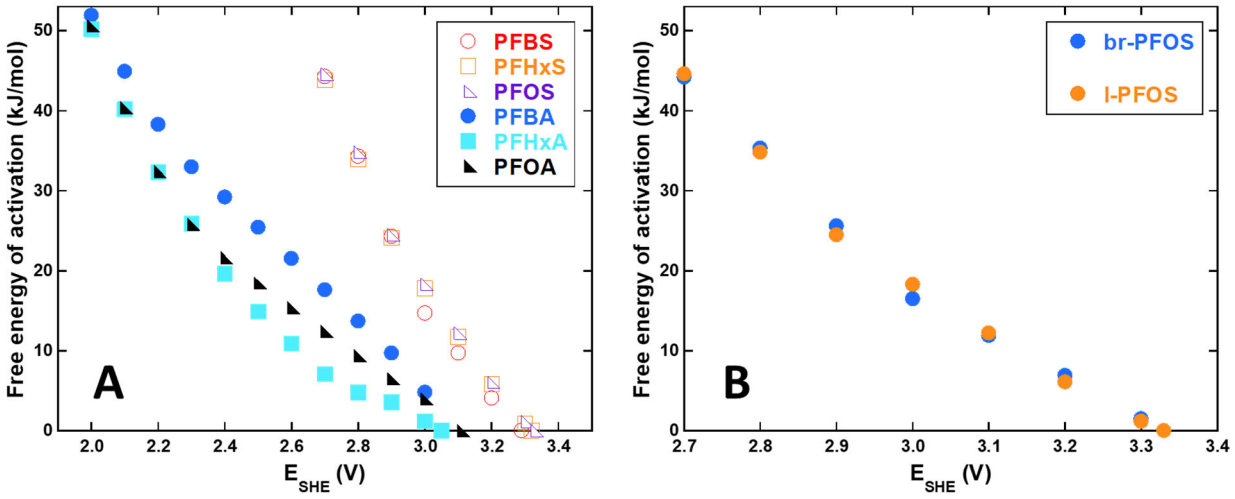

Figure 28: Density functional theory calculations of free energies of activation for direct electron transfer as a function of anode potential at the PCM/ωB97-XD/6-311+G(2d,2p) level of theory. A: PFSAs require higher anode potentials than PFCAs but impacts of chain length are negligible. B: Branched PFOS (br-PFOS) and linear PFOS (l-PFOS) show no difference in anode potential dependence on electrochemical oxidation kinetics.

More likely, the difference in reactivity as a function of chain-length can be explained by the more hydrophobic character of longer-chain PFASs, favoring adsorption to the anode surface [23]. This effect, however, cannot explain the observed difference in EO kinetics between PFCAs and their more hydrophobic PFSA counterparts. Given the anode potential was high enough to ensure barrierless DET for both classes, it appears plausible that electrochemically activated sulfate contributed to the removal of PFCAs [50]. Sulfate radicals are known to oxidize PFCAs but not PFSAs [15].

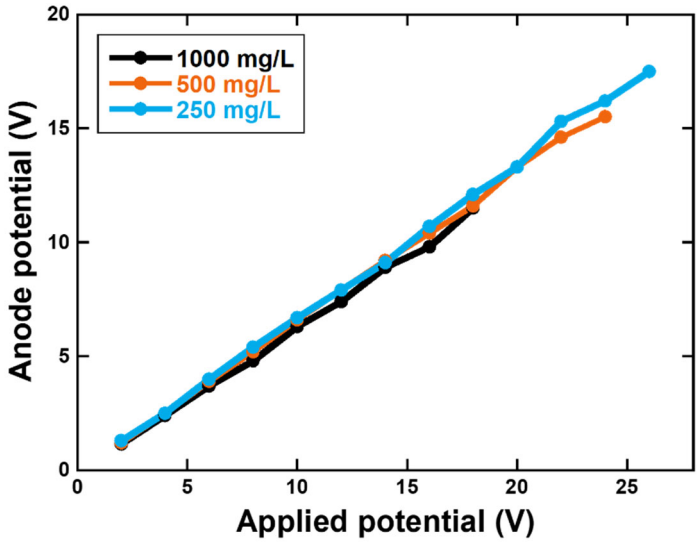

Figure 29: Anode potentials on the Magnéli-phase titanium suboxide surface as a function of Na_2SO_4 concentration and applied potential, measured against a flexible Ag/AgCl reference electrode (Flex-Ref; World Precision Instruments, Sarasota, FL).

4.4 Cost Comparison

To acquire a first rough understanding of treatment costs for this novel approach, we performed a cost estimate for the *in situ* electrochemical removal of one order of magnitude of PFOS (e.g., from 690 ng/L to 69 ng/L below the U.S. EPA health advisory for drinking water) and compared it to the estimated costs of incineration, currently the only destructive technology for PFASs available at the full scale. We note that this estimate bears great variability and given differences in hydrogeology, water quality, and other factors at impacted sites. Major parameters affecting the costs of *in situ* electrochemical groundwater treatment are as follows:

- Depth to water and other hydrogeological factors (e.g., sediment vs. rock).
- Electrode costs: PFAS-oxidizing anode possibly more expensive than cathode, whose sole purpose is to close the circuit.
- Durability of the electrode material.
- Electricity costs: may be mitigated by using solar power.
- Water quality: Especially precipitable species such as carbonate, calcium, and magnesium are of concern, and can degrade electrochemical oxidation performance rapidly if polarity reversals are not sufficiently frequent and long. This is the main reason why every single site needs individual performance pre-testing. Electrical conductivity of the water is an important parameter as well.

Other relevant parameters exist, some of which can be readily identified in Figure 22. In general, one of the major objectives during pilot testing should be the identification of an optimal voltage / current and polarity reversal schedule.

To obtain a reasonable, comparable cost estimate, we used the site parameters at Pueblo Chemical Depot (Colorado), where a 240 ft^2 *in situ* e^-Barrier had been built and a detailed cost estimate had been provided previously [26]. The average groundwater Darcy velocity at the site is 250 ft/y. Cost elements specific to the site but not specific to the contaminant were adopted with a total inflation of 25% since 2010. Other assumptions were:

- Replacement of electrodes every two years;
- Current density 50 mA/cm^2;
- ASA_O of 1,000 $m^2 \cdot h/m^3$ (based on 30 cm/d in Figure 22C);
- 10 years of operation.

Based on these assumptions, total costs of $2,000,000 can be expected, of which 25% are capital costs and 75% are operation & maintenance costs, largely driven by electrode service life (Table 3).

Table 3: Cost estimate for *in situ* electrochemical oxidation of one order of magnitude of PFOS in a 240 ft^2 e^-Barrier for 10 years total. Please note the assumptions stated in the text.

Cost element	Cost type	Description	Cost	Unit cost per ft^2
Material and panel fabrication	Materials (e^-Barrier)	Mesh anodes and cathodes	$ 146,136.82	$ 608.90
		Vinyl sheet pile	$ 4,011.00	$ 16.71
		Geonet/geoxtile	$ 309.00	$ 1.29
		Reference electrodes	$ 24,000.00	$ 100.00
	Materials (electrical system)	Solar array	$ 244,950.00	$ 1,020.63
		Miscellaneous hardware	$ 3,429.00	$ 14.29
		Data logger and communication syster	$ 3,639.00	$ 15.16
	Labor	Engineer/project lead	$ 13,749.00	$ 57.29
		Field Technician	$ 11,250.00	$ 46.88
	Subtotal		**$ 451,473.82**	**$ 1,881.14**
Installation	Contractor	Mobilization	$ 27,918.75	lump sum
		Installation	$ 8,874.00	$ 36.98
	Utilities	Solar array installation	$ 2,220.00	$ 9.25
	Labor	Engineer/project lead	$ 21,249.00	$ 88.54
		Field Technician	$ 7,500.00	$ 31.25
	Waste disposal	Off-site disposal of excavated soils	$ 2,694.00	$ 11.23
	Subtotal		**$ 70,455.75**	**$ 293.57**
Capital costs			**$ 521,929.57**	**$ 2,174.71**
Operational costs	Labor and expenses	Download data, review data, annual inspection for 10 years	$ 375,000.00	lump sum
Maintenance costs	Labor and expenses	Assuming 10-year life cycle with biannual exchange of electrodes	$ 1,099,038.29	$ 4,579.33
O & M costs			**$ 1,474,038.29**	**$ 6,141.83**
TOTAL COSTS		10 years of operation	$ 1,995,967.87	

These costs over 10 years are not insignificant, but likely considerably less compared to direct water incineration. At a Darcy velocity of 250 ft/y and a cross sectional area of 240 ft^2, 1,700 m^3

of groundwater would have to be incinerated per year, or 17,000 m^3 over a 10-year period. Based on personal communications with Chemours, the current costs of water incineration in the U.S. are on the order of $220 to $660 per m^3. In this example, using average incineration costs of $440 per m^3, the total costs over 10 years would amount to $7,480,000, not considering rather negligible costs for pumping well and piping installation (~$30,000) and electricity (~0.5 kWh per m^3). Clearly, direct water incineration, although currently practiced in the U.S., is inefficient. In this case, concentration prior to destructive treatment, for instance via nanofiltration [37], should be strongly considered.

4.5 Conclusions

In situ groundwater remediation technologies that can destroy PFASs are highly desirable. Previous work on other contaminants such as chlorinated solvents and energetic compounds has demonstrated that electrochemical oxidation can be implemented as an *in situ* PRB using mesh electrodes that remain operative for extended periods (>2 years) [26,59]. Our bench-scale performance testing of mesh electrodes in a flow-through EO reactor suggests that this approach may be a viable *in situ* solution for PFAS-impacted groundwater too, achieving >99% removal and full mineralization of highly refractory PFAAs as evidenced by fluoride release.

As with other destructive technologies, several challenges on the path to *in situ* implementation remain to be addressed. Some of our proof-of-principle experiments were conducted in recirculation mode. At field sites where recirculation may not be practicable, multiple electrode pairs need to be installed. The number of required electrodes must be determined based on site-specific parameters such as water quality, PFAS concentrations, and groundwater flow rate [28]. Furthermore, the high potentials and current densities required for PFAS mineralization may lead to considerable heat and gas generation. Gas generation needs to be managed and scrutinized, especially because our analyses detected HF and organofluorine intermediates in the reactor off-gas. It is unclear at this point whether this is an artifact of the small bench-scale, however, as volatile species may redissolve during longer travel paths and times in deeper field installations. Finally, energy consumption is substantially higher than in (*ex situ*) electrochemical systems with active pumping that have been optimized for enhanced mass transfer [22,35].

As our study demonstrates the general viability of *in situ* electrochemical PFAS destruction, future work should focus on optimizing design and implementation. For instance, the application of three-dimensional electrodes may substantially increase contaminant degradation rates and overall treatment efficiency by facilitating contaminant mass transfer and adsorption [60] at the typically low PFAS concentrations encountered in impacted groundwater, given the material has a sufficiently high hydraulic conductivity to avoid groundwater flow diversion. For impacted sites with excessively slow groundwater flow velocities, in-well installations may be a viable solution [61,62]. In conclusion, our performance testing evaluations herein demonstrate that electrochemical treatment is a promising approach for *in situ* destruction of PFASs and sets a foundation for further investigation and optimization.

4.5 Literature References

[1] M. Clara, S. Scharf, S. Weiss, O. Gans, C. Scheffknecht, Emissions of perfluorinated alkylated substances (PFAS) from point sources—identification of relevant branches, Water Sci. Technol. 58 (2008) 59–66. https://doi.org/10.2166/wst.2008.641.

[2] A.M. Trautmann, H. Schell, K.R. Schmidt, K.-M. Mangold, A. Tiehm, Electrochemical degradation of perfluoroalkyl and polyfluoroalkyl substances (PFASs) in groundwater, Water Sci. Technol. 71 (2015) 1569–1575. https://doi.org/10.2166/wst.2015.143.

[3] T.G. Schwanz, M. Llorca, M. Farré, D. Barceló, Perfluoroalkyl substances assessment in drinking waters from Brazil, France and Spain, Sci. Total Environ. 539 (2016) 143–152. https://doi.org/10.1016/j.scitotenv.2015.08.034.

[4] J.S. Boone, C. Vigo, T. Boone, C. Byrne, J. Ferrario, R. Benson, J. Donohue, J.E. Simmons, D.W. Kolpin, E.T. Furlong, S.T. Glassmeyer, Per- and polyfluoroalkyl substances in source and treated drinking waters of the United States, Sci. Total Environ. 653 (2019) 359–369. https://doi.org/10.1016/j.scitotenv.2018.10.245.

[5] A. East, R.H. Anderson, C.J. Salice, Per- and Polyfluoroalkyl Substances (PFAS) in Surface Water Near US Air Force Bases: Prioritizing Individual Chemicals and Mixtures for Toxicity Testing and Risk Assessment, Environ. Toxicol. Chem. 40 (2021) 859–870. https://doi.org/10.1002/etc.4893.

[6] B. Xu, S. Liu, J.L. Zhou, C. Zheng, J. Weifeng, B. Chen, T. Zhang, W. Qiu, PFAS and their substitutes in groundwater: Occurrence, transformation and remediation, J. Hazard. Mater. 412 (2021) 125159. https://doi.org/10.1016/j.jhazmat.2021.125159.

[7] Z.Y. Yong, K.Y. Kim, J.-E. Oh, The occurrence and distributions of per- and polyfluoroalkyl substances (PFAS) in groundwater after a PFAS leakage incident in 2018, Environ. Pollut. 268 (2021) 115395. https://doi.org/10.1016/j.envpol.2020.115395.

[8] E.M. Sunderland, X.C. Hu, C. Dassuncao, A.K. Tokranov, C.C. Wagner, J.G. Allen, A review of the pathways of human exposure to poly- and perfluoroalkyl substances (PFASs) and present understanding of health effects, J. Expo. Sci. Environ. Epidemiol. 29 (2019) 131–147. https://doi.org/10.1038/s41370-018-0094-1.

[9] J.L. Domingo, M. Nadal, Per- and Polyfluoroalkyl Substances (PFASs) in Food and Human Dietary Intake: A Review of the Recent Scientific Literature, J. Agric. Food Chem. 65 (2017) 533–543. https://doi.org/10.1021/acs.jafc.6b04683.

[10] U.S. Environmental Protection Agency Office of Water (4304T) Health and Ecological Criteria Division Washington, Drinking Water Health Advisory for Perfluorooctanoic Acid (PFOA), DC 20460, 2016. https://www.epa.gov/sites/default/files/2016-05/documents/pfoa_health_advisory_final-plain.pdf.

[11] P. McCleaf, S. Englund, A. Östlund, K. Lindegren, K. Wiberg, L. Ahrens, Removal efficiency of multiple poly- and perfluoroalkyl substances (PFASs) in drinking water using granular activated carbon (GAC) and anion exchange (AE) column tests, Water Res. 120 (2017) 77–87. https://doi.org/10.1016/j.watres.2017.04.057.

[12] M. Park, S. Wu, I.J. Lopez, J.Y. Chang, T. Karanfil, S.A. Snyder, Adsorption of perfluoroalkyl substances (PFAS) in groundwater by granular activated carbons: Roles of hydrophobicity of PFAS and carbon characteristics, Water Res. 170 (2020) 115364. https://doi.org/10.1016/j.watres.2019.115364.

[13] T.F. Mastropietro, R. Bruno, E. Pardo, D. Armentano, Reverse osmosis and nanofiltration membranes for highly efficient PFASs removal: overview, challenges and future perspectives, Dalt. Trans. 50 (2021) 5398–5410. https://doi.org/10.1039/D1DT00360G.

[14] M. Kah, D. Oliver, R. Kookana, Sequestration and potential release of PFAS from spent engineered sorbents, Sci. Total Environ. 765 (2021) 142770. https://doi.org/10.1016/j.scitotenv.2020.142770.

[15] T.A. Bruton, D.L. Sedlak, Treatment of perfluoroalkyl acids by heat-activated persulfate under conditions representative of in situ chemical oxidation, Chemosphere. 206 (2018) 457–464. https://doi.org/10.1016/j.chemosphere.2018.04.128.

[16] M.Y. Khan, S. So, G. da Silva, Decomposition kinetics of perfluorinated sulfonic acids, Chemosphere. 238 (2020) 124615. https://doi.org/10.1016/j.chemosphere.2019.124615.

[17] S. Singh Kalra, B. Cranmer, G. Dooley, A.J. Hanson, S. Maraviov, S.K. Mohanty, J. Blotevogel, S. Mahendra, Sonolytic destruction of Per- and polyfluoroalkyl substances in groundwater, aqueous Film-Forming Foams, and investigation derived waste, Chem. Eng. J. (2021) 131778. https://doi.org/10.1016/j.cej.2021.131778.

[18] R.K. Singh, S. Fernando, S.F. Baygi, N. Multari, S.M. Thagard, T.M. Holsen, Breakdown Products from Perfluorinated Alkyl Substances (PFAS) Degradation in a Plasma-Based Water Treatment Process, Environ. Sci. Technol. 53 (2019) 2731–2738. https://doi.org/10.1021/acs.est.8b07031.

[19] H. Park, C.D. Vecitis, J. Cheng, W. Choi, B.T. Mader, M.R. Hoffmann, Reductive Defluorination of Aqueous Perfluorinated Alkyl Surfactants: Effects of Ionic Headgroup and Chain Length, J. Phys. Chem. A. 113 (2009) 690–696. https://doi.org/10.1021/jp807116q.

[20] S. Hao, Y.-J. Choi, B. Wu, C.P. Higgins, R. Deeb, T.J. Strathmann, Hydrothermal Alkaline Treatment for Destruction of Per- and Polyfluoroalkyl Substances in Aqueous Film-Forming Foam, Environ. Sci. Technol. 55 (2021) 3283–3295. https://doi.org/10.1021/acs.est.0c06906.

[21] C.E. Schaefer, C. Andaya, A. Burant, C.W. Condee, A. Urtiaga, T.J. Strathmann, C.P. Higgins, Electrochemical treatment of perfluorooctanoic acid and perfluorooctane sulfonate:

Insights into mechanisms and application to groundwater treatment, Chem. Eng. J. 317 (2017) 424–432. https://doi.org/10.1016/j.cej.2017.02.107.

[22] T.X.H. Le, H. Haflich, A.D. Shah, B.P. Chaplin, Energy-Efficient Electrochemical Oxidation of Perfluoroalkyl Substances Using a Ti 4 O 7 Reactive Electrochemical Membrane Anode, Environ. Sci. Technol. Lett. 6 (2019) 504–510. https://doi.org/10.1021/acs.estlett.9b00397.

[23] J. Radjenovic, N. Duinslaeger, S.S. Avval, B.P. Chaplin, Facing the Challenge of Poly- and Perfluoroalkyl Substances in Water: Is Electrochemical Oxidation the Answer?, Environ. Sci. Technol. 54 (2020) 14815–14829. https://doi.org/10.1021/acs.est.0c06212.

[24] S. Salvestrini, A. Fenti, S. Chianese, P. Iovino, D. Musmarra, Electro-Oxidation of Humic Acids Using Platinum Electrodes: An Experimental Approach and Kinetic Modelling, Water. 12 (2020) 2250. https://doi.org/10.3390/w12082250.

[25] Y. Wang, R. “David” Pierce, H. Shi, C. Li, Q. Huang, Electrochemical degradation of perfluoroalkyl acids by titanium suboxide anodes, Environ. Sci. Water Res. Technol. 6 (2020) 144–152. https://doi.org/10.1039/C9EW00759H.

[26] T. Sale, M. Olson, D. Gilbert, M. Petersen, Field Demonstration/Validation of Electrolytic Barriers for Energetic Compounds at Pueblo Chemical Depot, 2010. https://apps.dtic.mil/sti/citations/ADA520569.

[27] J.R. Jasmann, P.B. Gedalanga, T. Borch, S. Mahendra, J. Blotevogel, Synergistic Treatment of Mixed 1,4-Dioxane and Chlorinated Solvent Contaminations by Coupling Electrochemical Oxidation with Aerobic Biodegradation, Environ. Sci. Technol. 51 (2017) 12619–12629. https://doi.org/10.1021/acs.est.7b03134.

[28] N.E. Pica, Y. Miao, N.W. Johnson, P. Ramos, S. Mahendra, J. Blotevogel, Bioelectrochemical Treatment of 1,4-Dioxane in the Presence of Chlorinated Solvents: Design, Process, and Sustainability Considerations, ACS Sustain. Chem. Eng. 9 (2021) 3172–3182. https://doi.org/10.1021/acssuschemeng.0c08152.

[29] S. Nayak, B.P. Chaplin, Fabrication and characterization of porous, conductive, monolithic Ti4O7 electrodes, Electrochim. Acta. 263 (2018) 299–310. https://doi.org/10.1016/j.electacta.2018.01.034.

[30] K.E. Carter, J. Farrell, Oxidative Destruction of Perfluorooctane Sulfonate Using Boron-Doped Diamond Film Electrodes, Environ. Sci. Technol. 42 (2008) 6111–6115. https://doi.org/10.1021/es703273s.

[31] B. Gomez-Ruiz, N. Diban, A. Urtiaga, Comparison of microcrystalline and ultrananocrystalline boron doped diamond anodes: Influence on perfluorooctanoic acid electrolysis, Sep. Purif. Technol. 208 (2019) 169–177. https://doi.org/10.1016/j.seppur.2018.03.044.

[32] H. Lin, J. Niu, S. Liang, C. Wang, Y. Wang, F. Jin, Q. Luo, Q. Huang, Development of macroporous Magnéli phase Ti4O7 ceramic materials: As an efficient anode for mineralization of poly- and perfluoroalkyl substances, Chem. Eng. J. 354 (2018) 1058–1067. https://doi.org/10.1016/j.cej.2018.07.210.

[33] C.E. Schaefer, C. Andaya, A. Urtiaga, E.R. McKenzie, C.P. Higgins, Electrochemical treatment of perfluorooctanoic acid (PFOA) and perfluorooctane sulfonic acid (PFOS) in groundwater impacted by aqueous film forming foams (AFFFs), J. Hazard. Mater. 295 (2015) 170–175. https://doi.org/10.1016/j.jhazmat.2015.04.024.

[34] Q. Zhuo, S. Deng, B. Yang, J. Huang, B. Wang, T. Zhang, G. Yu, Degradation of perfluorinated compounds on a boron-doped diamond electrode, Electrochim. Acta. 77 (2012) 17–22. https://doi.org/10.1016/j.electacta.2012.04.145.

[35] H. Shi, Y. Wang, C. Li, R. Pierce, S. Gao, Q. Huang, Degradation of Perfluorooctanesulfonate by Reactive Electrochemical Membrane Composed of Magnéli Phase Titanium Suboxide, Environ. Sci. Technol. 53 (2019) 14528–14537. https://doi.org/10.1021/acs.est.9b04148.

[36] J.R. Jasmann, T. Borch, T.C. Sale, J. Blotevogel, Advanced Electrochemical Oxidation of 1,4-Dioxane via Dark Catalysis by Novel Titanium Dioxide (TiO_2) Pellets, Environ. Sci. Technol. 50 (2016) 8817–8826. https://doi.org/10.1021/acs.est.6b02183.

[37] N.E. Pica, J. Funkhouser, Y. Yin, Z. Zhang, D.M. Ceres, T. Tong, J. Blotevogel, Electrochemical Oxidation of Hexafluoropropylene Oxide Dimer Acid (GenX): Mechanistic Insights and Efficient Treatment Train with Nanofiltration, Environ. Sci. Technol. 53 (2019) 12602–12609. https://doi.org/10.1021/acs.est.9b03171.

[38] H. Zöllig, A. Remmele, C. Fritzsche, E. Morgenroth, K.M. Udert, Formation of Chlorination Byproducts and Their Emission Pathways in Chlorine Mediated Electro-Oxidation of Urine on Active and Nonactive Type Anodes, Environ. Sci. Technol. 49 (2015) 11062–11069. https://doi.org/10.1021/acs.est.5b01675.

[39] J.-D. Chai, M. Head-Gordon, Systematic optimization of long-range corrected hybrid density functionals, J. Chem. Phys. 128 (2008) 084106. https://doi.org/10.1063/1.2834918.

[40] D.J. Van Hoomissen, S. Vyas, Early Events in the Reductive Dehalogenation of Linear Perfluoroalkyl Substances, Environ. Sci. Technol. Lett. 6 (2019) 365–371. https://doi.org/10.1021/acs.estlett.9b00116.

[41] H. Lin, R. Xiao, R. Xie, L. Yang, C. Tang, R. Wang, J. Chen, S. Lv, Q. Huang, Defect Engineering on a Ti 4 O 7 Electrode by Ce 3+ Doping for the Efficient Electrooxidation of Perfluorooctanesulfonate, Environ. Sci. Technol. 55 (2021) 2597–2607. https://doi.org/10.1021/acs.est.0c06881.

[42] A. Kapałka, G. Fóti, C. Comninellis, Kinetic modelling of the electrochemical mineralization of organic pollutants for wastewater treatment, J. Appl. Electrochem. 38 (2007) 7–16. https://doi.org/10.1007/s10800-007-9365-6.

[43] J. Niu, Y. Li, E. Shang, Z. Xu, J. Liu, Electrochemical oxidation of perfluorinated compounds in water, Chemosphere. 146 (2016) 526–538. https://doi.org/10.1016/j.chemosphere.2015.11.115.

[44] B.P. Chaplin, Critical review of electrochemical advanced oxidation processes for water treatment applications, Environ. Sci. Process. Impacts. 16 (2014) 1182–1203. https://doi.org/10.1039/C3EM00679D.

[45] T. Wu, G. Zhao, Y. Lei, P. Li, Distinctive Tin Dioxide Anode Fabricated by Pulse Electrodeposition: High Oxygen Evolution Potential and Efficient Electrochemical Degradation of Fluorobenzene, J. Phys. Chem. C. 115 (2011) 3888–3898. https://doi.org/10.1021/jp110149v.

[46] S. You, B. Liu, Y. Gao, Y. Wang, C.Y. Tang, Y. Huang, N. Ren, Monolithic Porous Magnéli-phase Ti4O7 for Electro-oxidation Treatment of Industrial Wastewater, Electrochim. Acta. 214 (2016) 326–335. https://doi.org/10.1016/j.electacta.2016.08.037.

[47] S. Yang, S. Fernando, T.M. Holsen, Y. Yang, Inhibition of Perchlorate Formation during the Electrochemical Oxidation of Perfluoroalkyl Acid in Groundwater, Environ. Sci. Technol. Lett. 6 (2019) 775–780. https://doi.org/10.1021/acs.estlett.9b00653.

[48] H. Lin, J. Niu, S. Ding, L. Zhang, Electrochemical degradation of perfluorooctanoic acid (PFOA) by Ti/SnO2–Sb, Ti/SnO2–Sb/PbO2 and Ti/SnO2–Sb/MnO2 anodes, Water Res. 46 (2012) 2281–2289. https://doi.org/10.1016/j.watres.2012.01.053.

[49] Q. Zhuo, X. Li, F. Yan, B. Yang, S. Deng, J. Huang, G. Yu, Electrochemical oxidation of 1H,1H,2H,2H-perfluorooctane sulfonic acid (6:2 FTS) on DSA electrode: Operating parameters and mechanism, J. Environ. Sci. 26 (2014) 1733–1739. https://doi.org/10.1016/j.jes.2014.06.014.

[50] A. Farhat, J. Keller, S. Tait, J. Radjenovic, Removal of Persistent Organic Contaminants by Electrochemically Activated Sulfate, Environ. Sci. Technol. 49 (2015) 14326–14333. https://doi.org/10.1021/acs.est.5b02705.

[51] T.A. Bruton, D.L. Sedlak, Treatment of Aqueous Film-Forming Foam by Heat-Activated Persulfate Under Conditions Representative of In Situ Chemical Oxidation, Environ. Sci. Technol. 51 (2017) 13878–13885. https://doi.org/10.1021/acs.est.7b03969.

[52] S. Barisci, R. Suri, Electrooxidation of short- and long-chain perfluoroalkyl substances (PFASs) under different process conditions, J. Environ. Chem. Eng. 9 (2021) 105323. https://doi.org/10.1016/j.jece.2021.105323.

[53] S. Li, D. Bejan, M.S. McDowell, N.J. Bunce, Mixed first and zero order kinetics in the electrooxidation of sulfamethoxazole at a boron-doped diamond (BDD) anode, J. Appl. Electrochem. 38 (2008) 151–159. https://doi.org/10.1007/s10800-007-9413-2.

[54] Y. Liu, X. Fan, X. Quan, Y. Fan, S. Chen, X. Zhao, Enhanced Perfluorooctanoic Acid Degradation by Electrochemical Activation of Sulfate Solution on B/N Codoped Diamond, Environ. Sci. Technol. 53 (2019) 5195–5201. https://doi.org/10.1021/acs.est.8b06130.

[55] T. Ochiai, Y. Iizuka, K. Nakata, T. Murakami, D.A. Tryk, A. Fujishima, Y. Koide, Y. Morito, Efficient electrochemical decomposition of perfluorocarboxylic acids by the use of a boron-doped diamond electrode, Diam. Relat. Mater. 20 (2011) 64–67. https://doi.org/10.1016/j.diamond.2010.12.008.

[56] C.E. Schaefer, D.M. Drennan, D.N. Tran, R. Garcia, E. Christie, C.P. Higgins, J.A. Field, Measurement of Aqueous Diffusivities for Perfluoroalkyl Acids, J. Environ. Eng. 145 (2019) 06019006. https://doi.org/10.1061/(ASCE)EE.1943-7870.0001585.

[57] L. Li, Y. Wang, Q. Huang, First-Principles Study of the Degradation of Perfluorooctanesulfonate and Perfluorobutanesulfonate on a Magnéli Phase Ti 4 O 7 Anode, ACS ES&T Water. 1 (2021) 1737–1744. https://doi.org/10.1021/acsestwater.1c00086.

[58] C. Eschauzier, E. Beerendonk, P. Scholte-Veenendaal, P. De Voogt, Impact of Treatment Processes on the Removal of Perfluoroalkyl Acids from the Drinking Water Production Chain, Environ. Sci. Technol. 46 (2012) 1708–1715. https://doi.org/10.1021/es201662b.

[59] Tom Sale, Matthew Petersen, Dave Gilbert, Final Report Electrically Induced Redox Barriers for Treatment of Groundwater (CU-0112), 2005. https://apps.dtic.mil/sti/pdfs/ADA438421.pdf.

[60] C. Zhang, Y. Jiang, Y. Li, Z. Hu, L. Zhou, M. Zhou, Three-dimensional electrochemical process for wastewater treatment: A general review, Chem. Eng. J. 228 (2013) 455–467. https://doi.org/10.1016/j.cej.2013.05.033.

[61] C.E. Divine, T. Roth, M. Crimi, A.C. DiMarco, M. Spurlin, J. Gillow, G. Leone, The Horizontal Reactive Media Treatment Well (HRX Well®) for Passive In-Situ Remediation, Groundw. Monit. Remediat. 38 (2018) 56–65. https://doi.org/10.1111/gwmr.12252.

[62] C.E. Divine, J. Wright, M. Crimi, J.F. Devlin, M. Lubrecht, J. Wang, J. McDonough, M. Kladias, J. Hinkle, A. Cormican, T. Osorno, B.N. Nzeribe, F. Laramay, D. Ombalski, K. Gerber, H. Anderson, Field Demonstration of the Horizontal Treatment Well (HRX Well®) for Passive In Situ Remediation, Groundw. Monit. Remediat. 40 (2020) 42–54. https://doi.org/10.1111/gwmr.12407.

5 BIOELECTROCHEMICAL TREATMENT OF PFASs IN COMPLEX AFFF

5.1 Introduction

Our success in combining electrochemical with biological degradation processes for 1,4-dioxane and CVOCs (Chapter 3) motivated us to explore synergies in the treatment of AFFF-impacted media. In general, the complex AFFF chemical composition can be divided into the three main categories of PFAAs, polyfluorinated precursor compounds, and non-fluorinated chemicals such as hydrocarbon surfactants [1,2]. While the non-fluorinated components are expected to be readily biodegradable, especially in the presence of O_2 as electron acceptor [2], question remain regarding the biotransformation of PFASs.

The transformation of polyfluorinated compounds has been widely documented. While bacteria generally transform polyfluorinated species to dead-end PFAAs [3], fungal transformation pathways produce more degradable polyfluoroalkyl carboxylic acids, such as 5:3 acid, with lower PFAA yields compared to microbial consortia [4]. As of 2021, the predominant belief is that PFAAs are biologically inert, but some studies have claimed that PFAA transformation by microorganisms or enzymes is possible. However, previous studies have not provided sufficient experimental evidence (e.g., defluorination, realistic metabolite identification) that definitively proves PFAA biodegradability, let alone mineralization [5-7]. Huang and Jaffé [8] reported removal of PFOS and PFOA accompanied by the generation of fluoride and short-chain PFAAs in the Feammox process. These observations are promising but, as of today, remain to be independently reproduced and mechanistically elucidated. Luo and co-workers [9-11] reported the degradation of PFOA and PFOS in a laccase-mediator system.

Laccase is an extracellular ligninolytic enzyme produced by wood-rotting fungi such as *Trametes versicolor*. Wood-rotting fungi and their enzymes have great potential for bioremediation because of their ability to mineralize large biological polymers like lignin and various environmental pollutants [12]. Laccase from *T. versicolor* is one of the highest redox potential laccases (785 mV). Like most laccases, it can oxidize compounds with higher redox potentials, which are not direct substrates, using the laccase-mediator system [13]. These mediator compounds can be synthetic or natural, phenolic, azo, hydroxamic acids, and oxime compounds, which are oxidized by laccase to produce radical species that can further assist in the transformation of the target compounds.

The overarching objective of this study was to explore whether fungal pre-treatment of AFFF-impacted water can increase the efficiency of subsequent electrochemical oxidation processes. As biotransformation of AFFF components was expected to be substantially slower than aerobic biodegradation of 1,4-dioxane (Chapter 3), the biological and electrochemical processes were spatially and temporally separated, i.e., AFFF-spiked synthetic groundwater was pre-treated with *T. versicolor* first and subsequently underwent electrochemical oxidation.

5.2 Materials and Methods

5.2.1. Chemicals

The AFFF sample was a 3M electrofluorination AFFF product. PFOS was supplied from Sigma Aldrich (>98%, USA). Surrogate standards (MPFAC-MXA, >99%) were purchased from Wellington Laboratories (Guelph, ON, Canada). KH_2PO_4 and Na_2HPO_4 were purchased from Sigma Aldrich (>99%, USA).

5.2.2. Biological Treatment

Trametes versicolor was cultivated on agar plates containing 4 g/L yeast extract, 10 g/L malt extract, 4 g/L glucose, and 16 g/L agar for 10 days at 30 °C and stored at 4 °C until used. All fungal treatment reactions were performed in Tisma medium [14] containing 10 g/L glucose, 0.3 g/L peptone, 0.5 g/L yeast extract, 1.6 g/L KH_2PO_4, 0.4 g/L Na_2HPO_4, 0.057 g/L $CaCl_2 \cdot 2H_2O$, 0.5 g/L $MgSO_4 \cdot 7\ H_2O$, 0.25 g/L citric acid, 0.1% Tween 80, 0.035 g/L $FeSO_4 \cdot 7H_2O$, 0.007 g/L $MnSO_4 \cdot H_2O$, 0.011 g/L $ZnSO_4 \cdot 7H_2O$, 0.002 g/L H_3BO_3, 0.00035 g/L KI, and 0.00064 g/L $CuSO_4$. Laccase for enzyme-catalyzed reactions was purchased for Sigma Aldrich.

For biological pretreatment of AFFF-spiked water, 2-L baffled Erlenmeyer flasks containing 400 mL Tisma medium were inoculated in triplicates at 104 spores/mL and the fungi were allowed to grow for 4 days before addition of the AFFF to a final dilution of 1:12,500. A killed fungal control was prepared to account for biosorption and other matrix effects. All reactors were incubated at 30 °C and 150 RPM for 19 days. Every 2 days, 200-µL samples were collected and diluted with an equal volume methanol to stop the reactions, filtered through a 0.2-µm polyethersulfone (PES) filter, and analyzed via LC/QToF-MS (see below). At the same time, 400-µL samples collected every 4 days were autoclaved to stop the reaction. These samples were also filtered through 0.2-µm PES filters and analyzed for aqueous fluoride via ion chromatography (see below). All reactors were kept open to atmosphere under sterile conditions for 30 minutes every day to supply oxygen required for aerobic metabolism.

5.2.3. Electrochemical treatment system

The electrochemical flow cell (Advanced Diamond Technologies Inc., Romeoville, IL) held a stainless steel cathode and a boron-doped diamond (BDD) anode with an active surface area of 44 cm^2. All solutions were recirculated from a 1-L polypropylene container at a flow rate of 3 L/min and an applied potential of 30 V. Two 0.5 M NaOH gas traps in series were used to capture volatile HF. Three treatment experiments were conducted: (1) PFOS in pure electrolyte solution (i.e., major Tisma medium salts 1.6 g/L KH_2PO_4, 0.4 g/L Na_2HPO_4), (2) AFFF in the same pure electrolyte solution, and (3) a composite sample of the fungal pretreated triplicate solution.

5.2.4. Chemical Analyses

Non-targeted and semi-targeted analyses were used to characterize the AFFF and treated samples. Samples were diluted 1:20 with methanol (UHPLC-grade, Sigma Aldrich) prior to analysis, spiked with appropriate internal standards, and analyzed on an Agilent 1290 Liquid Chromatograph paired with an Agilent 6530 Quadrupole Time-of-Flight Mass Spectrometer (LC/QToF-MS).

Liquid chromatography was performed with a 2.1 x 150 mm, 5 µm Atlantis dC18 column (Waters), a 2.1 mm x 5 mm, 5 µm Atlantis dC18 VanGuard guard column (Waters), and a mobile phase consisting of 5 mM ammonium acetate in water (A) and 1% water / 99% methanol (B) at a flow rate of 0.5 mL/min. A gradient method was used, starting at 20% B for 6 minutes, then constantly increasing to 90% B by 12 minutes. Electrospray ionization was operated in both positive and negative modes with a capillary voltage of 3500 V, a fragmentor voltage of 150, and a gas temperature of 350 °C. Nitrogen (>99.999% purity, Airgas) was used as the nebulizer and drying gas with flow rates of 9 and 11 L/min, respectively. High-resolution accurate mass spectra were recorded across the range *m/z* 100 - 1,000. Peaks were matched to a PFAS database that was generously provided by Dr. Chris Higgins (Colorado School of Mines) as well as to an in-house database of polyethoxylated surfactants, including polyethylene glycols, alkyl ethoxylates, and nonylphenol polyethoxylates, and of polypropylene glycols that we had previously analyzed in wastewater samples [15-18].

The total oxidizable precursor (TOP) assay was performed based on a protocol previously developed by Houtz & Sedlak [19] with some modifications. Potassium persulfate was added to a final concentration of 60 mM as dry powder to minimize sample dilution. Sodium hydroxide was added from a 5 M stock solution to a final concentration of 250 mM to ensure that the pH remained above 12 in the water samples for the entire duration of the oxidation. The samples were then transferred to a temperature-controlled water bath and treated at 85 °C for six hours. After cooling, samples were spiked with internal standard solution (MPFAC-24ES, Wellington Laboratories), sodium chloride added, and then vortexed. Liquid-liquid extraction was performed with 90% ethyl acetate / 10% trifluoroethanol solution for 30 mins on a rotary mixer. Samples were centrifuged for 2 minutes at 3500 rpm and the upper organic phase transferred to a clean vial. Solvent extraction was repeated, supernatants combined, and then dried under nitrogen. Samples were resuspended by vortexing with 500 µL of methanol and then diluted with 500 µL of water. Final samples were transferred to sample vials with polypropylene insert and polypropylene caps for PFAS quantification on an Agilent 1290 liquid chromatograph coupled to an Agilent 6460 triple quadrupole mass spectrometer (LC/QqQ-MS) equipped with an electrospray ionization (ESI) source using Agilent Jet Stream Technology (Agilent, Santa Clara, CA). The analytes were separated on an Agilent Poroshell C18 column (2.1 mm x 100 mm, 2.7 µm particle size) at 40 °C. A sample volume of 15 µL was injected into a binary mixture of 5 mM ammonium acetate in water (A) and 5 mM ammonium acetate in methanol (B) at a flow rate of 0.4 mL/min. The gradient used was 20% B for 1 minute, increasing to 45% B at 2 min, and finally increasing to 100% B at 5 min. The ionization source conditions used were as follows: negative ESI, nebulizer of 15 psi, gas flow of 4 L/min at 230°C, sheath gas flow of 12 L/min at 350 °C, nozzle voltage of 500 V, and capillary voltage at 3500 V. Analytes were identified by comparison of retention times with analytical standards, individual MRM mass transitions, and with MS/MS ion ratios. Peaks matching retention within 5% and with ion ratios at 20% of the standard ratio were considered acceptable for identification. The data collection and processing were performed by using Agilent MassHunter Quantitative software (v B.07.01). Quantitation was performed with linear regression using

calibration curves from 0.01-250 ng/mL. To minimize system-related interferences or background, an Agilent Eclipse Plus C18 column (4.6 mm x 50 mm, 5 μm particle size) was installed as a delay column immediately after the binary pump and prior to the injection port. The mobile phase degasser was bypassed allowing the mobile phase to enter the binary pump directly and avoiding contact with plastic filters. All plastic tubing in the LC/MS system was replaced with PEEK tubing and plastic frits were replaced with stainless steel. Five injections of pure methanol were made prior to sample analysis to determine if any system background analyte levels were present. With these system changes, background levels for each analyte were not detected in blank samples. The complete oxidative conversion of the quantified precursor compounds 4:2 FTS, 6:2 FTS, 8:2 FTS, and FOSA confirmed the effectiveness of our modified TOP assay protocol.

Fluoride was quantified via ion chromatography on a Dionex ICS 1500 using a Dionex IonPac AS16 (250 m x 4.0 mm ID) column with an IonPac AG16 guard column (4 x 50 mm). A sodium hydroxide gradient was applied, ramped from 5 mM to 100 mM NaOH over 60 minutes at flow rate of 0.8 mL/min, to achieve chromatographic separation of fluoride from formate and acetate, which may be formed during cathodic reduction of CO_2. Control samples confirmed there were no background sources of fluoride.

Total organofluorine was quantified via combustion ion chromatography by Dr. Thomas Holsen at Clarkson University [20].

5.3 Results and Discussion

5.3.1 Electrochemical treatment of AFFF

Figure 30 shows the electrochemical oxidation kinetics of PFOS, the main PFAS species in the AFFF sample, during treatment of the complex AFFF solution versus in clean background electrolyte solution. In the absence of other AFFF components, the pseudo-first-order rate constant was higher (0.0132 min^{-1}) than in the complex sample at the same PFOS concentration of 1 mg/L (0.0039 min^{-1}). Consequently, even at a high current density of 125 mA/cm^2, the treatment process was current-limited and other AFFF ingredients slowed down the electrochemical degradation rate of PFOS.

To further characterize the electrochemical treatment of the dilute AFFF solution, we tracked organofluorine compounds by total organofluorine via combustion ion chromatography and the TOP assay. Similar to the observed PFOS concentrations over time (Figure 30), total organofluorine concentrations decreased sharply during the first 30 minutes of treatment, but less pronounced afterwards (Figure 31). However, aqueous fluoride from C-F bond cleavage was generated almost constantly throughout the experiment (Figure 31). These data imply that PFASs initially adsorbed to the anode surface, but were continuously degraded. The incomplete but increasing fluorine mass balance towards the end of the experiment (Figure 31) indicated that after 420 minutes of treatment, PFASs were still adsorbed at the anode and kept breaking down.

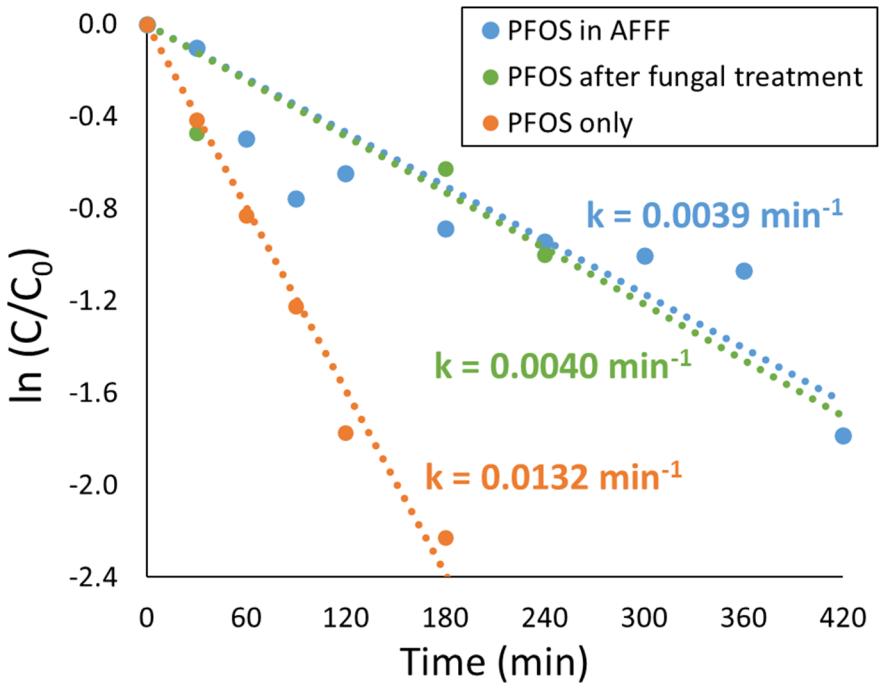

Figure 30: Pseudo-first-order kinetics of electrochemical PFOS oxidation in pure electrolyte solution, in untreated AFFF-spiked electrolyte solution, and in AFFF-spiked electrolyte solution pretreated with *Trametes versicolor*.

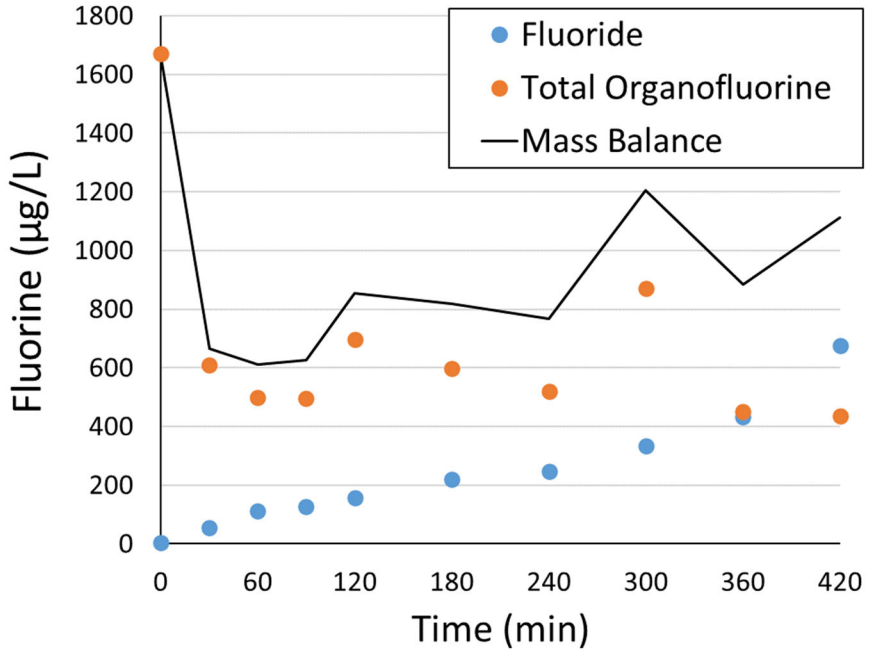

Figure 31: Concentrations of aqueous fluoride and total organofluorine measured via combustion ion chromatography during electrochemical oxidation of 1:12,500-diluted AFFF.

The TOP assay confirmed the observation of a steep PFAS concentration decrease in the first 30 minutes of the experiment. Notably, the concentration of PFAA precursor compounds decreased more strongly than the concentration of PFAAs (Figure 32). The underlying mechanism for this observation is likely related to the transformation of precursors by reactive oxygen species such as hydroxyl radicals, generated from water oxidation at the anode. While PFAAs are only degraded by direct electron transfer at the surface of the anode [21], the non-fluorinated moiety of the precursors can be oxidized by ROS [19] in the vicinity of the anode. We note that no PFOS was generated during the TOP assay, suggesting that the slower PFOS oxidation kinetics in the AFFF sample were not biased by precursor oxidation.

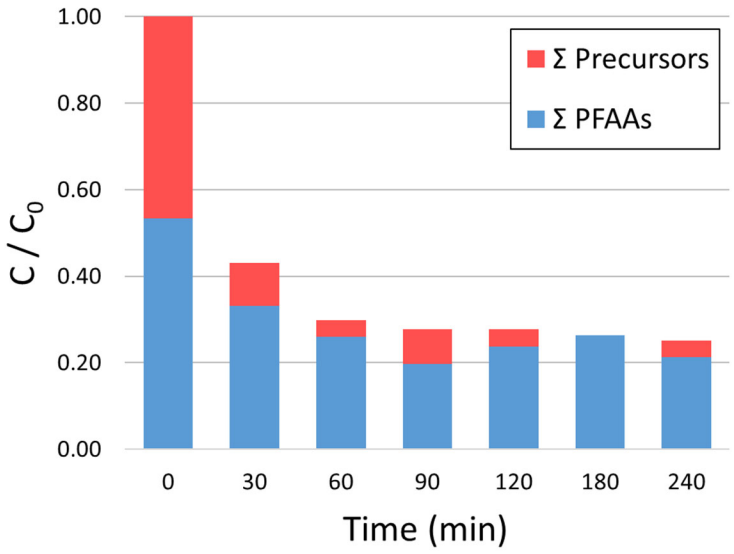

Figure 32: Concentrations of PFAAs and PFAA precursors quantified via the TOP assay during electrochemical oxidation of 1:12,500-diluted AFFF.

The total organofluorine analysis and the TOP assay were in good agreement on the fluorine content of the dilute AFFF sample (1,670 vs. 1,580 µg/L), indicating a total fluorine content of 2% in the original AFFF sample.

5.3.2 Fungal pretreatment of AFFF

Besides several PFSAs and PFCAs, non-targeted high-resolution mass spectrometry putatively identified several polyfluorinated species in the AFFF samples. Four of the major species based on abundance and selected for the assessment of biological treatability were *N*-dimethyl ammonio propyl perfluoropropane sulfonamide (AmPr-FPrSA), *N*-dimethyl ammonio propyl perfluoropentane sulfonamide (AmPr-FPeSA), 4:2 fluorotelomer sulfonamido propyl amine (4:2 FTSA-PrAn), and 6:2 fluorotelomer sulfonamido propyl amine (6:2 FTSA-PrAn).

Figure 33 shows the normalized PFAS concentrations at the end of the 19-day fungal pre-treatment. For some species, notable decreases in relative concentrations were observed, including PFBS and PFPeA. However, especially for two of the polyfluorinated compounds (AmPr-FPrSA

and 6:2 FTSA-PrAn), substantial increases by 63% and 27% were observed. Concentration increases may occur due to transformation if the parent analyte is also a transformation product of a different precursor. However, we note that no mass-labeled internal standards were available for the polyfluorinated compounds, so their peak areas were corrected based on the mass-labeled PFSA or PFCA internal standard with the closest chromatographic retention time. This step may dramatically increase the uncertainty related to (semi-)quantitation.

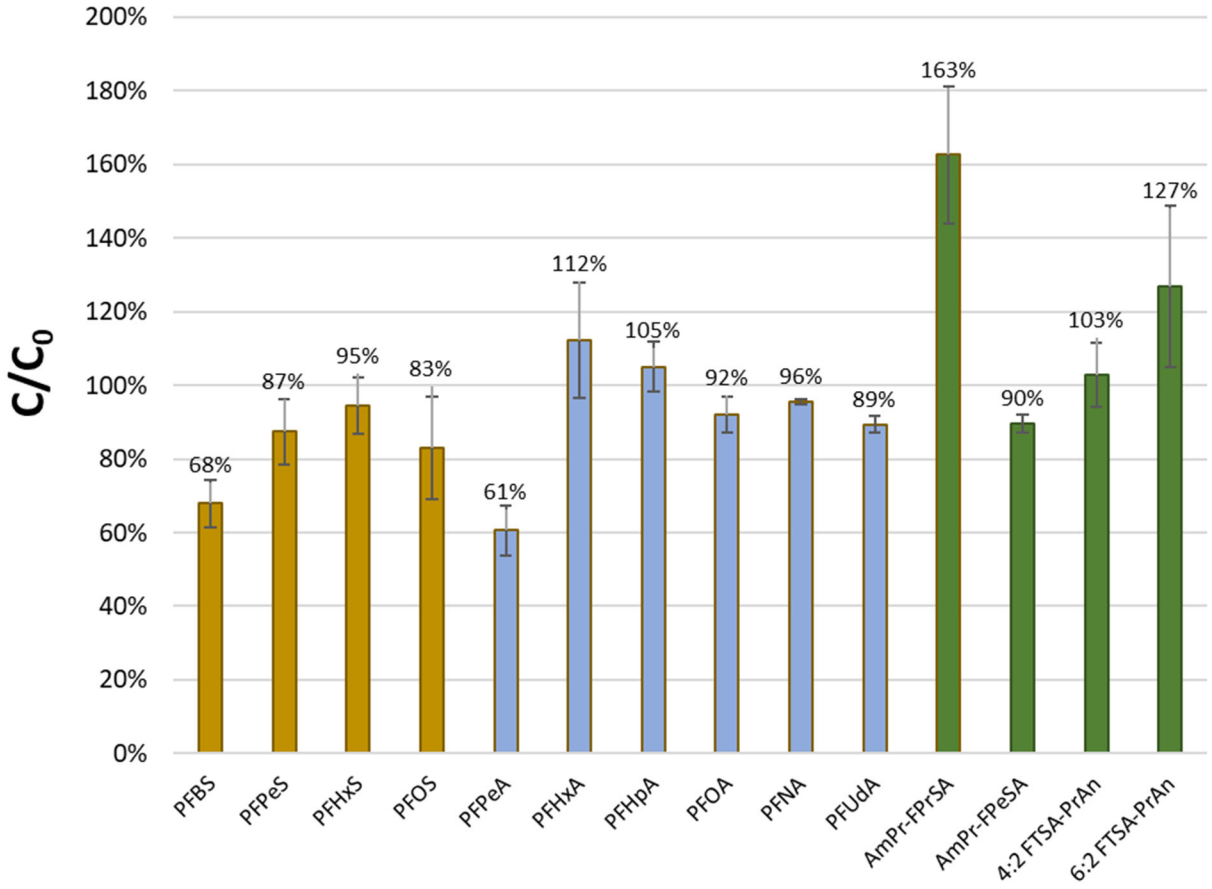

Figure 33: Normalized PFAS concentrations after 19 days of fungal pretreatment normalized to the initial concentrations.

To further assess the fate of the major PFASs in the samples treated by *T. versicolor*, and to distinguish biotransformation from sorption losses we determined the differences between active and killed batches. The raw data can be found in Figure A 2 and Figure A 3 in Appendix A. Figure 34 shows the differences in normalized PFSA concentrations through time. Substantial decreases (i.e., lower relative abundances in fungal versus killed treatments) were observed for all four major PFSAs. However, these decreases did not consistently evolve over time but showed substantial variability, possibly due to precursor transformation to PFSAs.

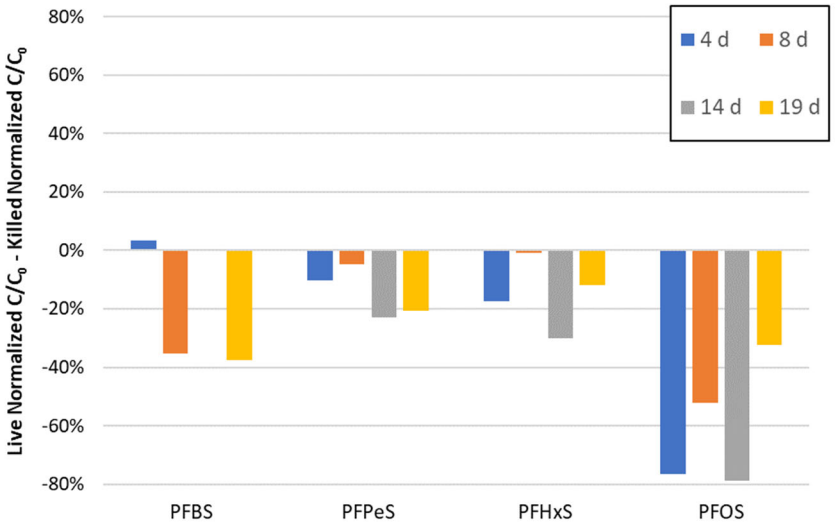

Figure 34: Differences in normalized PFSA concentrations between samples pretreated by *Trametes versicolor* and killed controls, averaged for triplicate samples. A negative value indicates a lower concentration in the fungal batches compared to the killed control batches, and vice versa.

For PFCAs, which were present at lower concentrations than PFSAs, no clear trend was evident (Figure 35). Similarly, no clear trends could be discerned for polyfluorinated species, again, possibly in part resulting from various formation, degradation, or conjugation reactions and in part caused by the lack of appropriate internal standards.

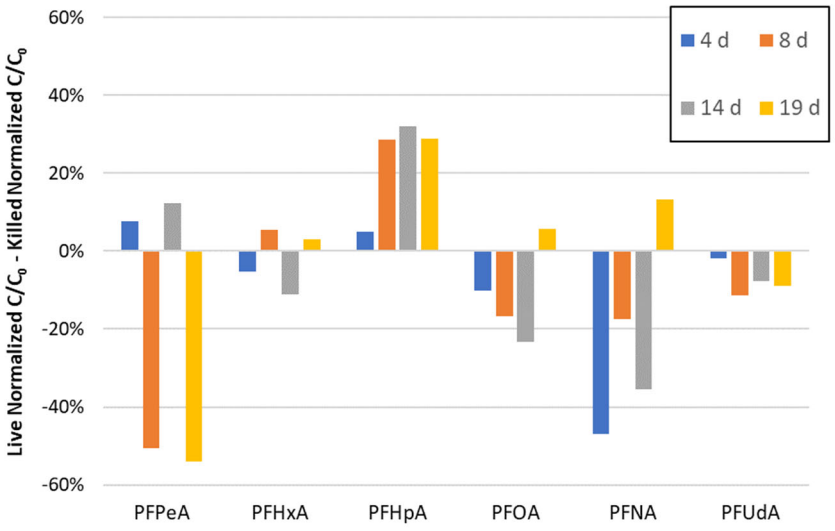

Figure 35: Differences in normalized PFCA concentrations between samples pretreated by *Trametes versicolor* and killed controls, averaged for triplicate samples. A negative value indicates a lower concentration in the fungal batches compared to the killed control batches, and vice versa.

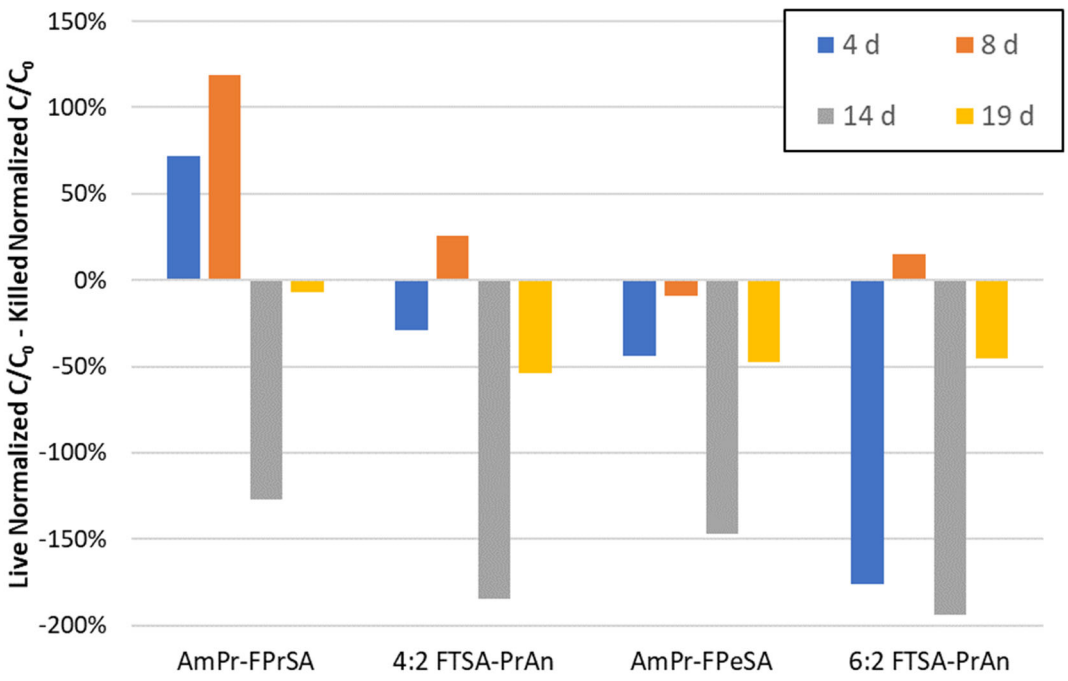

Figure 36: Differences in (select major) normalized polyfluorinated species concentrations between samples pretreated by *Trametes versicolor* and killed controls, averaged for triplicate samples. A negative value indicates a lower concentration in the fungal batches compared to the killed control batches, and vice versa.

We note that throughout the 19-day experiment, no aqueous fluoride as line of evidence for C-F bond cleavage was detected in any of the batches. Consequently, biotransformation resulting in defluorination of the PFAAs cannot be confirmed by these experiments despite strong observed concentration decrease for the highly concentrated PFSAs. One explanation for these observations may be that the fungal culture produced more biomass than in the killed control, leading to more biosorption of PFASs to cell material. Likewise, we cannot conclude that PFAAs are not biodegradable. Luo and co-workers [9-11] reported PFOA and PFOS transformation to occur in a laccase-mediator system over several months. Longer and more targeted experiments should be conducted to follow up on our and previous findings.

In contrast, fungal degradation of non-fluorinated AFFF components was readily observed. Figure 37 shows the degradation of one of the major hydrocarbon surfactants in the AFFF sample, a C_{10}-polyethoxylate homologous series. Concentrations decreased mostly within the first four days, when the activity of secreted enzymes was the highest in planktonic growth. Analytical variability was high in the killed control (Figure 38), likely at least in part due to lack of appropriate mass-labeled internal standards for alkyl ethoxylate surfactants. However, overall, the relative species concentrations were consistently and substantially higher in the killed control than in the fungal batches. Alkyl ethoxylates are known to readily biodegrade under both aerobic and anaerobic conditions [18].

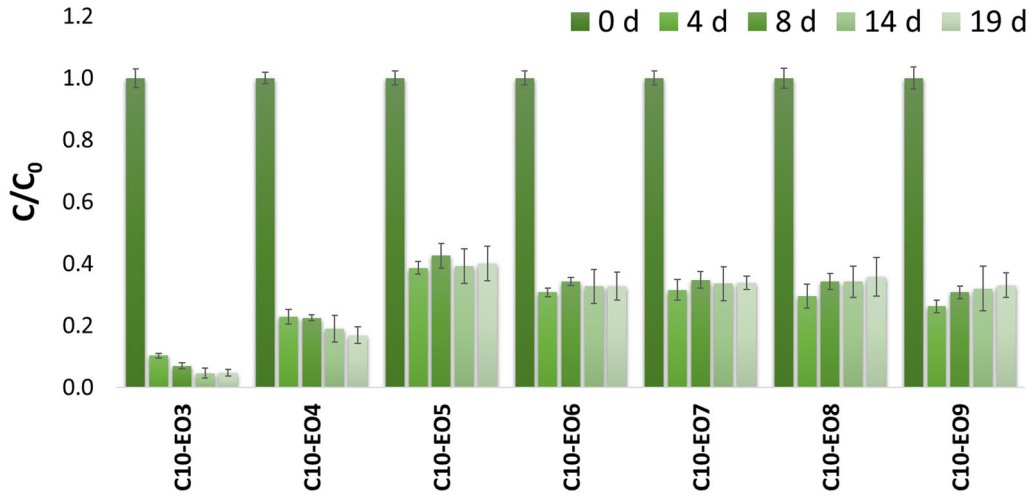

Figure 37: C_{10}-alkyl ethoxylate surfactant concentrations over time during fungal pretreatment normalized to the initial concentrations.

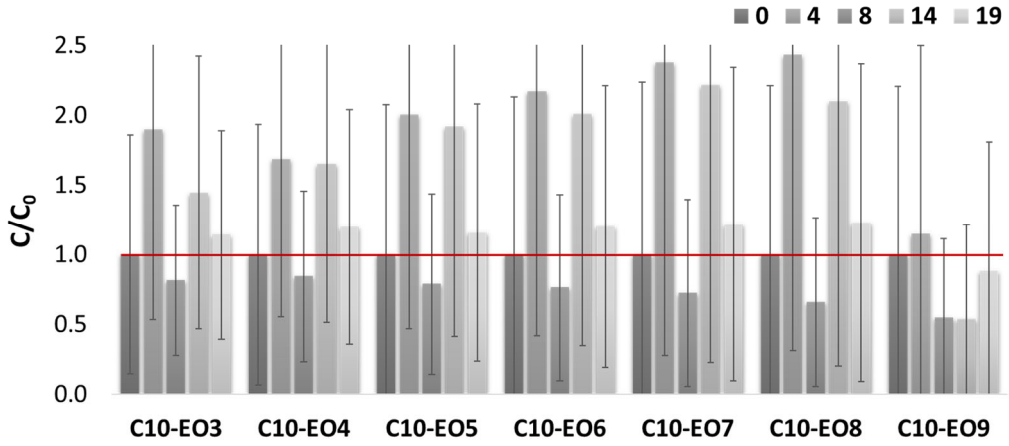

Figure 38: C_{10}-alkyl ethoxylate surfactant concentrations over time in the killed control normalized to the initial concentrations. The red line shows the initial concentration.

5.3.2 Combined fungal-electrochemical treatment of AFFF

Figure 30 shows the electrochemical oxidation kinetics of PFOS in the AFFF sample after fungal pre-treatment. While no meaningful improvement in the rate constant (0.0040 min^{-1}) was observed in comparison to the untreated AFFF sample (0.0039 min^{-1}), the current density had decreased by 20% to 100 mA/cm^2 at a constant applied potential of 30 V, likely due to fungal degradation of other, more readily biodegradable AFFF components. This led to a 20% lower energy consumption of the electrochemical treatment process, with the EEO decreasing from 1,600 to 1,200 kWh/m^{-3} for PFOS after fungal pretreatment (Figure 39).

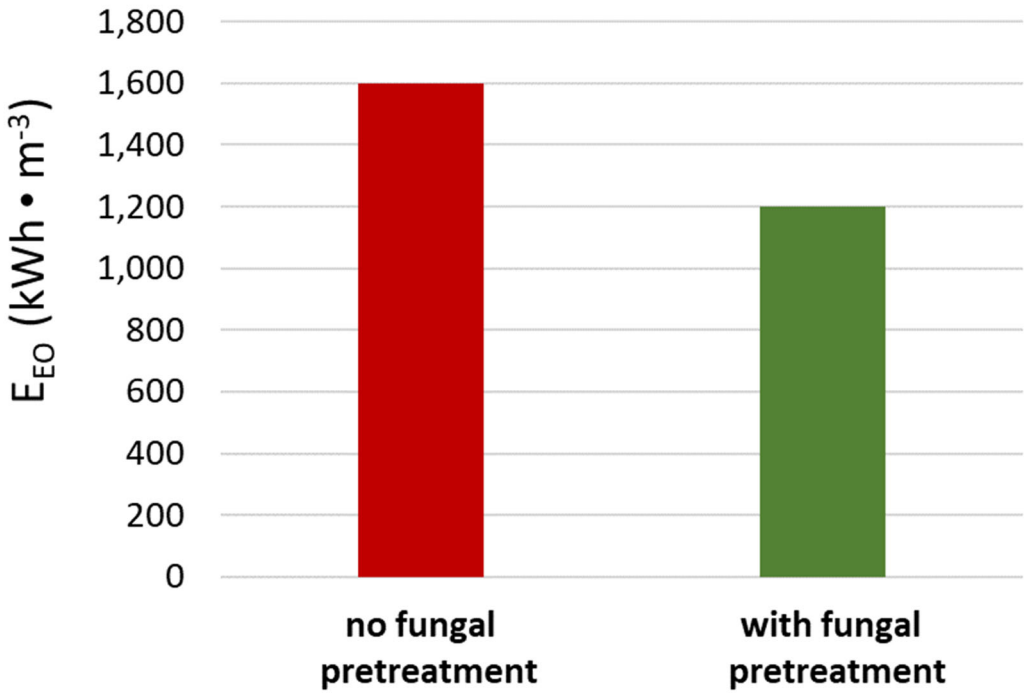

Figure 39: Electric energy per order of PFOS removed with and without fungal pre-treatment.

5.4 Conclusions

Destruction of PFASs in impacted environmental matrices is preferable over removal and disposal. However, destructive technologies that are effective for PFASs, including electrochemical treatment, are very expensive. While our relatively short-term experiments cannot confirm biodefluorination, biomineralization, or even biotransformation of highly persistent PFAAs (and likewise not exclude it), they do imply that many AFFF components such as hydrocarbon surfactants are readily biodegradable. For treatment processes whose efficiency is impacted by competition of co-occurring contaminants (e.g., electrochemical oxidation, but not incineration), remediation cost savings are possible by granting natural degradation processes time and space, and focus these expensive treatment methods on the most persistent species such as PFAAs only.

Nevertheless, it is our strong suggestion to keep exploring biological degradation processes for PFAAs. Besides experimental approaches, these investigations should make use of theoretical approaches to screen for thermodynamically and kinetically favorable mechanisms (e.g., references 9 and 11). Fungal degradation is a promising avenue as it generally accounts for up to 75% of the microbial biomass in surface soils, where typically the highest PFAS concentrations at AFFF-impacted soils are found [3,22].

5.5 Literature References

1. Barzen-Hanson, K. A.; Roberts, S. C.; Choyke, S.; Oetjen, K.;McAlees, A.; Riddell, N.; McCrindle, R.; Ferguson, P. L.; Higgins, C.P.; Field, J. A. Discovery of 40 Classes of Per-and Polyfluoroalkyl Substances in Historical Aqueous Film-Forming Foams (AFFFs) and AFFF-Impacted Groundwater. Environ. Sci. Technol. 2017, 51, 2047-2057.
2. Garcia, R.A., Chiaia-Hernández, A.C., Lara-Martín, P.A., Loos, M., Hollender, J., Oetjen, K., Higgins, C.P. and Field, J.A. Suspect Screening of Hydrocarbon Surfactants in AFFFs and AFFF-Contaminated Groundwater by High Resolution Mass Spectrometry. Environ. Sci. Technol. 2019, 53, 14, 8068-8077.
3. Sharifan, H., M. Bagheri, D. Wang, J.G. Burken, C.P. Higgins, Y. Liang, J. Liu, C.E. Schaefer, and J. Blotevogel. Fate and transport of per- and polyfluoroalkyl substances (PFASs) in the vadose zone. Science of the Total Environment 2021, 771, 145427.
4. Tseng, N.; Wang, N.; Szostek, B.; Mahendra, S. Biotransformation of 6:2 Fluorotelomer alcohol (6:2 FTOH) by the wood-rotting fungus *Phanerochaete chrysosporium*. Environ. Sci. Technol. 2014, 48, 4012-4020.
5. Mejia-Avendaño, S.; Zhong, G.; Liu, J. Comment on "Biodegradation of perfluorooctanesulfonate (PFOS) as an emerging contaminant". Chemosphere 2015, 138, 1037-1038.
6. Butzen, M.L.; Wilkinson, J.T.; McGuinness, S.R.; Amezquita, S.; Peaslee, G.F.; Fein, J.B. Sorption and desorption behavior of PFOS and PFOA onto a Gram-positive and a Gram-negative bacterial species measured using particle-induced gamma-ray emission (PIGE) spectroscopy. Chemical Geology 2020, 119778.
7. Presentato, A.; Lampis, S.; Vantini, A.; Manea, F.; Daprà, F.; Zuccoli, S.; Vallini, G. On the ability of Perfluorohexane Sulfonate (PFHxS) bioaccumulation by two Pseudomonas sp. strains isolated from PFAS-contaminated environmental matrices. Microorganisms 2020, 8, 92.
8. Huang, S. and P.R. Jaffe, Defluorination of Perfluorooctanoic Acid (PFOA) and Perfluorooctane Sulfonate (PFOS) by *Acidimicrobium* sp. Strain A6. Environmental Science & Technology 2019, 53, 11410-11419.
9. Luo, Q., J. Lu, H. Zhang, Z. Wang, M. Feng, S.-Y.D. Chiang, D. Woodward, and Q. Huang, Laccase-Catalyzed Degradation of Perfluorooctanoic Acid. Environmental Science & Technology Letters 2015, 2, 198-203.
10. Luo, Q., Z. Wang, M. Feng, D. Chiang, D. Woodward, S. Liang, J. Lu, and Q. Huang, Factors controlling the rate of perfluorooctanoic acid degradation in laccase-mediator systems: The impact of metal ions. Environmental Pollution 2017, 224, 649-657.
11. Luo, Q., X. Yan, J. Lu, and Q. Huang, Perfluorooctanesulfonate Degrades in a Laccase-Mediator System. Environmental Science & Technology 2018, 52, 10617-10626.

12. Harms, H., D. Schlosser, and L.Y. Wick. Untapped potential: exploiting fungi in bioremediation of hazardous chemicals. Nature Reviews Microbiology 2011, 9, 177-192.

13. Morozova, O.V.; Shumakovich, G.P; Shleev, S.V.; Yaropolov, Y.I. Laccase-mediator systems and their applications: A review. Applied Biochemistry and Microbiology 2007, 43, 523-535.

14. Tišma, M.; Žnidaršič-Plazl, P.; Vasić-Rački, Đ.; Zelić, B. Optimization of Laccase Production by *Trametes versicolor* Cultivated on Industrial Waste. Appl. Biochem. Biotechnol. 2012, 166, 36-46.

15. Thurman, E.M., Ferrer, I., Blotevogel, J., Borch, T. Analysis of hydraulic fracturing flowback and produced waters using accurate mass: Identification of ethoxylated surfactants. Anal. Chem. 2014, 86, 9653-9661.

16. McLaughlin, M.C., Borch, T., Blotevogel, J. Spill of hydraulic fracturing chemicals on agricultural topsoil: Biodegradation, sorption, and co-contaminant interactions. Environ. Sci. Technol. 2016, 50, 6071-6078.

17. Hanson, A.J., Luek, J.L., Tummings, S.S., McLaughlin, M.C., Blotevogel, J., Mouser, P.J. High total dissolved solids in shale gas wastewater inhibit biodegradation of alkyl and nonylphenol ethoxylate surfactants. Sci. Total Environ. 2019, 668, 1094-1103.

18. Heyob, K.M., Blotevogel, J., Brooker, M., Evans, M.V., Lenhart, J.J., Wright, J., Lamendella, R., Borch, T., Mouser, P.J. Natural Attenuation of Nonionic Surfactants Used in Hydraulic Fracturing Fluids: Degradation Rates, Pathways, and Mechanisms. Environ. Sci. Technol. 2017, 51, 13985-13994.

19. Houtz, E. F.; Sedlak, D. L. Oxidative Conversion as a Means of Detecting Precursors to Perfluoroalkyl Acids in Urban Runoff. Environ. Sci. Technol. 2012, 46, 9342-9349.

20. Singh, R.K.; Multari, N.; Nau-Hix, C.; Anderson, R.H.; Richardson, S.D.; Holsen, T.M.; Mededovic Thagard, S. Rapid removal of poly- and perfluorinated compounds from investigation-derived waste (IDW) in a pilot-scale plasma reactor. Environ. Sci. Technol. 2019, 53, 19, 11375-11382.

21. Chaplin, B. P. Critical review of electrochemical advanced oxidation processes for water treatment applications. Environ. Sci.: Processes Impacts 2014, 16, 1182-1203.

22. Harms, H.; Schlosser, D.; Wick, L. Y. Untapped potential: exploiting fungi in bioremediation of hazardous chemicals. Nature Reviews Microbiology 2011, 9, 177-192.

6 CONCLUSIONS AND IMPLICATIONS FOR FUTURE RESEARCH AND IMPLEMENTATION

The overarching goal of this project was to advance the efficacy of bioelectrochemical treatment for the remediation of groundwater contaminated by mixed contaminants. The guiding idea was to establish contaminant degradation by flow-through mesh electrodes, enabling *in situ* implementation such as in a permeable reactive barrier.

For mixed 1,4-dioxane and CVOC contaminations, we showed that both electrochemical and biological oxidation kinetics occur on similar time scales, meaning that these two treatments can be combined in one single simultaneous process. During bioelectrochemical treatment, 1,4-dioxane was reduced by several orders of magnitude from over 100,000 µg/L to below our detection limit of 3 µg/L. Consequently, this technology should be effective in source zones as well as in dilute plumes, possibly meeting the strict low- or sub-ppb 1,4-dioxane regulatory limits, where solely (co-)metabolic bioremediation approaches are challenged. While the presence of the strong inhibitor 1,1-DCE slowed bioelectrochemical 1,4-dioxane degradation, it did not stall it. Furthermore, we showed that the dimensionally stable mesh electrodes should be operative for extended periods (i.e., months, years) if proper scale management via polarity reversals is performed.

Prior to field implementation, limited bench-scale and pilot-scale testing is crucial because of site-specific variability in water chemistry, contaminant concentrations, and flow rates that will impact reactor design and operational parameters. Bench-scale should focus on the general feasibility by screening a broad range of applied potentials or current densities for contaminant degradation kinetics and mineral precipitation, acquiring a rough understanding of the number of electrodes needed to reach the target treatment goal. Pilot-testing should focus on optimizing applied potentials as well as polarity reversal duration and frequency, assessing the longevity of the electrodes, formation of reaction by-products, and general operational factors such as gas management and safety.

Due to the success of our research performed within this project, bioelectrochemical treatment of mixed 1,4-dioxane and CVOC contaminations has been scaled up and is currently pilot-tested at an undisclosed non-DoD site in the U.S. In collaboration with Jacobs Engineering, we built drum-scale reactors to test the treatment process at larger scale under real-world conditions (Figure 40). While final results will be reported at a later date, current results after ~1 year of operation look promising. Importantly, oxidation by-products generated from electrochemical oxidation are completely removed in a secondary biological reduction treatment. The findings of the pilot will be a critical first lesson in technology scale-up. Installations other than permeable reactive barriers are certainly possible, such as integration into subgrade biogeochemical reactors [1-3].

We believe that this technology is mature enough to move on to field trials, and that future efforts should be focused on scale-up. Other important questions that remain to be answered are whether bioelectrochemical oxidation can be combined with other types of bacteria including 1,4-dioxane- and CVOC-co-metabolizing strains and mixed cultures, and if reductive microbial processes can be integrated to take advantage of thus far unutilized cathodic processes.

Figure 40: Drum-scale bioelectrochemical reactor and rectifier for field testing, designed and constructed at Colorado State University in collaboration with Jacobs.

PFASs have been challenging largely any water treatment technology, and (bio)electrochemical treatment is no exception. In this process, electrochemical and biological degradation rates (if any) are very different, requiring a spatial and temporal separation of these two processes. Our findings show that various mesh electrode materials are capable of breaking down even the most persistent PFAAs, paving the way for *in situ* electrochemical groundwater treatment. As several previous studies have shown for other electrode and reactor configurations, Magnéli-phase titanium suboxides appear to be especially suited for PFAS degradation. This material is slowly becoming commercially available and, while currently still more expensive than other effective mixed metal oxide materials (e.g., Ti/IrO_2-Ta_2O_5), is seen as having the potential for economically feasible and competitive prices once more broadly adopted. As with other destructive treatment processes, concerns remain regarding the generation of organofluorine intermediates. While we did not observe any aqueous-phase organofluorine compounds, some were detected in the gas-phase exhaust of the electrochemical reactor. It seems possible, however, that these concerns can be mitigated through better (or possibly larger) future reactor design. Possibly greater concerns at this point are energy footprint and costs of *in situ* groundwater treatment. Electrochemical PFAS oxidation is notoriously mass transfer-limited, and typically slow groundwater seepage velocities in combination with high current densities needed for PFAS destruction results in low faradaic efficiency, resulting in excessive gas formation and low direct electron transfer rates to the target PFAS molecules. Future work should focus on optimizing process design (e.g., three-dimensional electrodes) and implementation (e.g., in-well installations [4]).

While we were unable to find conclusive evidence of fungal PFAA transformation during the relatively short experimental time frame (with "relative" pertaining to biological transformation of PFAAs in comparison to other organic pollutants), our experiments did demonstrate, however, that there are other non-fluorinated AFFF components that are readily biodegradable. As these substrates may compete with highly refractory PFAAs for sorption and degradation processes, such as direct electron transfer in the context of electrochemical treatment, biological processes should be granted time to degrade as many AFFF ingredients as possible. All water treatment and remediation technologies shown to break the C-F bond thus far are expensive, and these approaches will likely have to be focused on high-priority and/or high-concentration site locations. Historically, we have been depending on natural attenuation or source zone depletion processes for rational, sustainable, and economical site remediation. At most sites, biological processes have outcompeted our active engineered remedial approaches. Clearly, future research efforts should continue to explore natural biotic and abiotic removal and transformation of PFASs at the lab-scale, at the (matured) field-scale, and *in silico*, under consideration of the assimilative capacity [5]. This is not the time to give up – without nature's assistance in overall contaminant mass removals, low regulatory thresholds are hardly affordable.

As water treatment and remediation technologies have matured in recent years, combining processes in efficient treatment trains promises further economic and environmental benefits. In this project, we have advanced the efficacy of bioelectrochemical treatment for the remediation of groundwater contaminated by mixed contaminants of concern. While we recently scaled up this technology to field application for 1,4-dioxane and chlorinated solvents, future work and research remains to be done for more persistent PFASs. At the moment, any destructive PFAS treatment is expensive, but process and material optimizations leading to considerable cost savings are still waiting to be discovered.

6.1 Literature References

1. Gamlin, J.; Cox, J.; Castor, A. Innovative applications of subgrade biogeochemical reactors: Three case studies. Remediation 2019, 29, 33-43.
2. Gamlin, J.; Downey, D.; Shearer, B.; Favara, P. Design and performance of subgrade biogeochemical reactors. Journal of Environmental Engineering 2017, 204, 804-812.
3. Gamlin, J.; Downey, D. (2017). Subgrade biogeochemical reactor (SBGR). Enviro Wiki. https://www.enviro.wiki/index.php?title=Subgrade_Biogeochemical_Reactor_(SBGR).
4. Divine, C.E.; Roth, T.; Crimi, M.; DiMarco, A.C.; Spurlin, M.; Gillow, J.; Leone, G. The Horizontal Reactive Media Treatment Well (HRX Well®) for Passive In-Situ Remediation. Groundw. Monit. Remediat. 2018, 38, 56-65.
5. Cairns Jr, J. Assimilative capacity – the key to sustainable use of the planet. Journal of Aquatic Ecosystem Stress and Recovery 1998, 6, 259-263.

APPENDIX A: SUPPORTING DATA

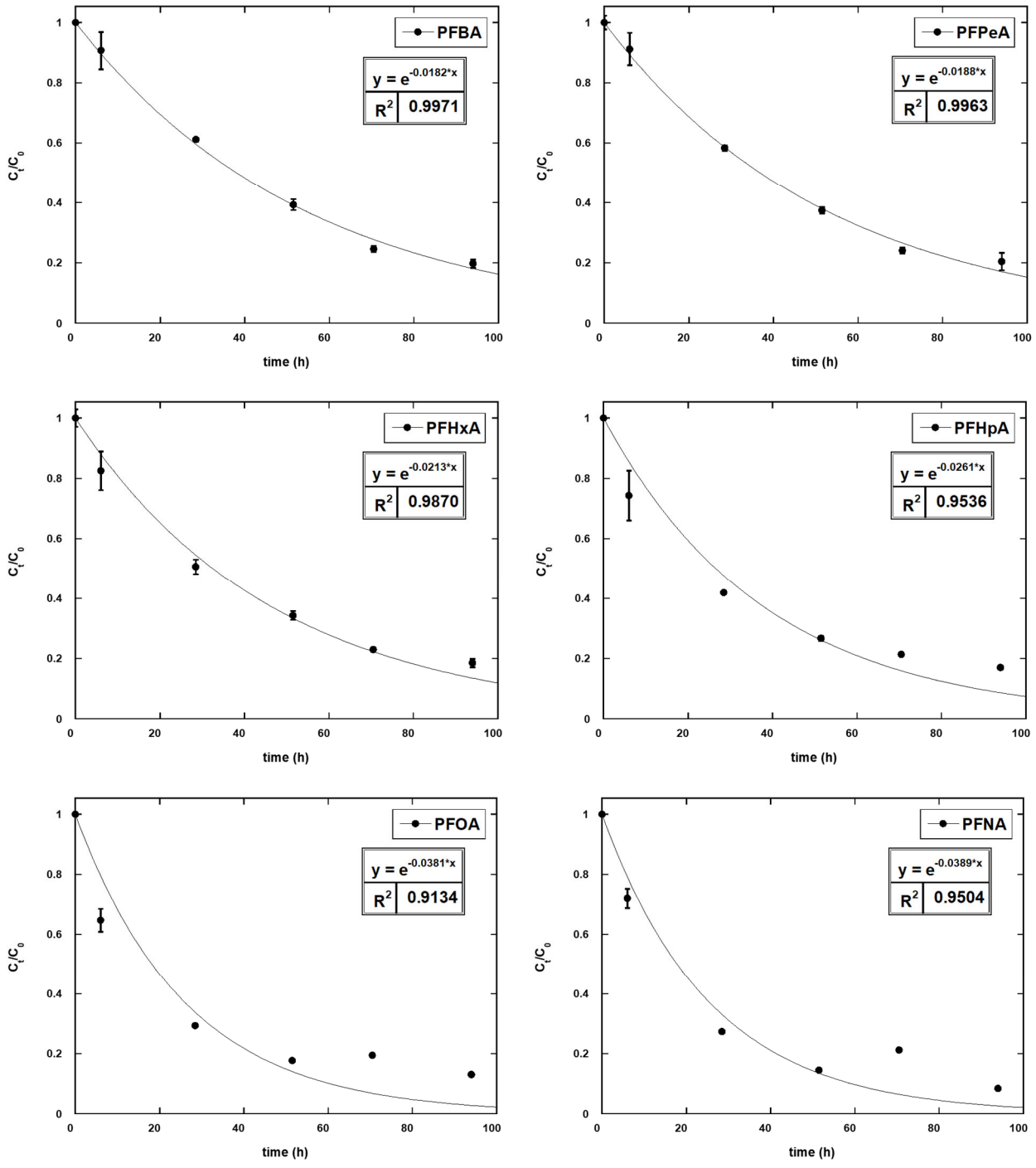

Figure A 1: Electrochemical oxidation kinetics for the PFAAs tested in this study.

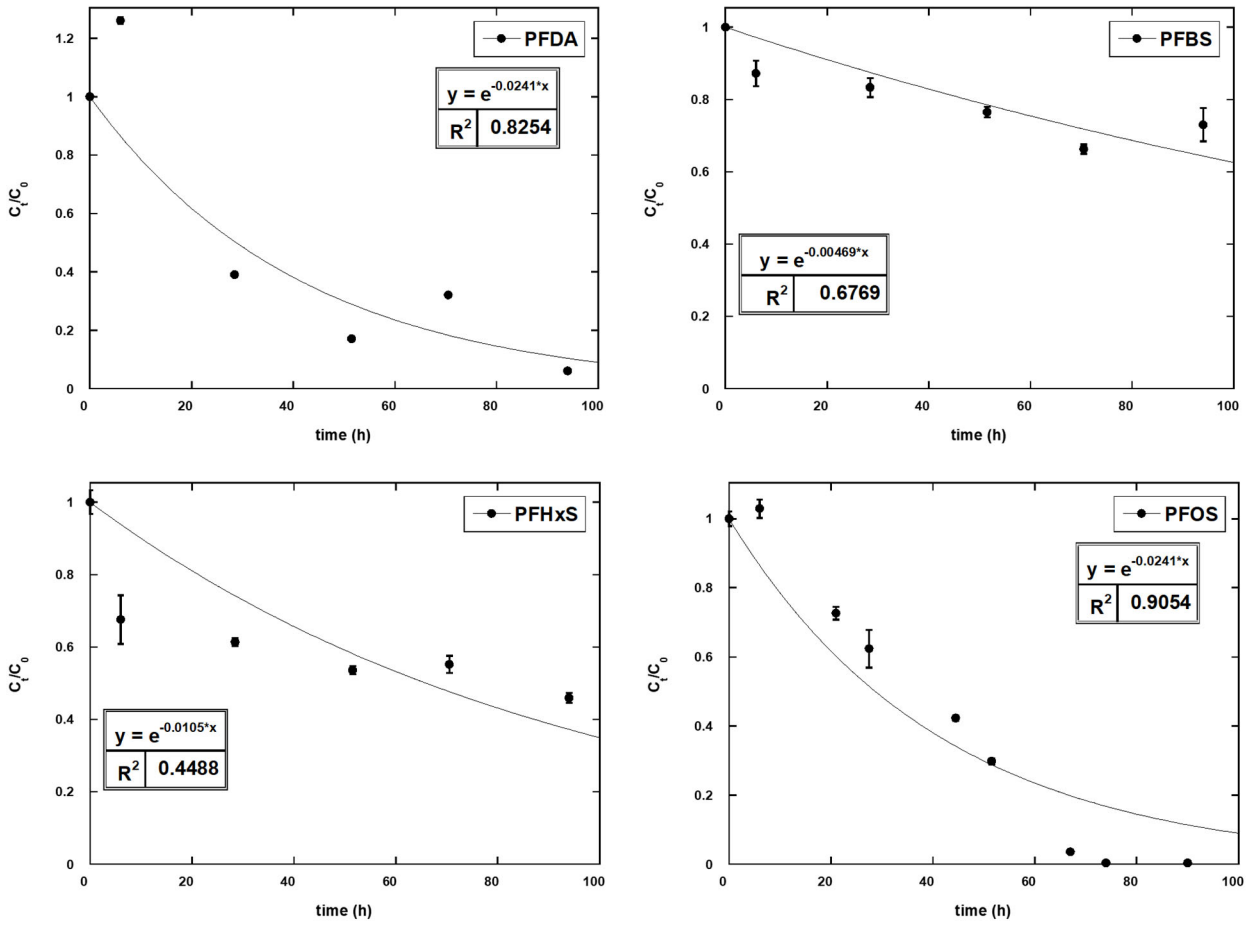

Figure A 1 (continued): Electrochemical oxidation kinetics for the PFAAs tested in this study.

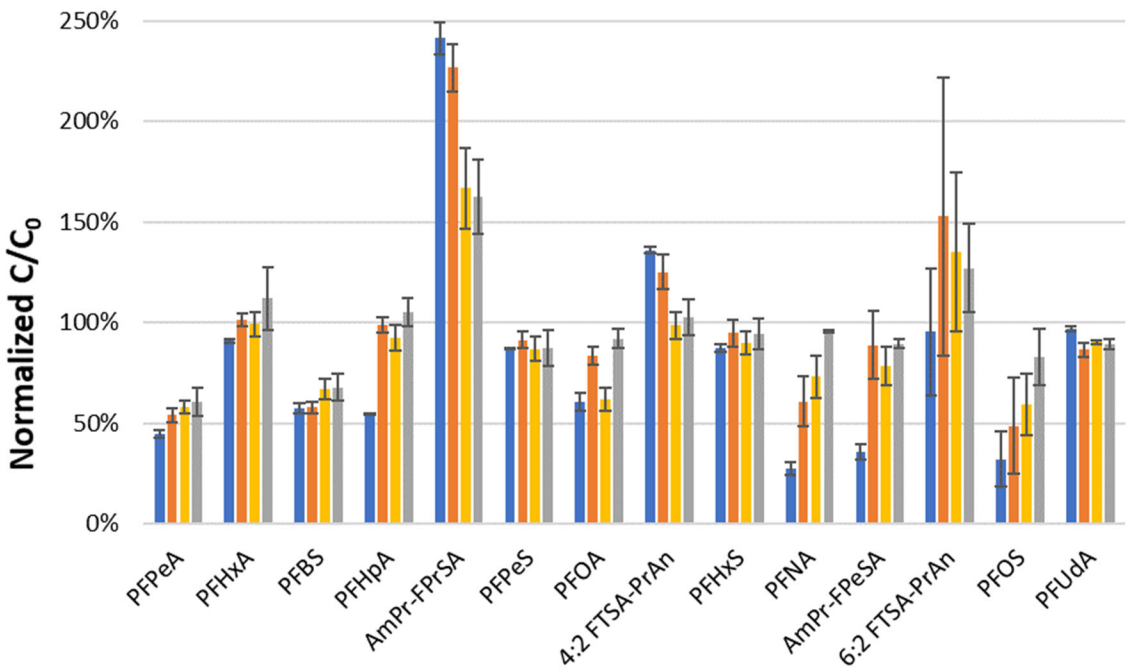

Figure A 2: Normalized PFAS concentrations over time in a dilute AFFF sample treated with *Trametes versicolor*.

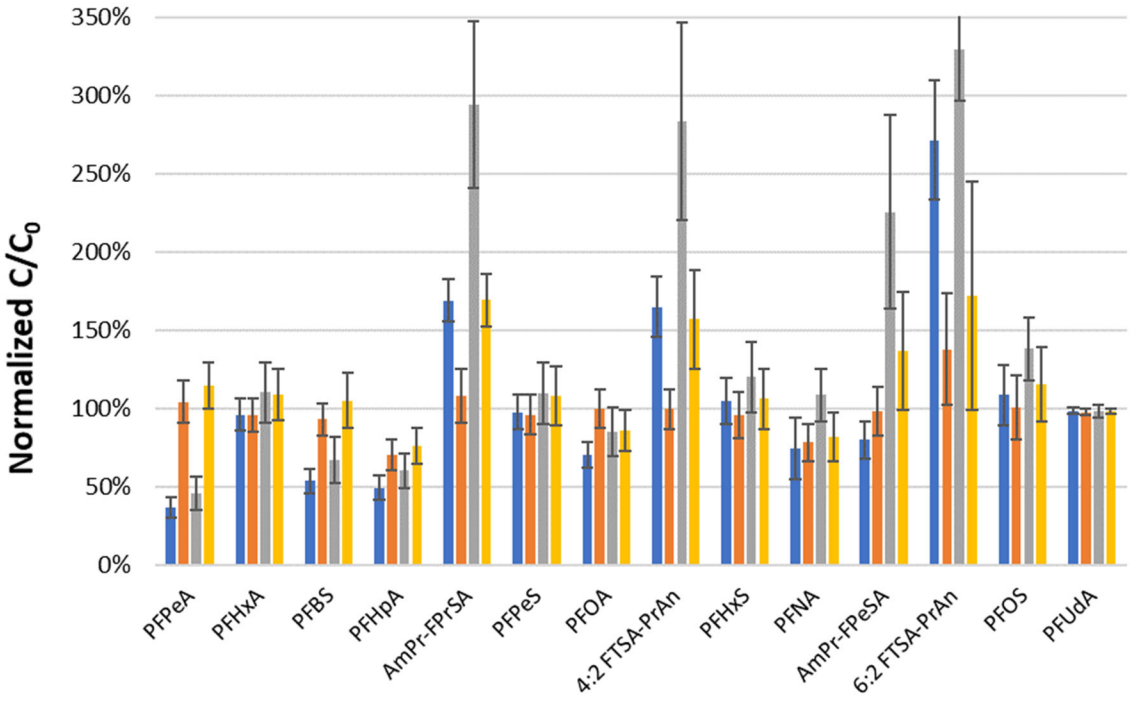

Figure A 3: Normalized PFAS concentrations over time in a dilute AFFF sample serving as killed control.

APPENDIX B: LIST OF PUBLICATIONS

Pica, N.E.; Johnson, N.W.; Miao, Y.; Ramos, P.; Mahendra, S.; Blotevogel, J. Bioelectrochemical treatment of 1,4-dioxane in the presence of chlorinated solvents: Design, process, and sustainability considerations. *ACS Sustainable Chemistry & Engineering* **2021**, *9*, 3172-3182.

Sharifan, H.; Bagheri, M.; Wang, D.; Burken, J.G.; Higgins, C.P.; Liang, Y.; Liu, J.; Schaefer, C.E.; Blotevogel, J. Fate and transport of per- and polyfluoroalkyl substances (PFASs) in the vadose zone. *Science of the Total Environment* **2021**, *771*, 145427.

Fenti, A.; Jin, Y.; Hanson, A.J.; Dooley, G.P.; Iovino, P.; Salvestrini, S.; Musmarra, D.; Mahendra, S.; Peaslee, G.F.; Blotevogel, J. Performance testing of mesh anodes for *in situ* electrochemical oxidation of PFAS. In review.